Universidade de Aveiro
2016

Departamento de Química

SARA RAQUEL DUARTE GAMELAS

DERIVADOS PORFIRÍNICOS E *SPLICING* ALTERNATIVO DO mRNA INDUZIDO POR TERAPIA FOTODINÂMICA

PORPHYRIN DERIVATIVES AND mRNA ALTERNATIVE SPLICING INDUCED BY PHOTODYNAMIC THERAPY

Universidade de Aveiro
2016

Departamento de Química

SARA RAQUEL DUARTE GAMELAS

DERIVADOS PORFIRÍNICOS E SPLICING ALTERNATIVO DO mRNA INDUZIDO POR TERAPIA FOTODINÂMICA

PORPHYRIN DERIVATIVES AND mRNA ALTERNATIVE SPLICING INDUCED BY PHOTODYNAMIC THERAPY

Tese apresentada à Universidade de Aveiro para cumprimento dos requisitos necessários à obtenção do grau de Mestre em Química, realizada sob a orientação científica da Doutora Maria do Amparo Ferreira Faustino, Professora Auxiliar do Departamento de Química da Universidade de Aveiro, Doutora Maria da Graça de Pinho Morgado Silva Neves, Professora Associada com Agregação do Departamento de Química da Universidade de Aveiro, e o Doutor Nuno Miguel Malavado Moura, aluno de Pós-Doutoramento do Departamento de Química da Universidade de Aveiro.

Thesis presented to the University of Aveiro to fulfil the requirements needed to obtain the degree of Master in Chemistry, performed under the scientific guidance of Dr Maria do Amparo Ferreira Faustino, Assistant Professor of the Chemistry Department of University of Aveiro, Dr Maria da Graça de Pinho Morgado Silva Neves, Associate Professor with aggregation of Chemistry Department of University of Aveiro and Dr Nuno Miguel Malavado Moura, Postdoc at the Chemistry Department of University of Aveiro.

Apoio financeiro da FEDER no âmbito do III Quadro Comunitário de Apoio

União Europeia
FEDER

Apoio financeiro da FCT e do FSE no âmbito do III Quadro Comunitário de Apoio

FCT
Fundação para a Ciência e a Tecnologia
MINISTÉRIO DA EDUCAÇÃO E CIÊNCIA

O júri

Prof. Dr. Artur Manuel Soares de Silva
Professor Catedrático- Departamento de Química- Universidade de Aveiro

Prof. Dr. Oscar Endrigo Dorneles Rodrigues
Professor Adjunto IV- Departamento de Química- Universidade Federal de Santa Maria, Rio Grande do Sul, Brasil. “

Prof. Dr. Maria do Amparo Ferreira Faustino
Professora Assistente – Departamento de Química- Universidade de Aveiro

Dr. Yvette Habraken
Cientista Sénior na F.R.S-FNRS- Universidade de Liège- Bélgica

agradecimentos

Gostaria de agradecer primariamente à minha orientadora Dr. Amparo Faustino e co-orientadora Dr. Graça Neves pois sem elas não seria possível a entrega desta tese. Gostaria também de agradecer ao Dr. Nuno Moura por ter despendido tempo para me ajudar com tudo o que precisei.
Não podia deixar de agradecer à minha família, nomeadamente aos meus pais por me terem aturado durante este ano, pelo esforço feito para a minha experiência Erasmus e porque sei que por vezes não dou o valor que eles merecem.
Também queria agradecer às minhas colegas de laboratório Kelly Castro e Letícia Costa, pela preocupação e pelo apoio.
Estes agradecimentos não podiam acabar sem agradecer aos meus amigos que me apoiaram e me aturaram durante este ano, em particular ao Vasco Batista, Daniela Machado, Carlos Silva, João Antunes, João Pereira, Emanuel Balsa, Patrícia Pescadinha, Leonardo Oliveira, Carolina Conceição, Pedro Reis, Cindy Rodrigues, Cristina Rodrigues, Alexandra Malta, Rafael Oliveira, Luís Bornes, Luís Alexandrino e Ana Guerrinha.

I would like to thank to my Erasmus friends: Flavio, Luís and Charlotte for being always there for me.
Finally, I would like to express my gratitude to professor Jacques Piette and Yvette Habraken for supporting me during my internship in their lab and helped me to develop this project. It was very important and made less hard the home/friends distance. I am very grateful for the way they received me in their lab and care for me, even when I was sick. This Erasmus experience would not be as much as enjoyable without you where I grew up as a professional and as individual. In their laboratory, I learned many new things that were very useful for me

palavras-chave

Macrociclos tetrapirrólicos, porfirinas regulares e *N*- confusas, porfirinas catiónicas, fotossensibilizador, terapia fotodinâmica, cancro, oxigénio singleto, células MCF-7, apoptose, necrose, necroptose, autofagia, splicing alternativo, *m*RNA

resumo

Neste trabalho é descrita a síntese de porfirinas regulares e *N*-confusas com o objetivo da realização de estudos acerca da sua eficiência como fotossensibilizadores (PSs) em terapia fotodinâmica (PDT) e a influência desta no *splicing* alternativo do mRNA. Os derivados porfirinicos foram preparados tendo como estrutura base a 5,10,15,20-tetraquis(1-metilpiridinio-4-il)porfirina.

Inicialmente irá ser realizada uma breve introdução sobre os macrociclos tetrapirrólicos, nomeadamente sobre porfirinas. Segue-se o capítulo 2 onde há a descrição sintética dos derivados porfirínicos usados neste trabalho. Desta forma, através das condições estabelecidas por Lindsey foram sintetizadas duas porfirinas: 5,10,15,20-tetraquis(4-bromometilfenil)-2-aza-21-carboporfirina e a 5,10,15,20-tetraquis(4-bromometilfenil)porfirina e procedendo-se à sua cationização com piridina que originou os derivados 5,10,15,20-tetraquis(4-(piridinio-1-il-metil)fenil)-2-aza-21-carboporfirina e 5,10,15,20-tetraquis(4-(piridinio-1-il-metil)fenil)porfirina. A formação das porfirinas neutras ocorreu com baixo rendimento, mas a sua cationização foi conseguida com rendimentos acima dos 80%. Neste mesmo capítulo ainda são apresentadas as caracterizações fotofísicas de todos os derivados porfirínicos, nomeadamente fluorescência e geração de oxigénio singleto. As porfirinas regulares foram aquelas que demonstraram bons rendimentos quânticos de fluorescência e capacidade para gerar oxigénio singleto em DMF.

No capítulo 3 são descritos todos os estudos biológicos realizados neste trabalho. Inicialmente foram realizados estudos de viabilidade celular em células MCF-7 e HeLa usando o teste com WST-1 e ATPlite^{TM} e como PS de referência a 5,10,15,20-tetraquis(1-metilpiridinio-4-il)porfirina. Foram realizados estudos de concentração (0.1 μM-5.0 μM) e tempo de irradiação (0, 5, 10 e 15 min).

A 5,10,15,20-tetraquis(4-(piridinio-1-il-metil)fenil)porfirina revelou ser o melhor PS, tendo sido selecionado um tempo de irradiação de 15 min e uma concentração até 5 μM para o estudos subsequentes. Os estudos de localização subcelular e *uptake* revelaram que a 5,10,15,20-tetraquis(4-(piridinio-1-il-metil)fenil)porfirina entra nas células mas não se localiza no núcleo como acontece com o controlo positivo. São ainda descritos estudos acerca do tipo de morte celular que as células podem sofrer depois da PDT com estes PSs. Por fim os estudos da influência da terapia fotodinâmica no *splicing* alternativo mostrou que a 5,10,15,20-tetraquis(4-(piridinio-1-il-metil)fenil)porfirina e a 5,10,15,20-tetraquis(1-metilpiridinio-4-il)porfirina parecem induzir um ligeiro *splicing* alternativo do mRNA.

keywords

Tetrapyrrolic macrocycles, regular and *N*-confused porphyrins, cationic porphyrins, photosensitizer, photodynamic therapy, cancer, singlet oxygen, MCF-7 cells, subcellular localization, apoptosis, necrosis, necroptosis, autophagy, alternative splicing, *m*RNA

abstract

In this work the synthesis of regular and *N*- confused porphyrins with the objective of assessing its efficiency as photosensitizers (PSs) in photodynamic therapy (PDT) and its influence in alternative splicing of mRNA is described. The porphyrin derivatives were prepared having as a template the 5,10,15,20-tetrakis(1-methylpyridynium-4-yl)porphyrin.

Initially, a brief introduction about tetrapyrrolic macrocycles, namely about porphyrins will be done. Then, chapter 2 will follow with the synthetic description of the porphyrin derivatives used in this work. Through Lindsey conditions, two porphyrins were synthesized: 5,10,15,20-tetrakis(4-bromomethylphenyl)-2-aza-21-carbaporphyrin; 5,10,15,20-tetrakis(4-bromomethylphenyl)porphyrin and then we proceeded to their cationization with pyridine to give: 5,10,15,20-tetrakis(4-(pyridynium-1-yl-methyl)phenyl)-2-aza-21-carbaporphyrin and 5,10,15,20-tetrakis(4-(pyridynium-1-yl-methyl)phenyl)porphyrin. The formation of the neutral porphyrins occurred with low yield but its cationization was achieved with yields higher than 80%. In the same chapter, the photophysical characterization of all porphyrins, namely singlet oxygen production and fluorescence quantum yield were described. The regular porphyrins demonstrated good fluorescence quantum yields and ability to generate singlet oxygen in DMF.

In chapter 3, all the biological assays done in this work are described. Initially, cellular viability studies were done in MCF-7 and HeLa cells using the WST-1 reagent and ATPlite^{TM} and as PSs reference the 5,10,15,20-tetrakis(1-methylpyridynium-4-yl)porphyrin. Studies of concentration (0.1 μM-5.0 μM) and irradiation time (0, 5, 10 and 15 min) were also done. The 5,10,15,20-tetrakis(4-(pyridynium-1-yl-methyl)phenyl)porphyrin showed to be the best PS and 15 min irradiation and a concentration up to 5 μM for the following studies were selected. The subcellular localization and uptake studies revealed that 5,10,15,20-tetrakis(4-(pyridynium-1-yl-methyl)phenyl)porphyrin can enter the cells but it is not localized in the nucleus, contrary to 5,10,15,20-tetrakis(1-methylpyridynium-4-yl)porphyrin. The studies regarding type of cell death that cells undergo after PDT treatment were also assessed. At last, the 5,10,15,20-tetrakis(4-(pyridynium-1-yl-methyl)phenyl)porphyrin and 5,10,15,20-tetrakis(1-methylpyridynium-4-yl)porphyrin seemed to induce a small alternative splicing of mRNA.

Index

Abbreviations xvii

CHAPTER 1 1

1.1 Tetrapyrrolic Macrocycles 3

1.1.1 General Remarks 3

1.1.2 Nomenclature of the tetrapyrrolic macrocycle 4

1.1.3 Physicochemical properties of porphyrin derivatives and *N*-confused porphyrins 5

1.1.4 Reactivity of the tetrapyrrolic macrocycles 9

1.1.5 Synthesis of porphyrinic macrocycles 11

1.1.6 Applications 17

1.1.7 Photodynamic process 17

1.2 PDT and alternative splicing 21

1.2.1 General background 21

1.2.1.1 Photodynamic therapy as a new alternative to cancer treatment 21

1.2.1.2 The photosensitizers 21

1.2.1.3 Subcellular localization 22

1.2.1.4 Effects of PDT and Immune Response 22

1.2.2 Cell Death: apoptosis, necrosis and autophagy 23

1.2.3 The alternative splicing process 25

1.2.4 Alternative splicing and cancer 26

1.3 Aim of Work 27

CHAPTER 2 29

2.1 N-Confused-porphyrin and porphyrin synthesis 31

2.1.1 General remarks 31

2.1.2 Synthesis of the precursors 5,10,15,20-tetrakis(4-bromomethylphenyl)-2-aza-21-carbaporphyrin and 5,10,15,20-tetrakis(4-bromomethylphenyl)porphyrin 33

2.1.3 Synthesis of 5,10,15,20-tetrakis(4-(pyridinium-1-yl-methyl)phenyl)porphyrin tetraiodide (6) and 5,10,15,20-tetrakis(4-(pyridinium-1-yl-methyl)phenyl)-2-aza-21-carbaporphyrin tetraiodide (2) 38

2.2 Photophysical Characterization 42

2.3 Material and methods 48

2.3.1 Chemicals and equipment 48

2.3.2 Synthesis of 4-bromomethylbenzaldehyde (4) 49

2.3.3 Synthesis of 5,10,15,20-tetrakis(4-bromomethylphenyl)-2-aza-21-carbaporphyrin (1) and 5,10,15,20-tetrakis(4-bromomethylphenyl)porphyrin (5) 50

2.3.4 Synthesis of 5,10,15,20-tetrakis(4-(pyridinium-1-yl-methyl)phenyl) porphyrin tetraiodide (6) 51

2.3.5 Synthesis of 5,10,15,20-tetrakis(4-(pyridinium-1-yl-methyl)phenyl)-2-aza-21-carbaporphyrin tetraiodide (2) 52

2.3.6 Irradiation conditions for $^1O_2$ generation 52

2.3.7 Singlet oxygen generation 53

CHAPTER 3 55

3.1 General remarks 57

3.2 Viability assays 57

3.2.1 Measurement of cell viability using the Cell Proliferation Reagent WST-1 57

3.2.1.1 Cell viability assay with WST-1 in HeLa Cells 58

3.2.1.2 Cell Viability assay with WST-1 in MCF-7 Cells 59

3.2.2 Cell viability assay using ATPlite^{TM} kit 64

4.2.2.1 Dose dependence assay 64

4.2.2.2 Time post-PDT dependence assay 66

3.2.3 Cell viability assay using Trypan Blue 67

3.3 Cellular uptake 70

3.4 Subcellular localization 72

3.5 Type of cell death induced by photodynamic therapy with porphyrin 6 and TMPyP 74

3.5.1 General background 74

3.5.2 General procedure to access type of cell death 76

3.5.3 Apoptosis and necroptosis pathway - the cleavage of PARP-1 77

3.5.4 Autophagy – Transformation of LC3-I into LC3-II 78

3.5.5 Necroptosis- Release of Cyclophilin A 79

3.6 Influence assessment of photodynamic therapy in alternative splicing of mRNA 80

3.7 Material and methods 86

3.7.1 Solutions and buffers 86

3.7.2 Statistical analysis 88

3.7.3 Eukaryotic cell line and cell culture 88

3.7.4 Photodynamic treatments 88

3.7.5 Light source 89

3.7.6 WST-1 assay 89

3.7.7 ATPlite^{TM} kit assay 89

3.7.8 Trypan Blue assay 90

3.7.9 Cellular uptake 90

3.7.10 Subcellular localization 90

3.7.11 The Western Blot Technique 91

3.7.12 Protein extraction 93

3.7.11.1 Harvest 93

3.7.11.2 Total Protein extraction 94

3.7.11.3 Protein Dosage 94

3.7.11.4 SDS-Page and Immuno-detection (Western Blotting) 94

3.7.13 Total RNA extraction 96

3.7.14 RNA dosage 96

3.7.15 Generation of cDNAs by reverse transcriptase and amplification by PCR . 96

3.7.16 Analysis on polyacrylamide gel 10%..... 99

CHAPTER 4..... 101

4. Conclusion and future outcomes. 103

5. References 107

Abbreviations

1,2 DBB	1,2-Dibenzoylbenzene
A	Absorbance
A.U	Arbitrary Units
A_0	Absorbance at time zero
AMZ2	Archaelysin family metallopeptidase 2
AS	Alternative splicing
ATF3	Activating Transcription Factor 3
ATP	Adenosine triphosphate
BSA	Bovine serum albumin
cDNA	Complementary DNA
cm^2	Square centimeter
CoASY	Coenzyme A synthase
CPT	Camptothecin
DDQ	2,3-Dichloro-5,6-dicyano-*p*-benzoquinone
DMEM	Dulbecco's Modified Eagle's medium
DMF	Dimethylformamide
DMSO	Dimethylsulfoxide
DNA	Deoxyribonucleic acid
DPiBF	Diphenylisobenzofuran
ESI	Electrospray ionization
FBS	Fetal bovine serum
H_2TPyNCPP	5,10,15,20-tetrakis(pyridyl-4-yl)-2-aza-21-carbaporphyrinn
H_2TPyTPP	5,10,15,20-tetrakis(pyridyl-4-yl) porphyrin
HMBC	Heteronuclear Multiple Bond Correlation spectroscopy
HRP	Horseradish peroxidase
HSP60	Heat Shock Proteins with 60 kDa
HSQC	Heteronuclear single quantum coherence spectroscopy
ISC	Intersystem crossing
IUPAC	International Union of Pure and Applied Chemistry
J	Coupling constant
LC3	Microtubule-associated protein 1A/1B-light chain 3

Ln	Napierian logarithm
m	Multiplet
m/z	mass/charge ratio
MCF-7	Human breast adenocarcinoma cell line
MDM2	Mouse double minute 2 homolog
min	minutes/minute
MMS	Methyl methanesulfonate
mRNA	Messenger ribonucleic acid
MSA	Methanesulfonic acid
mW	Milliwatts
NCP	*N*-Confused porphyrin
NCTPP	5,10,15,20-tetraphenyl-2-aza-21-carba-porphyrin
nm	nanometers
NMR	Nuclear magnetic resonance
PARP	Poly (ADP-ribose) polymerase
PBS	Phosphate-buffered saline
PCR	Polymerase chain reaction
PDT	Photodynamic therapy
ppm	Parts per million
PS	Photosensitizer
PVDF	Polyvinylidene fluoride
RBM4	RNA- binding protein 4
RNA	Ribonucleic acid
ROS	Reactive oxygen species
RT-PCR	Reverse transcriptase polymerase chain reaction
s	Singlet
s	Second/seconds
SDS-PAGE	Sodium dodecyl sulfate polyacrylamide gel electrophoresis
SRSF1	Serine/arginine-rich splicing factor 1

t	Triplet
TBST	Tris-buffered saline and Tween 20
TEMED	Tetramethylethylenediamine
TFA	Trifluoroacetic acid
THF	Tetrahydrofuran
TLC	Thin layer chromatography
TPP	5,10,15,20- tetraphenylporphyrin
UV-Vis	Ultraviolet-Visible
VEGF111	Vascular Endothelial Growth Factor-111
WST-1	Water soluble tetrazolium salt

CHAPTER 1

Introduction: Tetrapyrrolic Macrocycles: porphyrins, N-Confused Porphyrins and the alternative splicing process of mRNA and its correlation with cell death in cancer

1.1 Tetrapyrrolic Macrocycles

1.1.1 General Remarks

In general, the designation porphyrin is given to a family of compounds with intense colour formed by a nucleus of four units of pyrrole type joined by methinic bridges.[1] The designation porphyrin derives from the Greek term "*porphura*" which was used to describe the colour purple.

Porphyrins are also known as "the pigments of life" due to their important role in some biological processes like respiration, photosynthesis and electron transport.[2] In fact, the prostetic group of haemoproteins, as haemoglobin and myoglobin is a tetrapyrrolic macrocycle denominated *heme* group. This heterocyclic system coordinated with iron(II) by the four nitrogen atoms of the porphyrin core is able to bind reversibly to molecular oxygen and is responsible for the oxygen transportation and storage through the body (**Figure 1-A**).[3]

Chlorophylls are green pigments responsible for absorbing light and retain it in specific molecules.[4] This type of pigments has a porphyrin-type core similar to the heme group (**Figure 1-B**). However, instead of an iron ion, the inner core of the tetrapyrrolic macrocycle is coordinated with magnesium. Furthermore, one of the pyrrolic units in chlorophyll is reduced and the acid groups are esterified.[3]

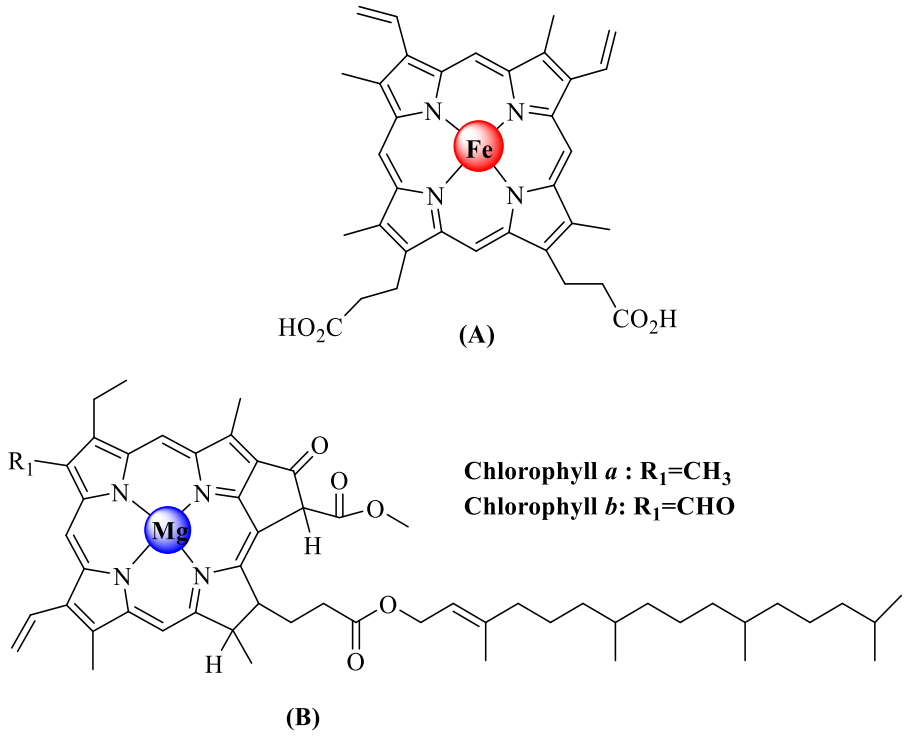

Figure 1. Structures of heme group (A) and chlorophylls (B).

Tetrapyrrolic macrocycles are also present in other biological systems like cytochromes, which are involved in electron transfer,[5] cellular energy production,[6] biosynthesis of steroids[7] and detoxification mechanisms.[8]

An important contribution for the development of this field is due to Hans Fisher who received the Nobel prize in Chemistry[9] in 1930 for his investigation in the composition of the *heme* group but mostly for its synthesis. He also reported the resemblance of the *heme* groups with the pigments responsible for the photosynthesis[3] and showed that these pigments have similar skeleton of porphyrins.[9]

1.1.2 Nomenclature of the tetrapyrrolic macrocycle

There are two types of nomenclature to indicate the name of porphyrins and analogues (**Figure 2**).[1,2] In the first one, due to H. Fischer, the pyrrole rings are denominated as A, B, C and D, the β-pyrrolic positions are numbered from 1 to 8 and the *meso*-positions are indicated by the Greek letters α, β, δ and γ. Posteriorly, IUPAC also created nomenclature rules for numerating this type of macrocycles, in which the numbers 5,10,15 and 20 correspond to the *meso* positions and the 2,3,7,8,12,13,17 and 18 ones are indicative of β-pyrrolic positions. In this work, the nomenclature used was the one proposed by IUPAC.

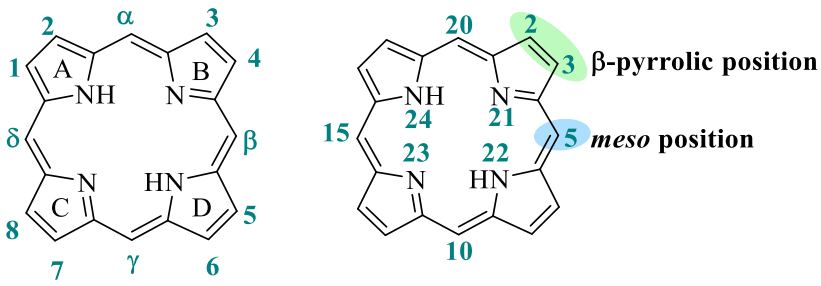

Figure 2. Nomenclature of tetrapyrrolic macrocycles proposed by Fischer and IUPAC, respectively

The tetrapyrrolic nucleus can also occur in chlorins, bacteriochlorins, corroles, calix[4]pyrroles, phtalocyanines among others. Additionally, there is a type of porphyrins 2-aza-21-carbaporphyrin called *N*-confused porphyrins (**NCP**), which will be also very relevant to the present work. So, in this chapter, some considerations about the unique characteristics of this type of porphyrins are made.

A *N*-confused porphyrin is an isomer of a "regular" porphyrin with an inverted pyrrole ring linked to the *meso* carbons through an α and β position.[10] This type of compounds can also be numbered according to IUPAC nomenclature as it is shown in **Figure 3**. It is important to highlight that in *N*-confused porphyrins the nitrogen in the inverted pyrrole ring is numbered as 2.

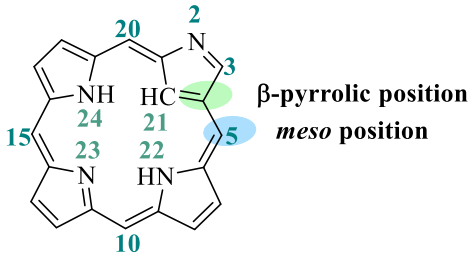

Figure 3. IUPAC recommendation to the *N*-confused porphyrinic core numeration.

1.1.3 Physicochemical properties of porphyrin derivatives and *N*-confused porphyrins

Porphyrins have 22 π electrons but only 18 of these are involved in electronic delocalization, in order to satisfy the Huckel's rule regarding aromaticity ($4n+2\pi$ electrons, n=4).[11] As it happens with porphyrins, *N*-confused porphyrins have 18 π electrons involved in delocalization and consequently are aromatic compounds.

Also, when the porphyrin nucleus is reduced losing one double bond in one of the β-pyrrolic positions, the new macrocycle designated by chlorin is still aromatic (**Figure 4-a**). The aromaticity is also maintained in derivatives known as bacteriochlorins with two opposite pyrrolic units reduced (**Figure 4-b**) and in isobacteriochlorins (**Figure 4-c**)where the reduction occurs in two contiguous pyrrolic units.[12,13]

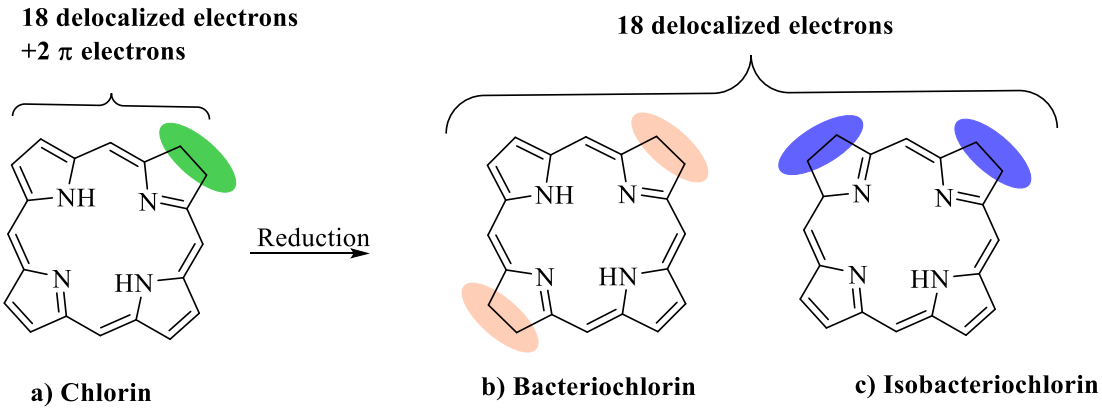

Figure 4. Structures of reduced macrocycles like chlorin (a), bacteriochlorin (b) and isobacteriochlorin (c).

Porphyrins and their derivatives can lose two internal protons and form complexes with the majority of metals in the periodic table, especially copper(II), zinc(II), iron(III), magnesium(II) and nickel(II). Tetrapyrrolic macrocycles, which do not appear coordinated with any metal, are usually denominated as *free-bases*.[14]

Porphyrins and their derivatives have unique absorption spectra. This type of macrocycles has in general a strong band around 400 nm denominated *Soret* band and several bands with lower intensity at 500-650 nm named Q bands.[11,15] In the UV-Vis spectrum, the appearance of the Soret band is due to the delocalization of π electrons of the macrocycle; so this band appears also in chlorins, bacteriochlorins and isobacterochlorins although with different intensities.[2,15]

Free-base porphyrins have four Q bands with increasing wavelength denoted as I, II, III and IV (**Figure *5***). The intensity ratio of the absorption bands in the porphyrins spectra depends on their structure. For example, when the relative intensities of these bands are in the order IV>III>II>I, the spectrum is called ethio-type (**Figure 5 - a).**

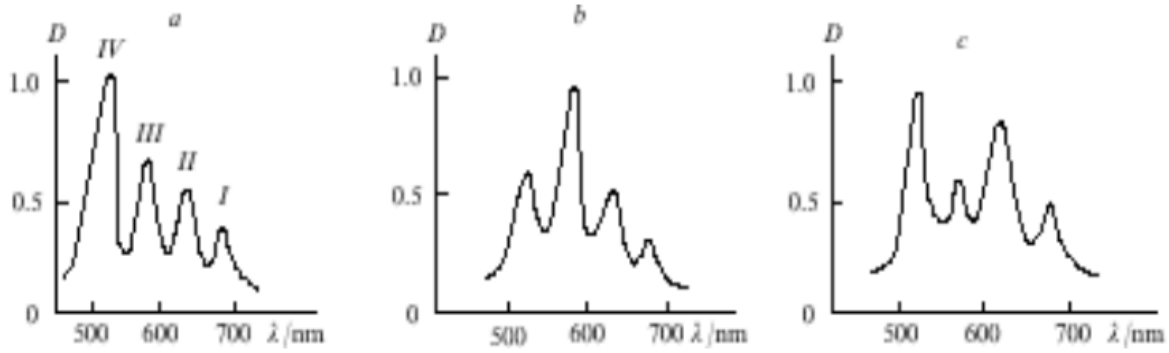

Figure 5. Ethio (a), rhodo (b) and phylo (c)-type UV-Vis spectrum.[16]

In porphyrins with a rhodo-type spectrum the relative intensity of Q bands follows the sequence III>IV>II>I (**Figure 5 b**), and in the ones with phyllo-type spectrum the sequence is IV>II>III>I (**Figure 5 c)**.[16] As it can be seen in **Figure 6**, the UV-Vis spectrum of a chlorin has also four Q bands. Comparatively to porphyrins, the band I which is centred at 650 nm is much more intense. Bacteriochlorins have one strong absorption band I between 700-750 nm. Isobacteriochlorins, in turn, have three Q bands with an increasing intensity from 500 to 600 nm. In general, the UV-Vis spectra of metalloporphyrins show only two Q bands due to the symmetry induced by the metal ion in the macrocycle core.[2,11] These variations in position and intensity of the Q bands allow the distinction of reduced derivatives and if the macrocycle is coordinated or not with a metal in the inner core.[17]

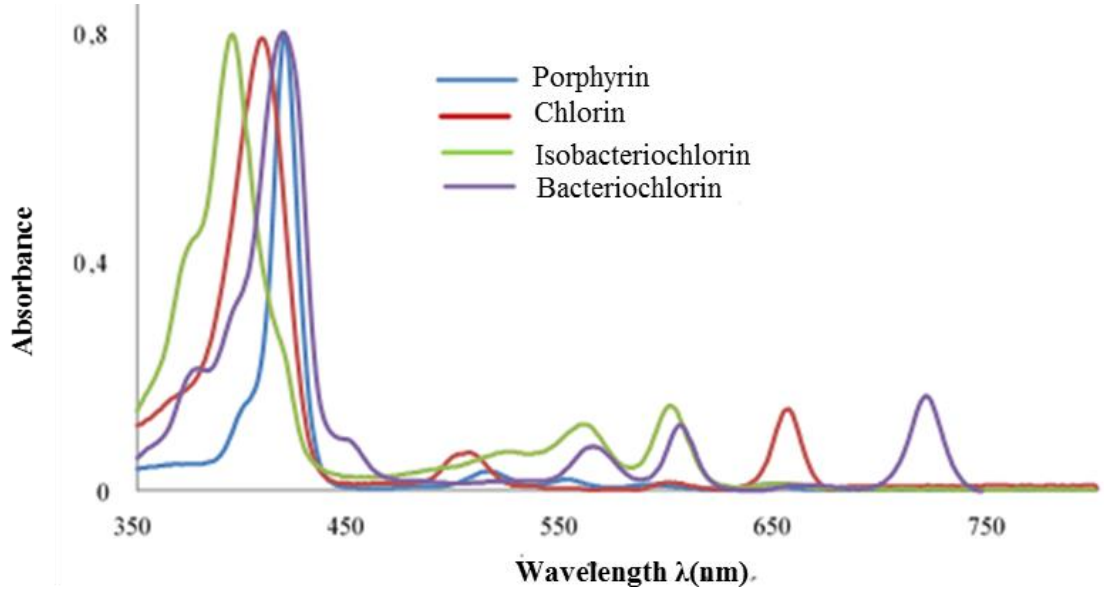

Figure 6. UV-Vis spectra in CH_2Cl_2 regarding a *meso*-substituted porphyrin and the corresponding reduced analogues bacteriochlorin, isobacteriochlorin and chlorin.

The UV-Vis spectrum of a *N*-confused porphyrin in CH_2Cl_2 shows a red-shifted for the whole bands due to the macrocycle distortion from planarity. In the *N*-confused derivatives, the last band (band I) that appears at 725 nm is much more intense than the band I in porphyrins at 650 nm. In **Figure 7** is shown the spectra of 5,10,15,20-tetraphenylporphyrin (**TPP**) and of the corresponding *N*-confused porphyrin, the 5,10,15, 20-tetraphenyl-2-aza-21-carbaporphyrin (**NCTPP**) where these features are patent.

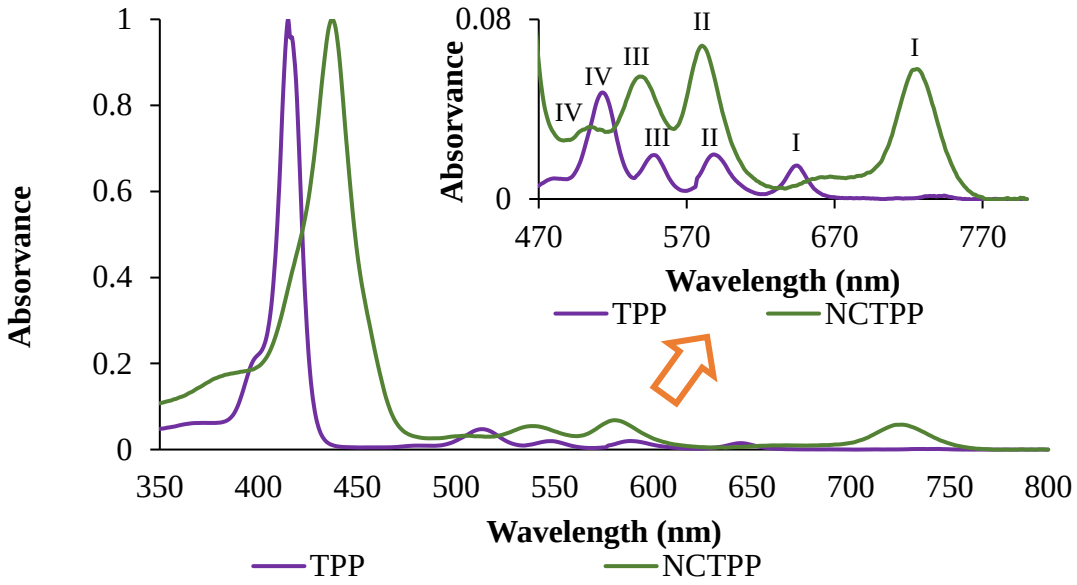

Figure 7. UV-Vis spectra in CH_2Cl_2 of 5,10,15,20-tetraphenylporphyrin (TPP) and of 2-aza-5,10,15,20-tetraphenyl-21-carbaporphyrin (NCTPP).

As it can be seen in the spectra, the Q bands of **NCTPP** are distorted because band I becomes more intense than the band III and IV. It is important to highlight that when a substituent is introduced in the *para* positions of the phenyl moiety, the spectrum undergoes a red-shifted delocalization.[16]

Another important technique that allows structural identification of these compounds is the Nuclear Magnetic Resonance (NMR). For *meso*-arylporphyrins, the signals corresponding to the resonance of the β-pyrrolic protons appear between δ 8-9 ppm and the signals corresponding to the resonance of the inner *N*-H appear at high field, between δ -2 and -4 ppm.[11,18] These chemical shifts are due to an anisotropic effect, caused by the electronic flow originated by π delocalized electrons, which protects the protons inside the ring and unprotects the ones outside it.[18] Additionally, in case of *meso*-unsubstituted porphyrins the signals generated by the resonance of the *meso* protons appear at δ 10 ppm. As mentioned earlier, the saturation of β-pyrrolic bonds does not affect the aromaticity of the macrocycle but this reduction of peripheral double bonds leads to a decrease in the ring current. This is demonstrated by the upfield shift of peripheral proton signals and a down field shift of the *N*-H signals. This decrease is moderate in chlorins and bacteriochlorins but highly noted in isobacteriochlorins.[11]

Regarding *N*-confused porphyrins, the ^{1}H NMR of this type of compounds has characteristic signals in the high field region at δ -2.5 ppm for inner *N*H's and at δ -5.1 ppm

corresponding to the inner CH.[10,19] The β-pyrrolic protons give rise to several signals due to the asymmetry caused by the inverted pyrrole ring.

N-confused porphyrins have three inner core nitrogens and one peripheral. Given its asymmetric structure, six *N*H-tautomers can be formed. They can be separated into type-A and type B-tautomers. Type A possess [18] annulenic circuits and show strong aromaticity isomers. However, when the outer nitrogen is protonated the type-B tautomers are accomplished where the [18]annulenic circuits do not exist and the aromaticity is only moderate (**Scheme 1)**.[20,21]

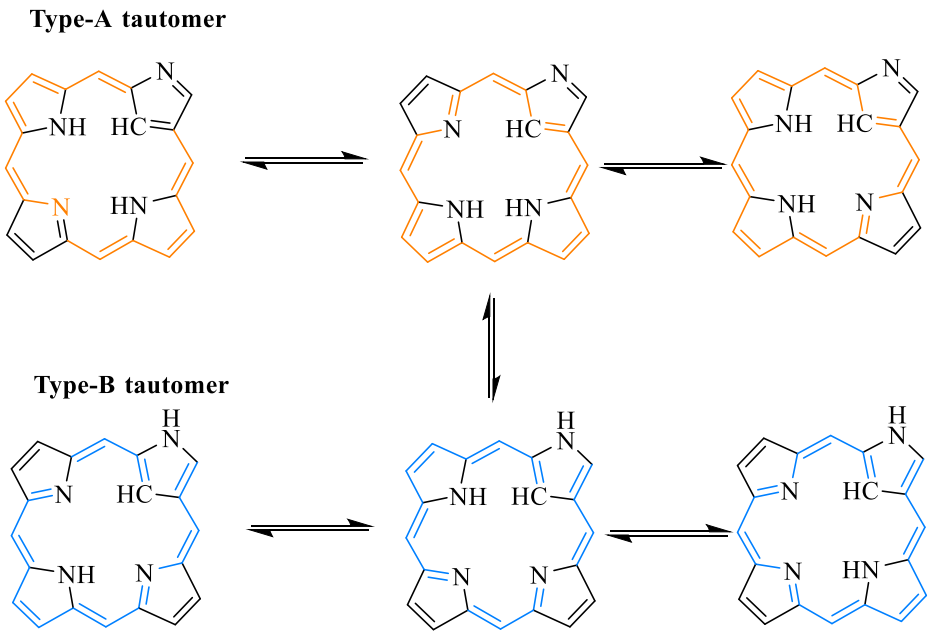

Scheme 1. *N*H. -tautomerism of *N*-confused porphyrins.

Another important feature of the tetrapyrrolic macrocycles are their solubility in organic solvents and their insolubility in water. However, the solubility in organic solvents depends on the substituents present in the pyrrolic rings, *meso* positions or in the macrocycle inner core coordination.[23]

1.1.4 Reactivity of the tetrapyrrolic macrocycles

Macrocycles may undergo some reactions either in the inner core or on the peripheral positions of the macrocycle.[2,11,18] Reactions that occur in the inner core of the ring can involve *N*-alkylation processes[23] or acid-base type reactions (**Scheme 2**). For instance, strong

induce the deprotonation of the inner *N*H leading to anionic species (P^{2-}-**Scheme 2**). These anions can suffer further alkylation. In addition, the formation of cationic species comes from the protonation of the other nitrogens in the presence of acids (PH_3^+ and PH_4^{2+}-**Scheme 2**).[24]

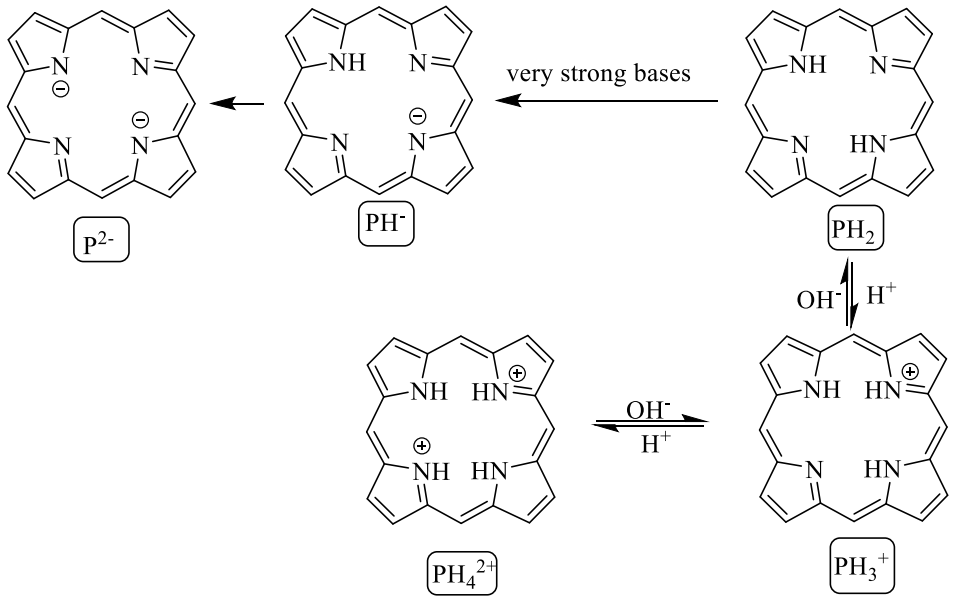

Scheme 2. Acid-base reactions that occur in the inner *N*H of porphyrin core.

In the macrocycle's inner core of the ring complexation with metallic ions can also occur. These reactions have great importance because either the absence or the presence of a metallic ion in the inner core can determinate the reactivity of the macrocycle. These metallic atoms can also protect the inner nitrogen atoms from nucleophilic attacks or protonation.[2,18]

As well as aromatic hydrocarbons, porphyrins can suffer electrophilic aromatic substitution reactions namely formylation,[25] halogenation,[26] nitration,[27] sulfonation,[28] alkylation[29] and acylation.[30] The reactions mentioned can occur in the *meso* and/or in the β-pyrrolic positions.[31,32]

N-confused porphyrins have a peripheral nitrogen atom which has less steric constraint, and it is much more nucleophilic than the interior nitrogen atoms; for that reason this nitrogen atom can be alkylated.[33] Furthermore, *N*-confused porphyrins can undergo complexation with metals, alkylation in the inner carbon of the inverted pyrrole ring and acid-base reactions.[34] Some common reactions which can be accomplished with *N*-confused

porphyrins are present in **Figure 8**. Regarding complexation, it can bind with many metallic ions but **Figure 8** only shows the most common ones.

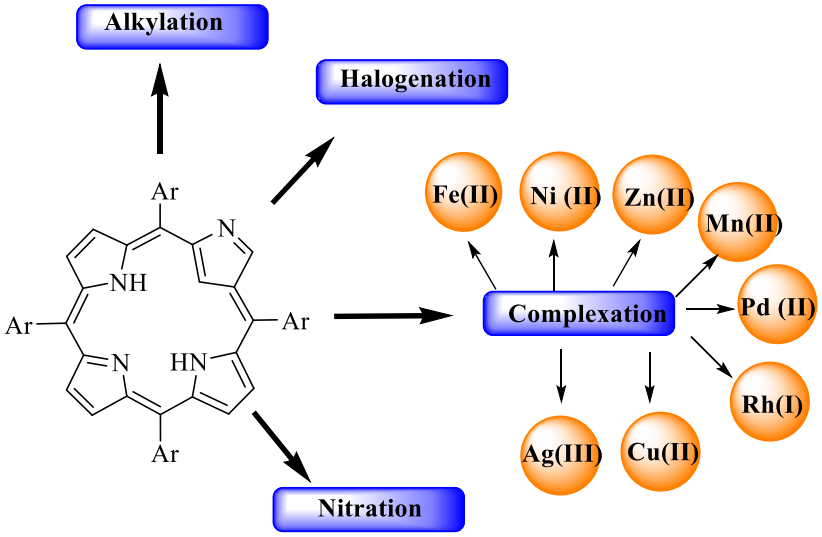

Figure 8. Possible reactions for *N*-Confused Porphyrins.[35–42]

It is important to highlight that when complexing to palladium, it was reported that when this complexation is done with the outer nitrogen, dimers can be formed.[39] Moreover, the complexation can also occur with the inner nitrogen. Regarding some other metallic ions, the complexation can occur in the outer nitrogen as well.[36,40]

1.1.5 Synthesis of porphyrinic macrocycles

In the past century, there were several research groups that studied and developed synthetic methods to prepare selectively *meso*-tetraarylporphyrins, corrole, cálix [4] pyrrole, phthalocyanines, expanded porphyrins like saphyrins and hexaphyrins and *N*-confused porphyrins (**Figure 9**).

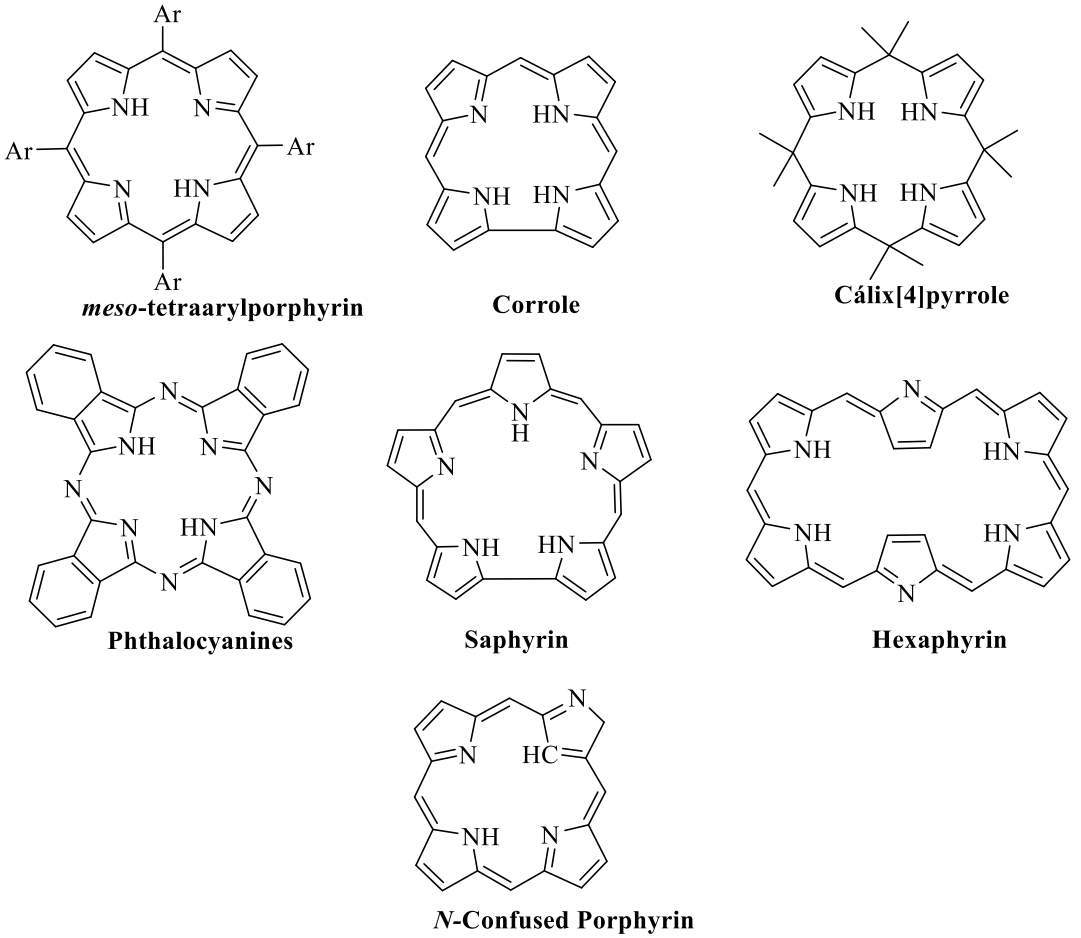

Figure 9. Structures of some macrocycle derivatives.

The synthesis of porphyrins derivatives can occur by several distinct pathways: through pyrrole intermediates, by introducing modifications in natural pigments or in pre-synthesized porphyrins. In this chapter, it will be discussed the synthesis of 5,10,15,20-tetraarylporphyrins and also of *N*-confused porphyrins since in this work it will be developed either "regular" and *N*-confused porphyrins. There are many synthetic approaches regarding *meso*-substituted porphyrins preparation, being the condensation between a pyrrole and an aldehyde the most common method.

The first synthetic route used to prepare *meso*-tetrasubstituted porphyrins was described by Rothemund in 1936 and it consisted in the condensation between pyrrole and aldehydes (**Scheme 3**). In his work, he could prepare 5,10,15,20-tetramethylporphyrin and porphine from the reaction of pyrrole with gaseous acetaldehyde and gaseous formaldehyde, respectively, in pyridine. The two reactional mixtures were heated in sealed tubes at 90-95ºC for 30 h under anaerobic conditions affording after this time the expected macrocycles.[43]

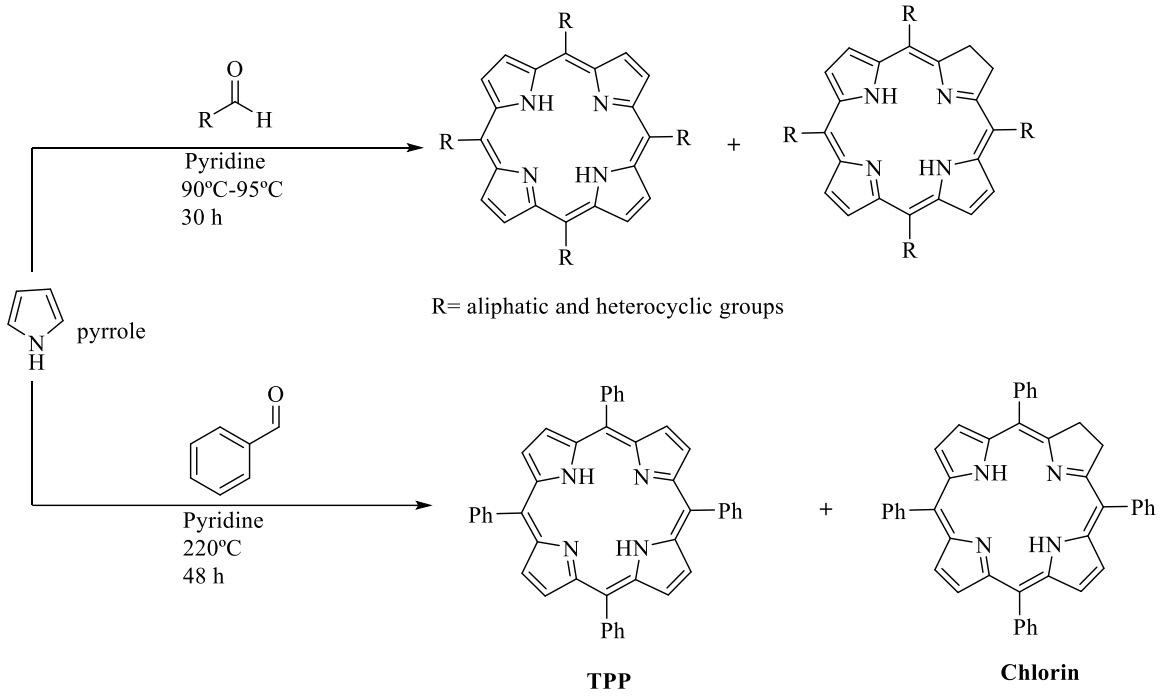

Scheme 3. Preparation of *meso*-tetrasubstituted porphyrins according to Rothemund conditions.

After testing more than 25 aldehydes (aliphatic, aromatic and heterocyclic ones) with optimized conditions,[44] Rothemund prepared and isolated **TPP** through condensation of pyrrole and benzaldehyde in pyridine at 220ºC for 48 h **(Scheme 3)**. The porphyrin yield of this reaction was about 5% and it was contaminated with the correspondent chlorin. This contamination could vary depending on temperature and reactants concentration. However, the conclusions of Rothemund studies also showed that by adding the adequate agents like $PbCrO_4$ or a mixture of calcium carbonate and magnesium oxide, the reaction yield could be increased.[45]

After the method proposed by Rothemund, in 1964 Alder and Longo suggested new conditions for preparation of *meso*-arylporphyrins (**Scheme 4**). The authors studied several reaction conditions such as solvents, absence or presence of salts and temperature range in order to optimize the reaction conditions in order to produce the desired porphyrins.[46]

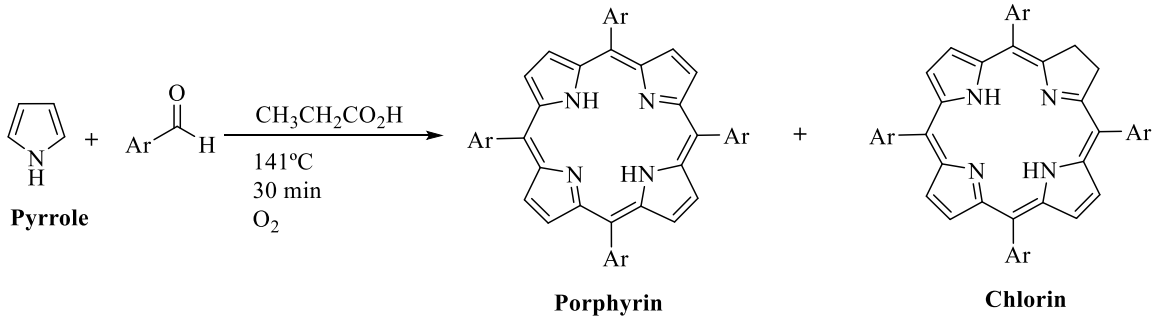

Scheme 4. The best Adler-Longo conditions to prepare *meso*-arylporphyrins.

The best conditions founded by these authors consisted in the reaction of pyrrole with the adequate aldehyde and refluxing it with propionic acid for 30 min at open air. Using these conditions, Adler and Longo synthetized **TPP** in 20% yield in a fast and reproducible way.[47] This method is efficient to prepare porphyrins in a multi-gram scale due to the fact that porphyrins precipitate in the reactional mixture.[47] However, this method has its own disadvantages such as the contamination with the corresponding chlorin[48] and the impossibility of using aldehydes with functional groups sensible to acidic media.[47]

The conditions established by Alder-Longo are also used to synthetize asymmetric porphyrins. In this case, the stoichiometric amounts of the aldehydes must be adjusted to favour the formation of the desired derivative.[47]

In order to prepare this type of macrocycles there is another approach developed by Rocha Gonsalves and later by Lindsey and co-workers. This method is based in three basic assumptions.[49,50]

I) Pyrrole and aldehyde are very reactive species

II) The formation of porphyrinogen, which is an intermediate without aromatic character, is thermodynamically favourable when the reaction between aldehyde and pyrrole occur in appropriate conditions;

III) In order to reach equilibrium, the reaction conditions must be suitable for a wide variety of aldehydes.

In 1985 Rocha Gonsalves proposed a method where the formation of porphyrinogen occurred through condensation of pyrrole and an aliphatic aldehyde in CCl_4 with the presence of trifluoroacetic acid (TFA) at 60ºC and where the oxidation was achieved by adding 2,3-dichloro-5,6-dicyano-1,4-benzoquinone (DDQ) or *p*-chloranil.[49] After almost 6 years, Rocha Gonsalves and his collaborators proposed another method where the

condensation of pyrrole and aldehyde were done in refluxing acetic or propionic acid and in the presence of nitrobenzene for 1 h. These oxidative conditions solved the problem of porphyrins being contaminated with the correspondent chlorin.[51]

In the Lindsey methodology (**Scheme 5**), the first step consisted in the condensation of pyrrole and aldehyde in dry CH_2Cl_2 in the presence of an acid catalyst (BF_3, TFA or BCl_3) at room temperature under nitrogen atmosphere and protected by light for 30-60 min. The second step involved the oxidation of porphyrinogen by adding an oxidant agent, like DDQ or *p*-chloranil, resulting in the correspondent porphyrin. With these conditions, **TPP** is obtained with an yield of 20%.[52]

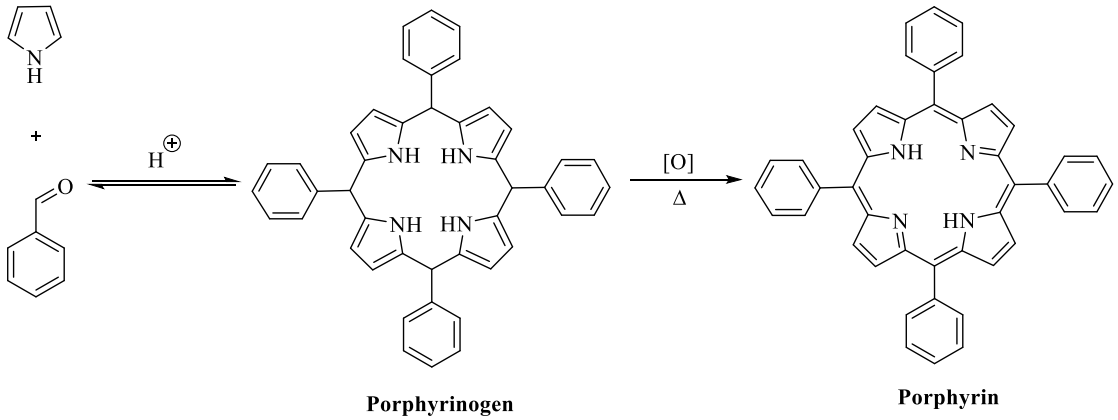

Scheme 5. Lindsey method for synthesis of 5,10,15,20-tetraphenylporphyrin (TPP).

Although the Lindsey method allowed the synthesis of porphyrins with good yields from sensible aldehydes in acidic conditions, the reaction requires an elevated dilution, which implicates large volumes of solvent. Therefore, this method becomes less viable when synthetizing in a high scale. Furthermore, the utilization of high quantities of oxidizing agents leads to an inviable reaction purification.[53]

The synthesis of *N*-confused porphyrin can be accomplished by methodologies which are similar to the ones described for porphyrins:

a) Condensation of pyrrole and aldehyde[54,55]
b) Condensation of "building-blocks"[56,57]

Given that in this work all porphyrins derivatives were synthetized by condensation between pyrrole and aldehyde, only this methodology will be emphasized.

The first studies involving *N*-confused porphyrins were reported in an independent way by Furuta[10] and Latos-Granzinsky[58] in 1994 (**Scheme 6**). In both cases, the method used to synthetize *N*-confused tetraarylporphyrin was an adaptation of the Lindsey methodology

to prepare porphyrins. That methodology consisted in the condensation between a pyrrole and the adequate aldehyde under catalytic acidic conditions followed by an oxidation step. Furuta selected HBr as the acid catalyst while Latos-Granzynski selected $BF_3.Et_2O$, but in both cases *p*-chloranil was used as the oxidizing agent. In these reactions the *N*-confused porphyrin was obtained with a yield of 5% and it was considered a by-product of the regular porphyrin synthesis.[58]

In 1999, Lindsey described the preparation of NCTPP using as catalyst $BF_3.Et_2O$ or TFA and DDQ as oxidizing agent.[54] Later, Lindsey did the same reaction using methanesulfonic acid (MSA) as catalyst (**Scheme 6**). With this modification, Lindsey obtained a much better yield (39%) comparatively with all methods described until then but still obtained **TPP** (5% yield) as a by-product.[55] This reactional conditions are the basis for preparing the *N*-confused porphyrin in the present work (**Scheme 6,** condition 4).

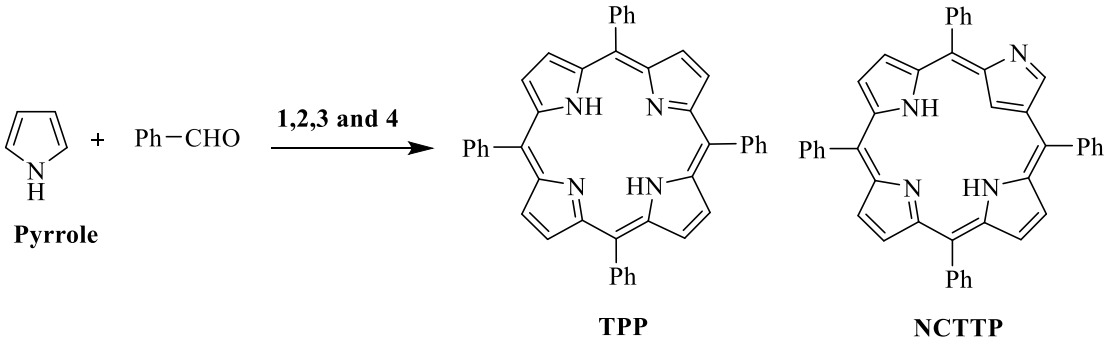

1- a). HBr, 48 h room temperature; b) *p*-chloranil
2- a) CH_2Cl_2, BF_3OEt_2, room temperature; b) *p*-chloranil
3- a) CH_2Cl_2 , BF_3OEt_2 or TFA room temperature; b) DDQ
4- a) CH_2Cl_2, MSA, room temperature; 30 min b) DDQ 5 min

Scheme 6. Synthesis of NCTPP according to Furuta (1), Latos-Granzynski (2) and Lindsey(3 and 4).[10,54,55,58]

The literature yields of the *N*-confused porphyrin obtained from the condensation of pyrrole with benzaldehyde under different reaction conditions discussed above are summarized in **Table 1**

Table 1. Reactional conditions for synthesizing *N*-confused porphyrins and their respective yields.

Reactional conditions	Yield	
	TPP	**NCTPP**
1-a). HBr, 48 h room temperature; b) *p*-chloranil	20%	5-7%
2-a) CH_2Cl_2, BF_3OEt_2, room temperature; b) *p*-chloranil		4% (less than 1% of the crude)
3-a) CH_2Cl_2, BF_3OEt_2 or TFA room temperature; b) **DDQ**	32%	7.5%
4-a) CH_2Cl_2, **MSA**, room temperature; 30 min b) **DDQ** 5 min	5%	39%

1.1.6 Applications

Tetrapyrrolic macrocycles are present in many forms in Nature with important roles as it was already mentioned before. Due to their biological, photophysical and photochemical properties, tetrapyrrolic macrocycles can also be applied in areas such as catalysis,[59] artificial oxygen transporter,[60] biomimetic models,[61] sensors,[62] semiconductors and superconductors.[63] However, Medicine is the most relevant area where this type of compounds is being used, namely in photodynamic therapy (PDT)[64] and in diagnostic field.[65]

Nowadays tetrapyrrolic macrocycles are also being considered as intercalating agents of desoxyribonucleic acid (DNA).[66] It is known that some DNA damaging agents (neoplastic therapeutic drugs) can affect alternative splicing (AS) as it will be shown later.[67]

1.1.7 Photodynamic process

Nowadays, cancer is one of the main causes of death in the world. Despite of numerous existing treatment, there are many secondary effects and disadvantages associated with it and sometimes these treatments do not even work. Therefore, it is required to find different and more efficient approaches. Porphyrins and their derivatives shown a photosensitizing ability in photodynamic therapy (PDT), making these macrocycles suitable candidates for this type of cancer therapy.[68–70]

PDT requires the combination of three different components: a photosensitizer (PS), light and molecular oxygen. The association of these components allows the generation of highly reactive oxygen species (**ROS**) which when in contact with cells can induce cell death or cause cell damage.[64] One of those **ROS** species is singlet oxygen $^1O_2$. (**Figure 10**) Therefore, the efficiency of the photodynamic process is dependent on the presence of molecular oxygen and on the way that the PS transfers the energy from its triplet state to O_2 in fundamental triplet energy state.

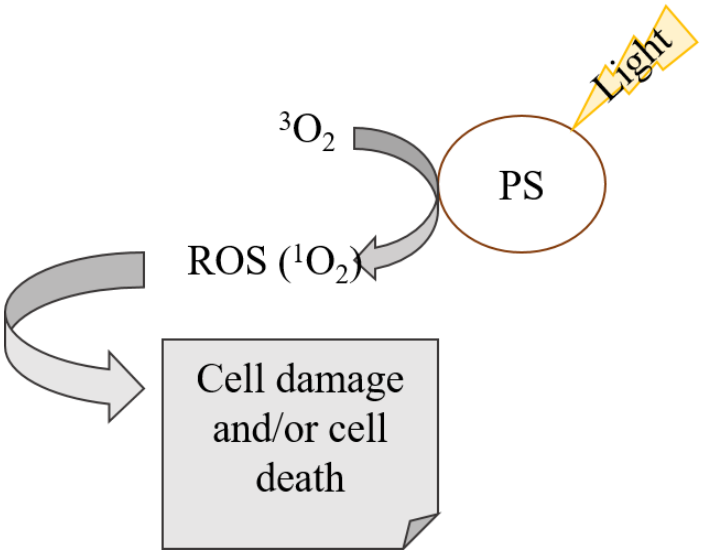

Figure 10. Principle of the photodynamic therapy (PDT) process.

The mechanism involved in PDT process can be explained by using a modified Jablonski's diagram (**Figure 11**). This illustrates the several transitions that an electron can suffer after light absorption and transition to an excited state.

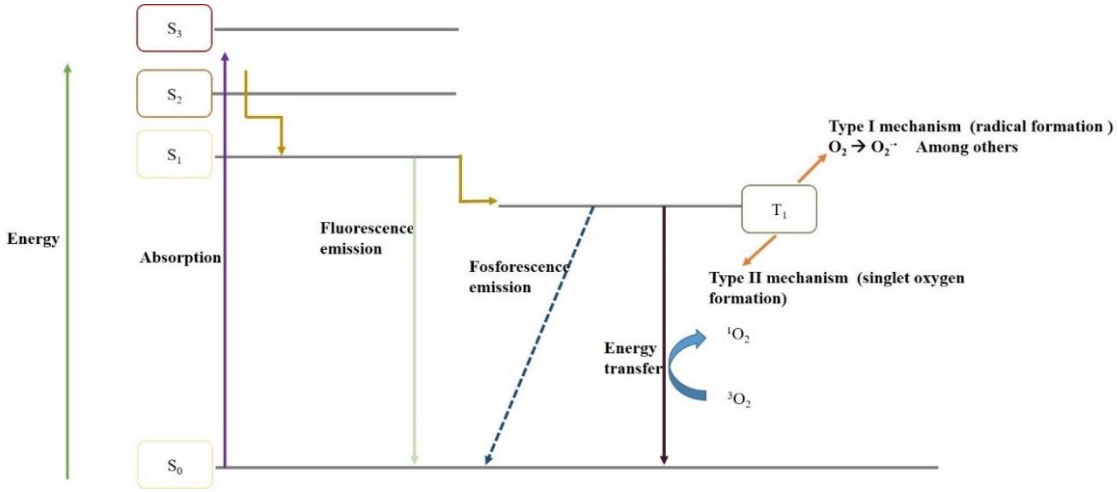

Figure 11. Modified Jablonski's diagram.

When a photosensitizer is irradiated with light, it is excited and transits from a fundamental state (S_0) to a more excited singlet state (S_2 or S_3). This excited molecule has a short lifetime.[71]

The PS transits to an excited singlet state with lower energy (S_1) through internal conversion processes.[72] After some nanoseconds this excited state tends to return to the ground state (S_0). This transition can be done through three different processes:

- Radiative decay with light emission, namely fluorescence emission with wavelength higher than the absorbed radiation.[71]
- Non-radiative decay with release of heat.[72,73]
- By intersystem crossing (ISC) where a spin inversion of the electron occurs. This inversion is quantum forbidden and the PS is transformed into an excited triplet state (T_1). The decay to S_0 can occur with phosphorescence emission and spin inversion again. However, being this transition forbidden, the photosensitizer reveals long lifetimes which allows the interaction with other molecules.[12,71]

So, a good photosensitizer is the one that suffers intersystem crossing (ISC) with high efficiency. Given the long lifetime of the exited triplet state, this can interact with close molecules through two types of mechanism: type I and type II.

Type I mechanism

In this mechanism, the abstraction of a hydrogen atom or the electron transference between the photosensitizer and a biological substrate is involved and it results in the formation of free radicals.[18,71,73]

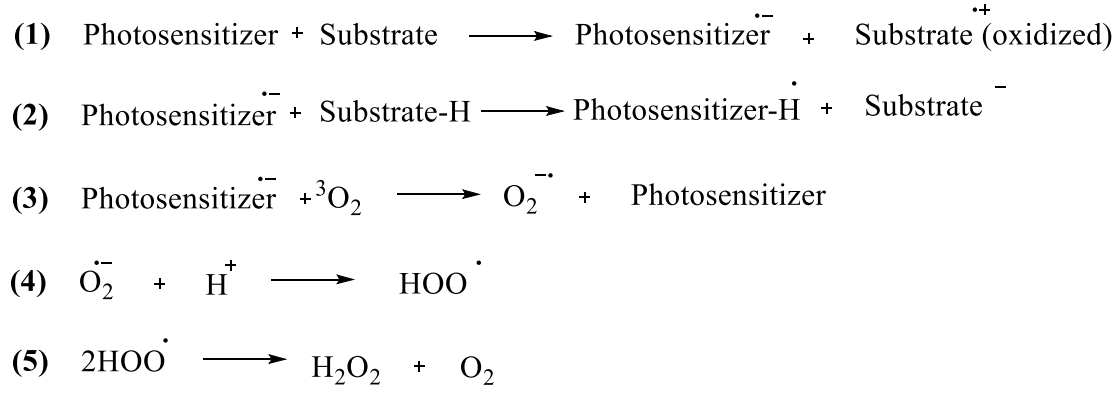

Scheme 7. Type I mechanism reactions.

The anionic photosensitizer can react with the molecular oxygen O_2 and generate the superoxide anion ($O_2^{\cdot-}$).[34,71,74] The superoxide anion radical is not particularly reactive in biological systems but when protonated (**Scheme 7- (4)**) can produce hydrogen peroxide and molecular oxygen (**Scheme 7-(5)**) or highly reactive hydroxyl radicals. This hydrogen peroxide is highly toxic and can be removed by catalases.[71]

Type II mechanism

This type of mechanism is less complex and involves the formation of a reduced number of products when compared with the previous mechanism. In mechanism type II, the photosensitizer in its triplet state can transfer the energy in excess to the molecular oxygen in the ground state ($^3O_2$), relaxing to its ground state and producing singlet oxygen ($^1O_2$).[71]

The $^1O_2$ is a high reactive oxygen species and despite of its short lifetime in the biological systems, it is considered the principle mediator of photochemical damage caused to cells by several photosensitizers. This $^1O_2$ can interact with several enzymes leading to the inhibition of protein synthesis and modification of several DNA chains. This change leads to an alteration in the transcription and the replication process which can lead to cell death. Even the unsaturated lipids can be a target to this triplet oxygen.[71]

There are several authors reporting photodynamic effect using tetrapyrrolic macrocycles[68,75,76], being the most interesting to this work the 5,10,15,20-tetrakis(1-methylpyridinium-4-yl)porphyrin **TMPyP**.[69,77,78]

1.2 PDT and alternative splicing

1.2.1 General background

1.2.1.1 Photodynamic therapy as a new alternative to cancer treatment

Photodynamic therapy is a clinically approved therapy which overlap to the orthodox ones for being minimally invasive and targeting only the malignant cells. It is used successfully for neoplastic and non-malignant diseases.[79]

As it was said before, PDT consists of three essential components: PS, light and oxygen.[64] The combination of these components can generate singlet oxygen that it is toxic to the cells and can cause their death through apoptosis, necrosis or autophagy. PDT involves two steps: administration of a light sensitive PS and the irradiation of the tumour location by light with appropriate wavelength. The main characteristic of photosensitizers in PDT is its high selectivity to localize in a neoplasm instead of the healthy cells. This can also be a disadvantage because this treatment cannot be applied to metastatic lesions which is the most frequent cause of death in cancer patients. It is important that the PS do not accumulate in the cell nucleus, leading to resistant clones or by limiting DNA damage that can be carcinogenic.[64,79]

PDT has been recently used to treat several types of cancer such as skin tumours, digestive system tumours, prostate cancer and brain tumours. [64]

1.2.1.2 The photosensitizers

There are several main characteristics that made certain compounds suitable for PS in PDT. A PS should be stable in storage and not have dark toxicity, having a rapid pharmacokinetic elimination.[80] These compounds have to ideally absorb light in the red or far-red in order to penetrate the tissues. The high absorption peak must be between 600 and 800 nm because if it is longer than 800 nm, there is not enough energy to excite the molecular oxygen to its singlet state.[64] The PS should not aggregate under biological conditions

because it diminishes its capacity of absorbing light and consequently its photochemical efficiency to generate singlet oxygen.[80]

It is important to highlight that the synthesis of the desirable PS should be cheap, easy and the starting materials available to make large-scale production or in some cases the PS can be commercial available. It is better for the photosensitizers to be water-soluble because they can easily travel in the body. When insoluble in water, the PS should be incorporated in liposomes or in an emulsion.[64,80,81]

There are many photosensitizers used in PDT. Among them there are the ones with tetrapyrrolic core [80] such as chlorins,[81] phtalocyanines and porphyrins.[82] The first and the most widely used photosensitizer employed in cancer was a mixture of porphyrins called purified hematoporphyrin derivative, usually known as Photofrin®.[64] This shows that tetrapyrrolic macrocycles are very studied for PDT application and that porphyrins derivatives can be promising as PS.

1.2.1.3 Subcellular localization

The precise cellular localization of a PS is very important because ROS act close to its site generation and depending on the location, there is a difference in the damage caused to the cell. So, the study of the PS localization is useful in order to select the correct PS according to the desired application. There are several structural characteristics that determine the intracellular distribution such as the net ionic charge (can vary from -4 to +4), the degree of asymmetry of the molecule and the degree of hydrophobicity.

The easiest way to detect the intracellular location of a PS is by confocal laser scanning fluorescence microscopy. This technique is more sensible and has a better special resolution than non-confocal techniques.[80,83,84]

1.2.1.4 Effects of PDT and Immune Response

PDT causes, sometimes, a strong acute inflammatory reaction at the target site which is triggered by the oxidative stress induced by PDT. The tumour vasculature is changed and the inflammatory cells (neutrophils/macrophages followed by mast cells and monocytes/macrophages) rapidly invade tumours going through PDT. The damage in the

treated tumour makes its vasculature to block the tumour tissue preventing it from spreading the disrupted homeostasis until these cells are eliminated by the white cells. It was shown that if these blood cells were depleted, the effect of PDT is diminished.[64]

1.2.2 Cell Death: apoptosis, necrosis and autophagy

PDT can induce three different pathways of cell death: apoptosis, necrosis and autophagy. The first is the most found in cells which underwent PDT. However, if the cells have deficient caspases (see later), the cells undergo necrosis. On the other hand, it was reported recently that the cells can undergo autophagy to preserve cell viability after photodynamic injury.[64]

Necrosis

This type of death results from enzymatic digestion of the injured cells. The membrane integrity is often affected and the necrotic cell contents leak out. The enzymes which digest these cells are derived from its lysosomes or from the white cells' lysosomes that take part in the inflammatory reaction.[85]

This type of cell death is often observed due to a response to severe stress as physical injury or long periods of ischemia (reduced blood flow which leads to a decrease in oxygen and nutrients). It was thought that necrosis was not a regulated process. However, there are evidence that this type of cell can be regulated (in that case called necroptosis), occurring as an alternative to apoptosis.[86]

Necroptosis

This type of death is known to be the regulated necrosis and it occurs often in cells in which the normal apoptotic pathway is blocked or deficient. Necroptosis is often associated with depletion of ATP which can lead to an increase in Ca^{2+} concentration which, in turn, can induce the activation of calpains (protease). These enzymes can lead to lysosomal rupture and release of another enzymes that can destruct the cells.[86,87]

Apoptosis

Apoptosis (**Figure 12**) is a type of programmed cell death with a tightly regulated pathway in which cells that are designated to die activate enzymes that degrades its own DNA and proteins. The apoptotic cells become apoptotic bodies that contain pieces of the cytoplasm and nucleus after disrupting into fragments. However, the plasma membrane stays intact but its structure is altered in a way that they become easy targets for phagocytes. These changings can include the movement of some phospholipids from the internal to the external membrane surface, where they are identified by phagocytes' receptors. Besides this change, there is DNA breakdown and activation caspases, essential enzymes to the apoptotic pathway.[85,86]

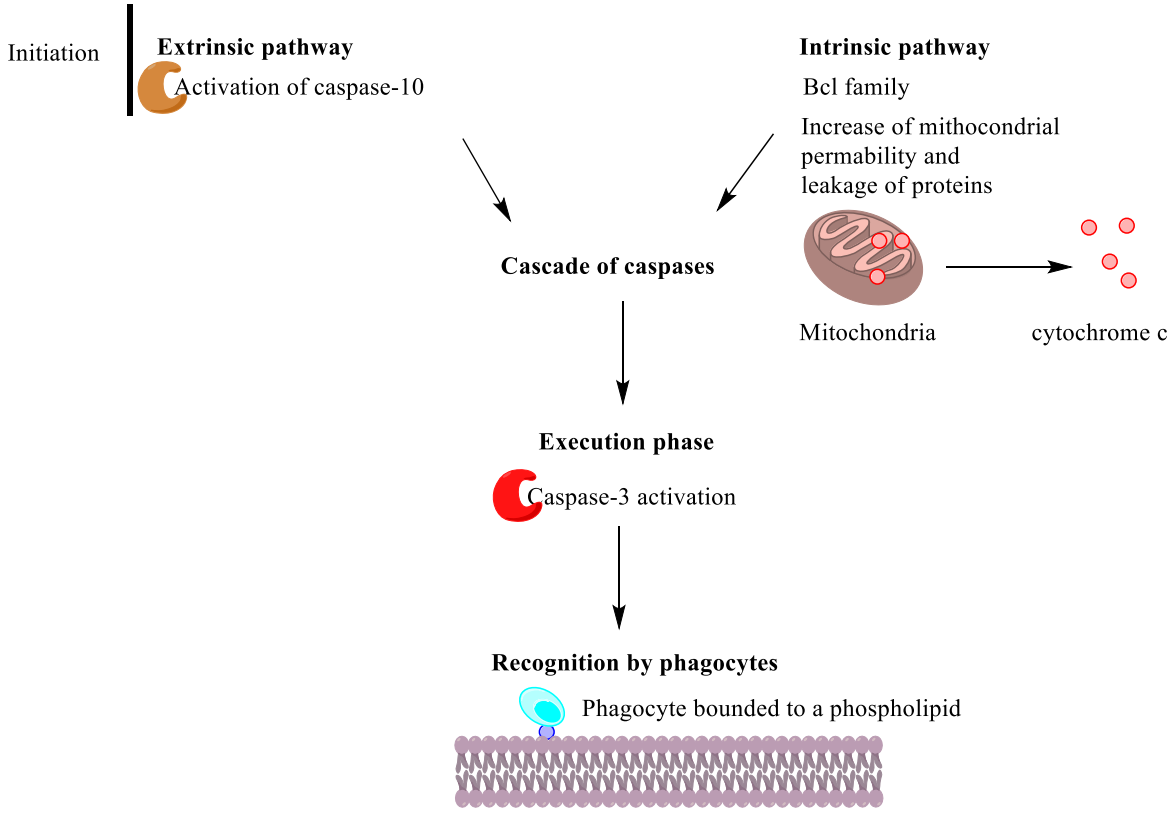

Figure 12. The apoptosis pathway.

There are two different initiating pathways which converge to a cascade of caspase activation: the intrinsic (mitochondrial) pathway and the extrinsic (death receptor mediated) pathway. The first one is mediated by anti and pro-apoptotic family of proteins, called Bcl and is characterized by an increase in mitochondrial permeability. These proteins cause activation of another proteins which will cause the leakage to the cytoplasm of essential

proteins that can cleave caspase-9 (a critical initiator caspase) and initiate the caspase cascade. In the extrinsic pathway, membrane death receptors are involved. The name death receptors came from its role in the apoptotic pathway. In the initiation pathway, there is an activation of caspase-10 which triggers the cascade of caspases by cleaving and activating the thereby inactive caspases. The now active caspases will mediate the execution phase.[87]

These two pathways have different molecules involved in the initiation phase and for that reason they were described in separated.

As it was said before, the two initiation phases converge to a cascade of caspase activation which mediates the execution and final phase of the apoptosis. This involves caspase-3 which act in many cellular components that will lead to the several changes that were mentioned before.

Autophagy

Autophagy is a type of cell death that occur when there is nutrient deprivation and the cell eats its own contents in order to survive. In the beginning of this process, intracellular organelles are put in a autophagic vacuole that later will fuse with the lysosomes and become the autophagosome.[85]

There are several ways to assess the type of cell death. For example, by doing a Western Blot in order to detect specific key proteins of apoptosis, necrosis, autophagy and necroptosis. In this work, this technique will be used and for that reason some considerations about it are made in chapter 4.

1.2.3 The alternative splicing process

It is known that eukaryotic genes contain introns which are segments of genes that do not code for polypeptides. The introns are removed from the primary transcript while the RNA molecule is still being synthesized before transportation into the cytoplasm. The removal of introns (non-coding regions) and the joining of the remaining exons (coding regions) is named splicing. This process is like a movie edition when a single part is cut and then the rest of the movie is re-joined together. The splicing process is conducted by the spliceosome, a large and dynamic ribonucleoproteic complex, regulated by the interaction

between *cis*-acting elements and over 200 *trans*-regulating proteins. The activity of the regulatory proteins depends of their intracellular localization, their post-translational modifications and binding to other proteins.

Alternative splicing results in different mature mRNAs which in turn results in different protein isoforms which can have opposite functions[88]. This type of splicing can produce different mRNAs and different proteins from the same primary transcript.

Modes of alternative Splicing

Exons present in the expressed mature transcript are termed constitutive exons opposing to alternative exons which only appears in particularly transcripts. There are five possible alternative splicing as shown in **Figure 13**.[88] The most common is exon skipping where a selected exon is removed from the mature mRNA.

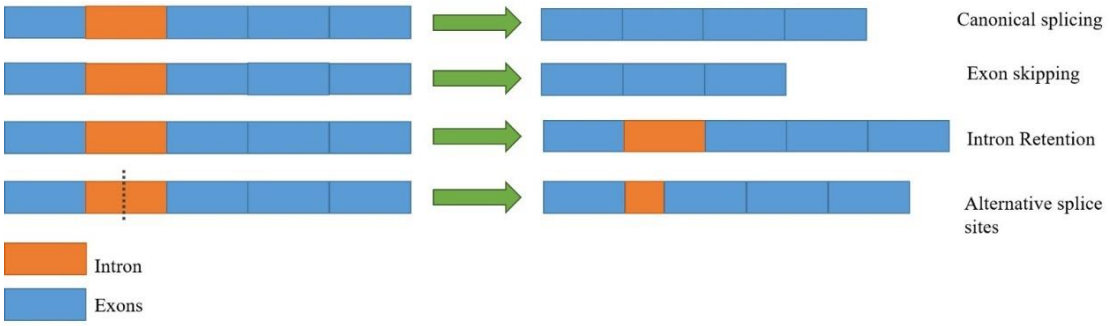

Figure 13. Types of splicing. [88,89]

Alternative 3' or 5' splice site occurs when a partial sequence of an intron is included. There is also intron retention in which an intron remains in the mature mRNA and is the rarest alternative splicing event.[90] At last, there is the mutually exclusive exons where the targeted exons are never simultaneously in the same transcript.

1.2.4 Alternative splicing and cancer

Ninety-five percent of the pre-mRNA undergoes alternative splicing (AS). This process contributes largely to the diversity and the flexibility of the proteome compare to the genome. The isoforms generated from a single pre-mRNA often have modified functions and in some instance opposite functions.

Given that alternative splicing controls several essential processes like cell division and differentiation, alteration on this process can lead to many diseases such as cancer. It is known that many oncogenes and tumour suppressors are alternatively spliced in cancer. p53 known to be inactivated in cancer, functions as a transcription factor and is responsible for maintain the genetic stability.[88] p53 has 9 different isoforms that result from alternative splicing. Several isoforms are known to be associated with loss of p53 function and cancer. In case of the splicing factor SRSF1 which can act as proto-oncogene and its overexpression can result in tumour formation. However, RBM4 (another splicing factor) was found to have tumour suppressor function unlike other splicing factors.[88,91,92]

With the recognition of the role for pre-mRNA splicing in cancer, there is an attempt to understand how this contributes to anticancer drug resistance. The aberrant pre-mRNA splicing can promote cell survival in response to chemotherapy by dysregulation of the apoptosis process.[88,92–94]

The regulation of apoptosis depends on the pro and anti-apoptotic factors, which in turned can result in a decrease on drug sensitivity. There are many genes involved in apoptosis which are regulated by alternative splicing. Bcl-x when alternative spliced forms two isoforms: the anti-apoptotic Bcl-xL and the pro-apoptotic Bcl-xS (as mentioned above). Cancer cells have elevated expression of the Bcl-xL which results in apoptosis inhibition. Also, caspase-2S (anti-apoptotic) has high expression in cancer cells and it enhances survival of this cells.[88,94,95]

Alteration in splicing of genes involved in pro-drug activation can lead to resistance of specific chemotherapeutics.

Giving all of this, different therapies are being developed to target splicing aberrations like inhibitors of the spliceosome or oligonucleotides.[88]

1.3 Aim of Work

It is known that the most common drugs used in chemotherapy (like cisplatin, doxorubicin and oxaliplatin) have been losing their efficiency due to a mechanism of DNA damage repair of cells creating a drug resistance. These mechanisms can repair the monoadducts and intra-strand cross links induced by platinum-based compounds with DNA.[96,97] More recently, over 600 cisplatin-related AS events in MCF-7 (breast cancer cell

line) cells were identified and observed that the reduction of AS led to a reduction of the stress related apoptosis.[93]

PDT relies on a photosensitiser that accumulates in tumour cells and is activated by visible light, which leads throughout an oxidative stress to cell death by apoptosis and necrosis.[64] It was shown that are different tetrapyrrolic macrocycles used effectively in PDT namely porphyrins, chlorins, among others. Having in mind that PDT and AS of mRNA can cause cell death, the final aim of this work was to study the effect of PDT using porphyrinic PS on alternative splicing of mRNA. Thus, a set of cationic porphyrin derivatives [5,10,15,20-tetrakis(4-(pyridinium-1-yl-methyl)phenyl)porphyrin and 5,10,15,20-tetrakis(4-(pyridinium-1-yl-methyl)phenyl)-2-aza-21-carbaporphyrin] were prepared and their biological properties compared with 5,10,15,20-tetrakis(1-methylpyridinium-4-yl)porphyrin which is known to be a good PS. Considering that AS can origin several protein isoforms which can lead to a specific type of cell death, it is important to study which cell type of death the cells undergo after PDT treatment and to study its effect on alternative splicing of mRNA.

CHAPTER 2

Synthesis of porphyrinic derivatives

2.1 *N*-Confused-porphyrin and porphyrin synthesis

2.1.1 General remarks

As it was mentioned in the previous chapter, it is known that cationic porphyrins are promising photosensitizers in PDT. One of the most studied cationic porphyrin is 5,10,15,20-tetrakis(1-methylpyridinium-4-yl)porphyrin (**TMPyP**) (**Figure 14**) due to their good properties for PDT.[98,99] Based on **TMPyP** structure and knowing that *N*-confused porphyrins recently discovered, possess interesting photosensitizing properties,[100,101] it seemed attractive to design a *N*-confused porphyrin considering **TMPyP** structure. So, our first target was to evaluate the possibility to synthesise the 5,10,15,20-tetrakis(pyridyl-4-yl)-2-aza-21-carbaporphyrin (**H_2TPyNCPP**) (see **Scheme 8**).

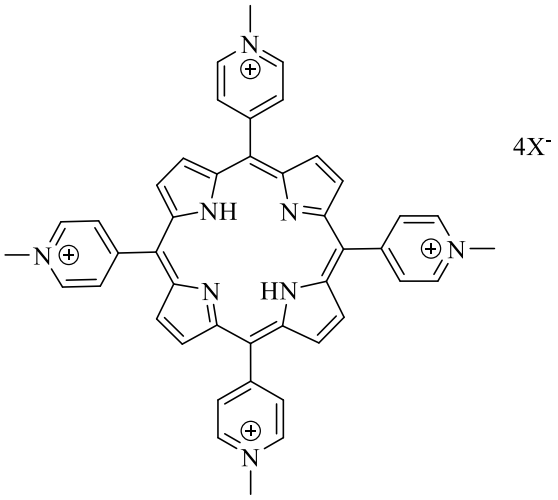

TMPyP

Figure 14. Structure of 5,10,15,20-tetrakis(1-methylpyridinium-4-yl)porphyrin (TMPyP).

The synthetic strategy to prepare **H_2TPyNCPP** was based on Lindsey methodology, considering that it is the most efficient one to prepare *N*-confused porphyrins.[55] The first step involved the condensation between pyrrole and 4-pyridinecarboxaldehyde in CH_2Cl_2, using a catalytic amount of MSA**,** at room temperature for 30 min. After this period DDQ was added and the reaction was stirred for 1 min. The oxidation step was followed by TLC which showed the formation of a less

polar compound than it was expected to obtain; in general *N*-confused porphyrins are more polar than regular porphyrins.

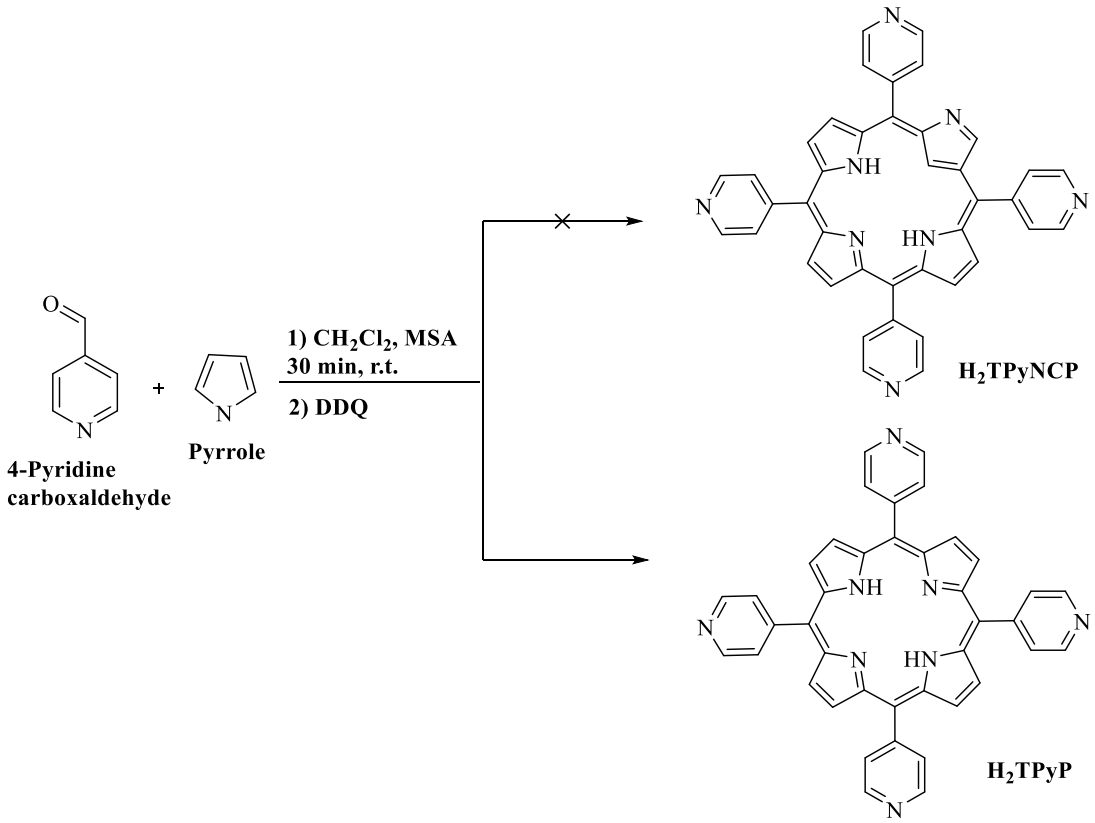

Scheme 8. Synthesis of H_2TPyP under Lindsey conditions.

After the reaction purification by column chromatography, using as eluent a mixture of CH_2Cl_2/MeOH (3%), two main fractions were obtained although only one showed a UV-Vis spectrum with Soret and Q bands, typical of a porphyrin derivative. This polar fraction was posteriorly identified by TLC as being constituted by the regular **H_2TPyP.**

So, the synthesis of the *N*-confused **H_2TPyNCP** was not successful and instead it was isolated **H_2TPyP** but in small amount. Probably, the high oxidant environment required by the Lindsey conditions for this aldehyde, in the second step is not ideal to generate **H_2TPyNCP.**

These results prompt us to try the synthesis of the *N*-confused cationic porphyrin 5,10,15,20-tetrakis(4-(piridinium-1-yl-methyl)phenyl)-2-aza-21-carbaporphyrin tetrabromide salt (**2, X = Br**) (**Figure 15-right**) reported by Ikawa and co-workers. [102] These authors were able to prepare the *N*-confused porphyrin **2** by introducing cationic side-arms at the *meso*-positions of 5,10,15,20-tetrakis(4-bromomethylphenyl)-2-aza-21-

carbaporphyrin (**1**) (**Figure 15- left**).[102] So, porphyrin **2 (X = I)** and the correspondent cationic regular porphyrin 5,10,15,20-tetrakis(4-(pyridinium-1-yl-methyl)phenyl)porphyrin tetraiodide were the ones selected to be prepared in this work. In the next sections a detailed description of the experimental work performed concerning the synthesis of these two derivatives it is discussed.

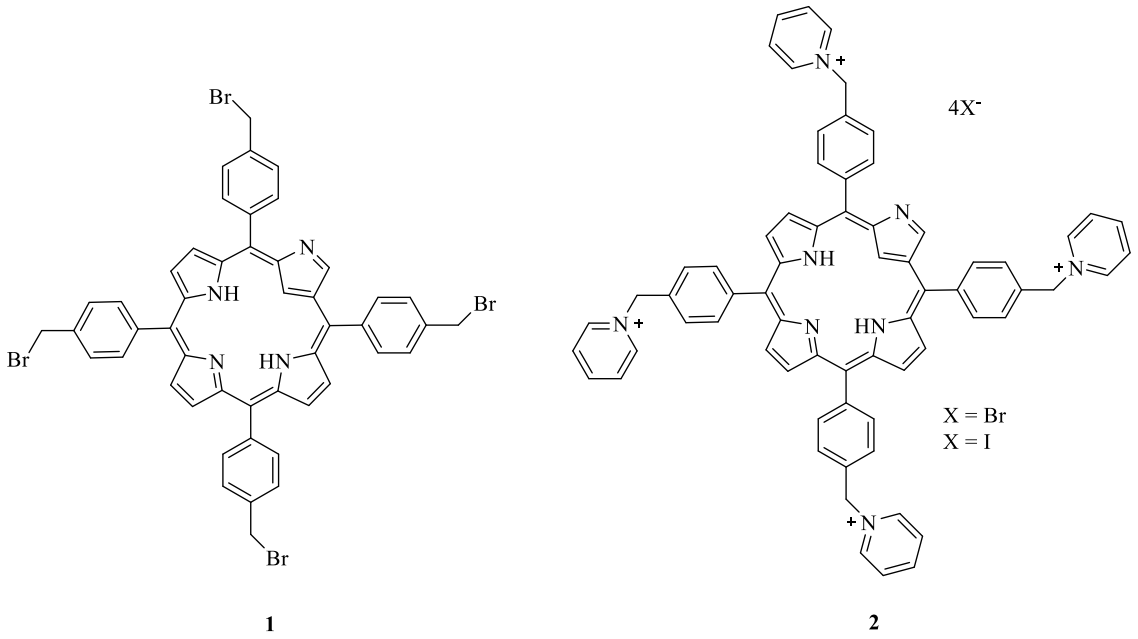

Figure 15. Structure of 1 and of its cationic derivative 2.

2.1.2 Synthesis of the precursors 5,10,15,20-tetrakis(4-bromomethylphenyl)-2-aza-21-carbaporphyrin and 5,10,15,20-tetrakis(4-bromomethylphenyl)porphyrin

In order to prepare the desired porphyrinic derivatives 5,10,15,20-tetrakis(4-bromomethylphenyl)-2-aza-21-carbaporphyrin (**1)** and 5,10,15,20-tetrakis(4-bromomethylphenyl)porphyrin (**5) (Scheme 9**), it was necessary first to prepare the 4-bromomethylbenzaldehyde **4**.

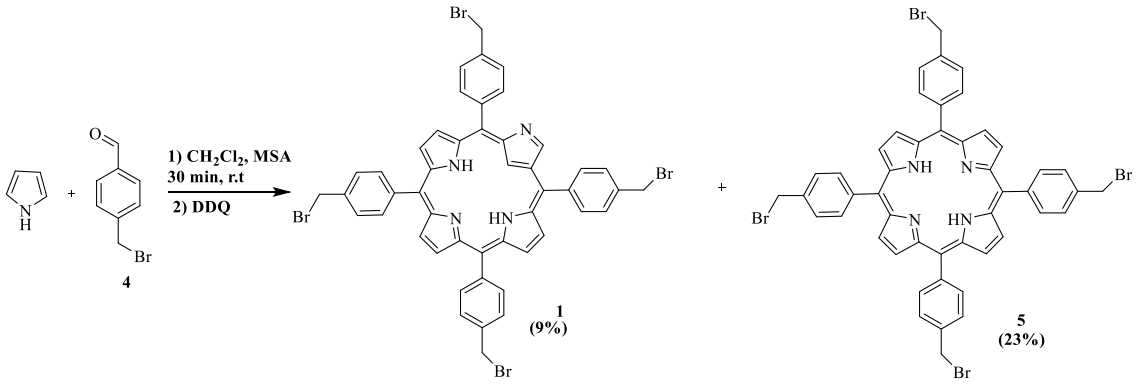

Scheme 9. Synthesis of 5,10,15,20-tetrakis(4-bromomethylphenyl)porphyrin 5 and 5,10,15,20-tetrakis(4-bromomethylphenyl)-2-aza-21-carbapophyrin 1.

According to literature this aldehyde can be obtained by oxidation of 1,4-bis(bromomethyl)benzene **3** using manganese oxide(IV) (**Scheme 10**).[103] The reaction was carried out in refluxing $CHCl_3$ using 4.6 equivalents of MnO_2. After 72 h, the reaction mixture was filtered through a celite column and then it was purified by column chromatography using a mixture of hexane/CH_2Cl_2 (1:1) as eluent. In this purification process was isolated two main fractions; the less polar one corresponded to the starting compound **3** (confirmed by TLC and ^{1}H NMR) and the more polar one it was identified as being the desired compound **4.** This derivative was isolated in 19% yield and its structure was confirmed by ^{1}H NMR and mass spectroscopy.

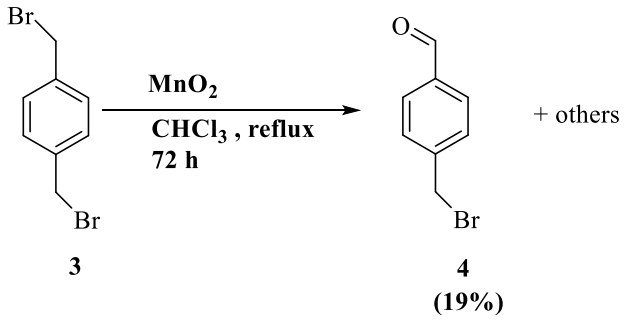

Scheme 10. Oxidation of 1,4-bis(bromomethyl)benzene 3 into 4-bromomethylbenzaldehyde 4

The ^{1}H NMR spectrum of compound **4** (**Figure 16)** shows a typical spectrum of a *para*-substituted aromatic system with two doublets and two singlets. The characteristic singlet at δ 10.02 ppm corresponds to the resonance of the carbonyl proton (-CHO) and the two doublets at δ 7.56 and δ 7.87 ppm (J = 8.2 Hz) are due to the aromatic protons H-

2,6 and H-3,5. The resonances due to the aliphatic protons CH_2 appear as a singlet at 4.52 ppm.

In the mass spectrometry analysis $[ESI]^+$, a peak at *m/z* 199.0 corresponding to $[M+H]^+$ ion of compound **4**, allowed also to confirm its structure.

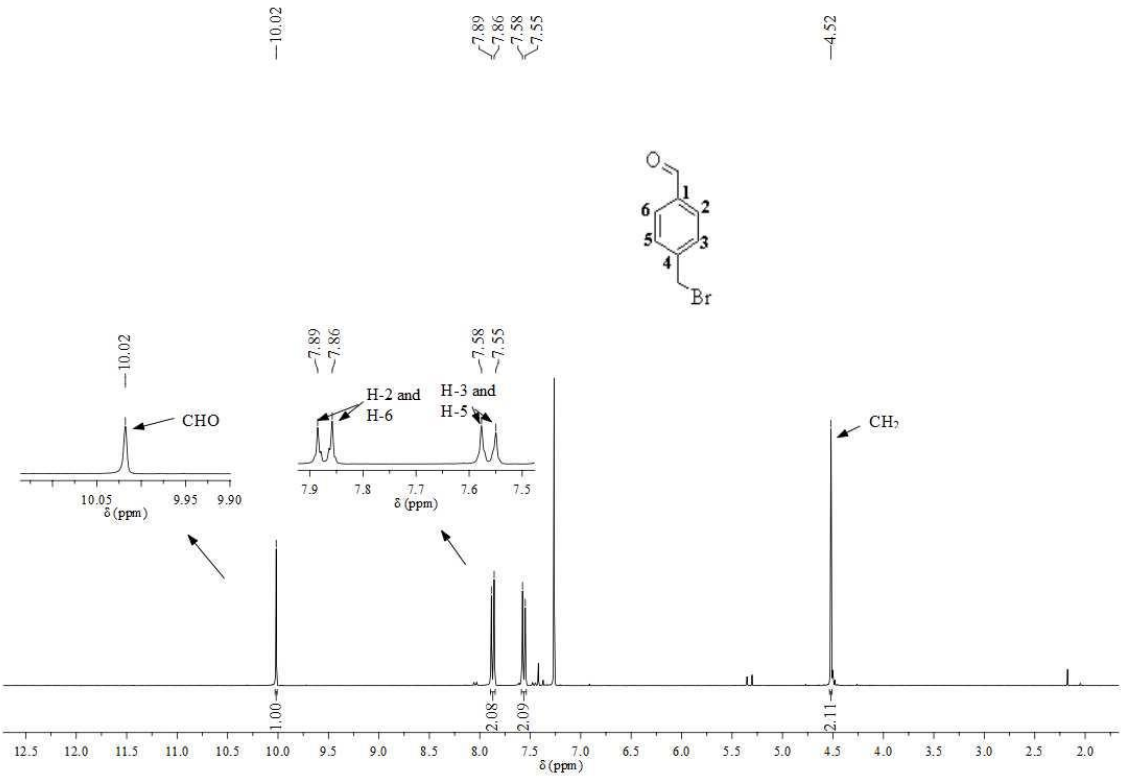

Figure 16. ^{1}H NMR spectrum of compound 4 (300MHz, $CDCl_3$).

The condensation of the synthesised 4-bromomethylbenzaldehyde **4** with pyrrole, in order to obtain 5,10,15,20-tetrakis(4-bromomethylphenyl)-2-aza-21-carbaporphyrin (**1**) (**Scheme 9**) was performed according to Lindsey conditions.[102] This condensation was performed in CH_2Cl_2 in the presence of MSA and under nitrogen atmosphere at room temperature. The reaction was stirred for 30 min and after this period DDQ was added to promote the oxidation; the TLC control shown the formation of two main compounds. Then, the mixture was purified by preparative TLC using a mixture of CH_2Cl_2/CH_3OH (92:8) as eluent. The first fraction with a reddish colour was identified as being the regular porphyrin **5** and was isolated in 23% yield; the second fraction, with a dark green colour, showed to be the *N*-confused porphyrin **1** and was obtained in 9% yield (**Scheme 9**).

The structure of both compounds was confirmed by spectroscopic data namely ^{1}H NMR and mass spectrometry.

The analysis of the ^{1}H NMR spectrum of compound **5** (**Figure 17**) confirms as expected, the presence of a highly symmetric structure and the singlet that appear at δ -2.82 ppm corresponds to the resonance of the two *N*-H protons of the porphyrin inner core.

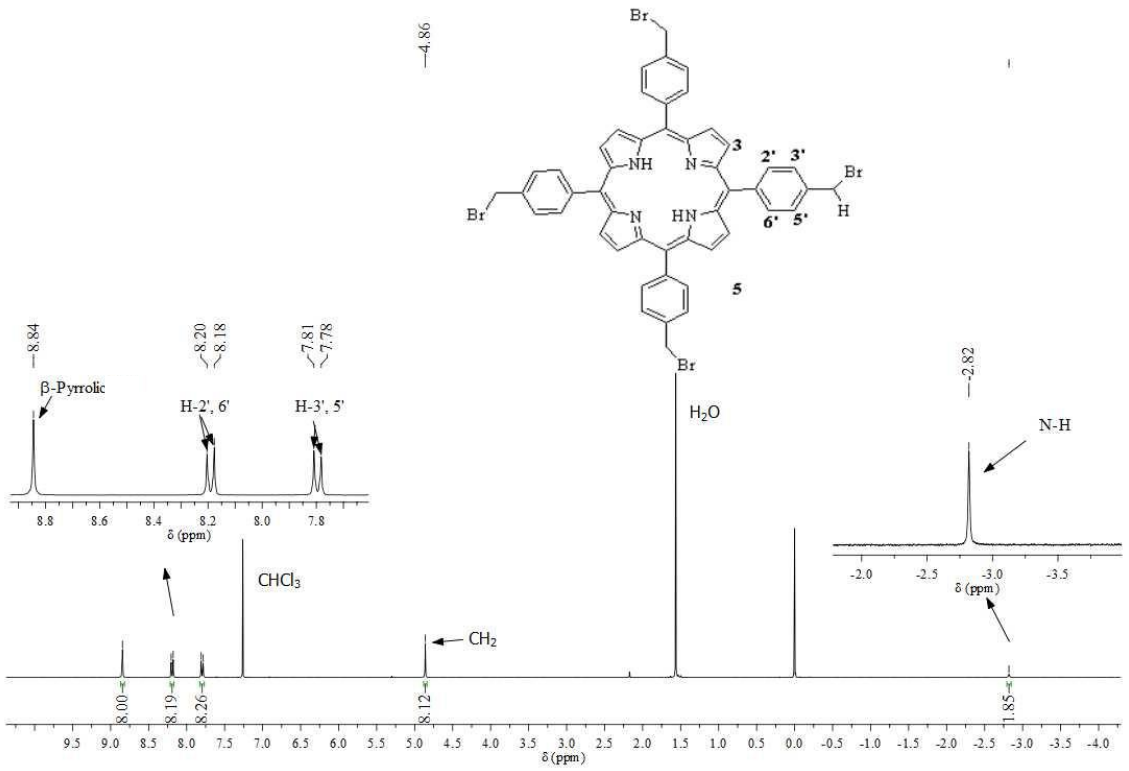

Figure 17. ^{1}H NMR spectrum of porphyrin 5 (300MHz, $CDCl_3$).

These protons are highly protected due to the anisotropic effect induced by the electron delocalization of the macrocycle. Still in the aliphatic region it is possible to observe a singlet at δ 4.86 ppm which corresponds to the resonance of the four -CH_2 protons. Regarding the aromatic region, it is possible to observe three different signals. Two doublets at δ 7.80 and δ 8.19 ppm with a coupling constant of J = 8.1 Hz due to the resonance of the protons H-3', 5' and proton H-2', 6', respectively, and a singlet at δ 8.84 ppm generated by the resonance of the β-pyrrolic protons.

The ESI mass spectrum of compound **5** corroborated also the structure proposed, showing the peak of $[M+H]^+$ ion at *m/z* 987.1.

As it was mentioned above, the structure of the more polar compound was identified by ^{1}H NMR (**Figure 18**) and mass spectroscopy techniques as being the *N*-

confused derivative **1**. The ^{1}H NMR spectrum is representative of a compound with a much less symmetric structure than **5**.

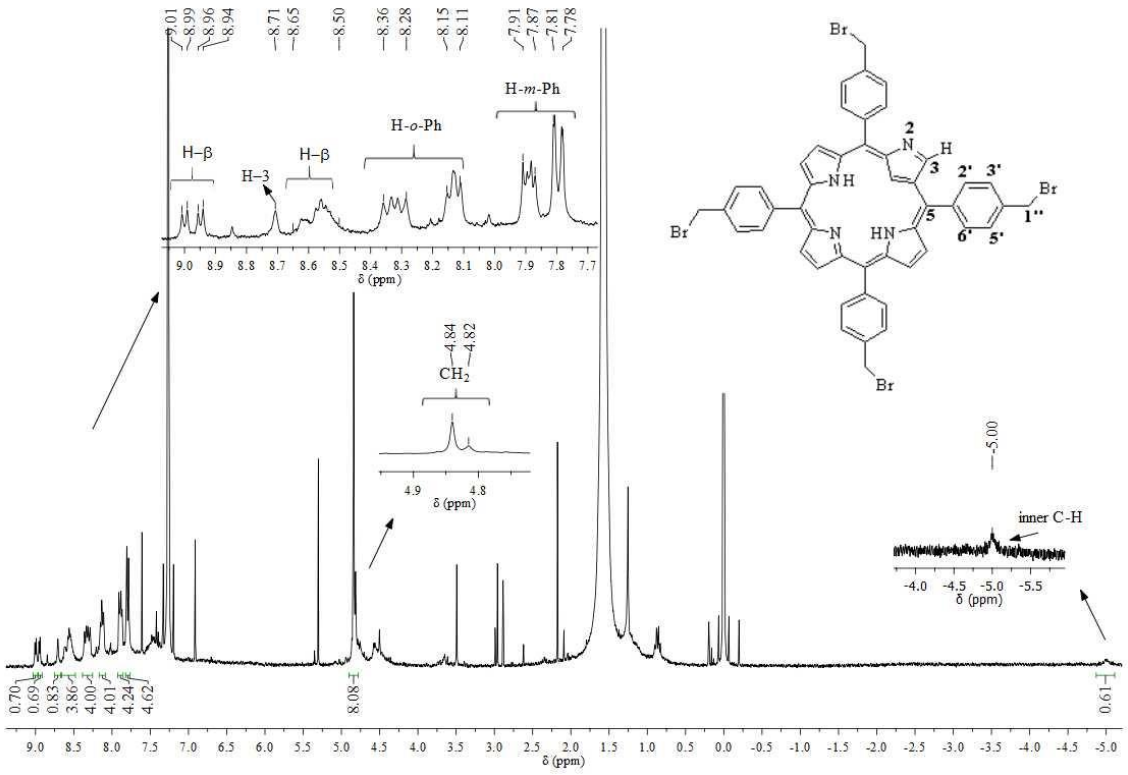

Figure 18. ^{1}H NMR spectrum of porphyrin 1 (300MHz, $CDCl_3$).

It was very difficult to obtain a ^{1}H NMR spectrum with well defined peaks because derivative **1** is very unstable during the purification work-up probably due to some self-polymerization. However, it is possible to detect a broad singlet at δ -5.0 ppm which corresponds to the resonance of the highly protected C-H inner core. Still in the aliphatic region at δ 4.82 and δ 4.84 ppm it is possible to observe two singlets that correspond to the resonance of the 4 -CH_2 protons. In the aromatic area it is possible to observe the signals corresponding to the resonance of the β-pyrrolic protons: two doublets at δ 8.95 ppm (J = 4.7 Hz) and δ 9.0 ppm (J = 5.1 Hz) and one multiplet between δ 8.50 and 8.65 ppm; in this region it is still possible to observe the signals corresponding to the *orto* and *meta* protons of the *para*-substituted phenyl rings: a multiplet at δ 8.22-8.36 ppm and another at δ 8.11-8.15 ppm; a doublet at δ 7.80 ppm (J = 9.2 Hz) and a multiplet between δ 7.87 ppm and δ 7.91 ppm, respectively. This ^{1}H NMR spectrum is consistent with the one already described in the literature.[102]

The structure of compound **1** was also confirmed by the ESI(+) mass spectrum which revealed a peak at *m/z* 987.1 corresponding to the $[M+H]^+$ ion.

2.1.3 Synthesis of 5,10,15,20-tetrakis(4-(pyridinium-1-yl-methyl)phenyl)porphyrin tetraiodide (6) and 5,10,15,20-tetrakis(4-(pyridinium-1-yl-methyl)phenyl)-2-aza-21-carbaporphyrin tetraiodide (2)

The synthetic approach to obtain the cationic porphyrins **1** and **5 (Scheme 11)**, was based on the nucleophilic substitution of the bromine atoms in the *meso*-aryl groups by pyridine. In contrast with the described procedure[102] it was added sodium iodide (**NaI**) in order to favour the nucleophilic substitution.

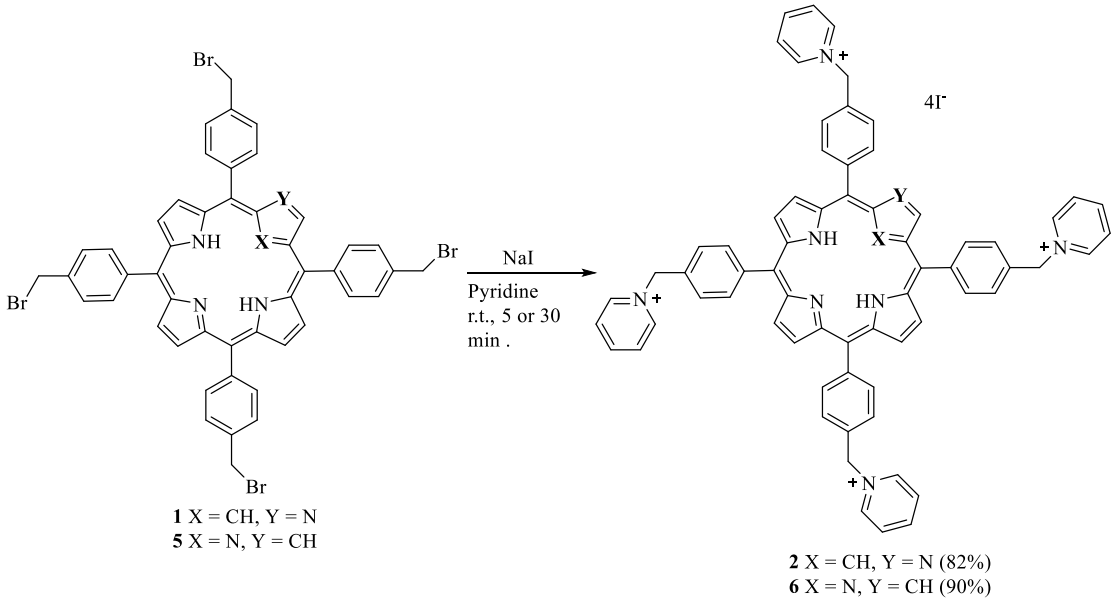

Scheme 11. Synthesis of 5,10,15,20-tetrakis(4-(pyridinium-1-yl-methyl)phenyl)-2-aza-21-carbaporphyrin tetraiodide (2) and 5,10,15,20-tetrakis(4-(pyridinium-1-yl-methyl)phenyl)porphyrin tetraiodide (6)

Therefore, both cationic porphyrins were prepared by adding 6.0 equivalents of **NaI** to the appropriate porphyrin derivative (**1** or **5**) in pyridine at room temperature. After 30 min, the formation of the cationic *N*-confused porphyrin **2** was confirmed by TLC and after the work up, the desired porphyrin was isolated in 82% yield. Porphyrin **6** was obtained in 90% yield from the regular porphyrin **5** after 5 min of reaction.

The structure of both compounds was confirmed by ^{1}H NMR and mass spectroscopy (**Figure 19, Figure 20** and **Figure 21**).

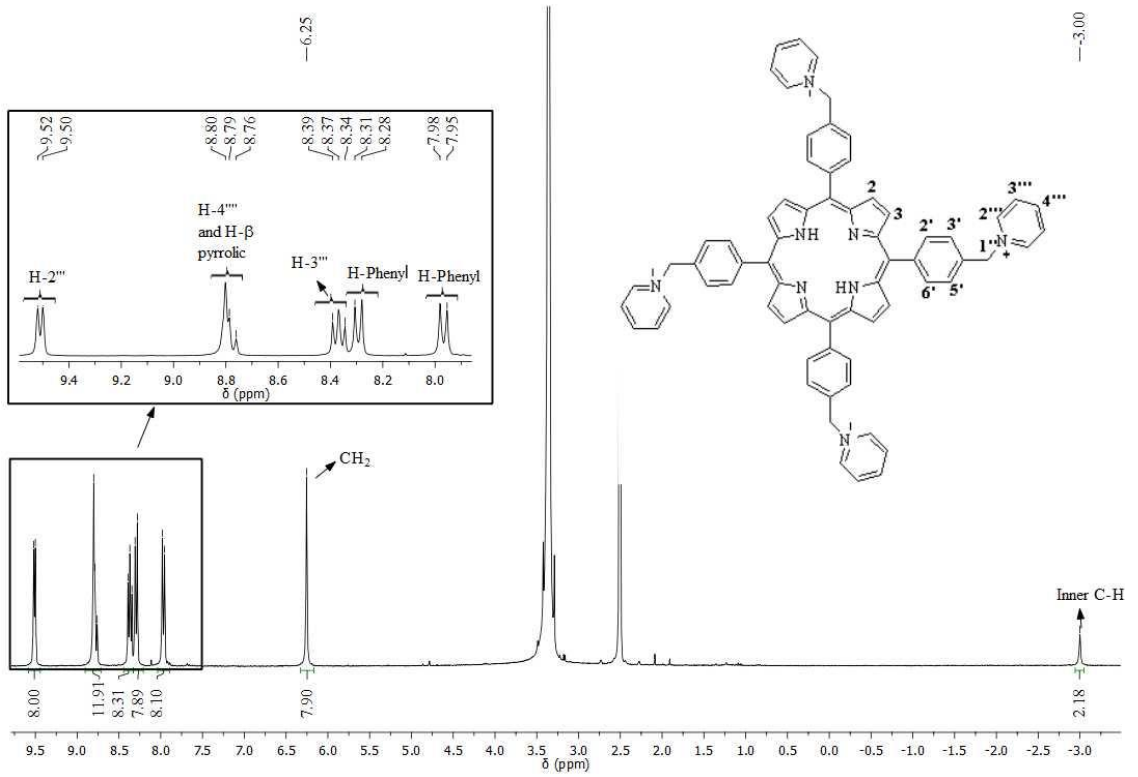

Figure 19. ^{1}H NMR spectrum of porphyrin 6 (300MHz, DMSO-d$_6$).

The insertion of the pyridinium group in porphyrin **5** induced some changes in the ^{1}H NMR spectrum of **6**. This introduction leads to the shift of the -CH_2 resonance singlet to low field region of the spectrum, appearing now at δ 6.25 ppm. These protons become more unshielded due the new pyridinium moiety linked to the -CH_2 carbon by the nitrogen atom. The signals corresponding to the protons of the pyridinium group H-2''', 6''' appear as a doublet at 9.51 ppm (J = 5.6 Hz) being these the most unshielded proton of the pyridinium ring due the proximity of the positive charged heteroatom. The other protons corresponding to H- 3''',5''' resonate as a doublet of doublets at δ 8.37 ppm (J_1 = 6.7 Hz and J_2 = 7.8 Hz) because it couples differently with H-2''',6''' and H-4'''. The identification of the protons of the pyridinium moiety was confirmed by 2D spectra (see **Figure 20).** These experiments allowed to verify that the signal corresponding to protons H-4''' appears overlapped with the multiplet generated by the β-pyrrolic protons between δ 8.76 ppm and δ 8.80 ppm. As expected the resonance of the two protons in the inner core of the porphyrinic macrocycle appear as a singlet at δ -3.0 ppm. The 2D experiments (COSY, HSQC and HMBC) allowed also to identify some carbons (see experimental part).

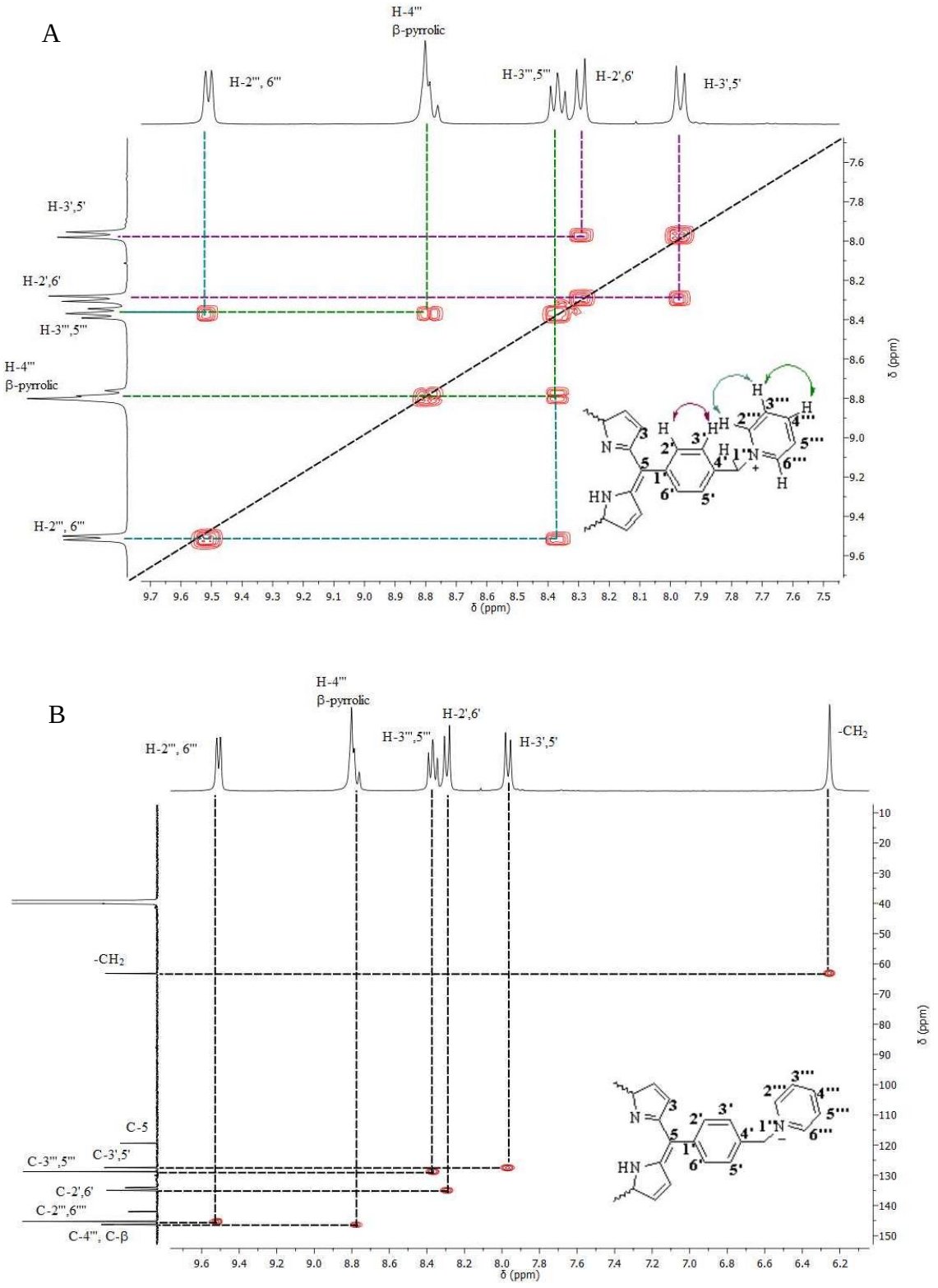
A
H-4'''
β-pyrrolic
H-2''', 6'''
H-3''',5'''
H-2',6'
H-3',5'
H-3',5'
H-2',6'
H-3''',5'''
H-4'''
β-pyrrolic
H-2''', 6'''
δ (ppm)
B
H-4'''
β-pyrrolic
H-2',6'
H-3''',5'''
H-3',5'
-CH2
H-2''', 6'''
-CH2
C-5
C-3',5'
C-3''',5'''
C-2',6'
C-2''',6'''
C-4''', C-β
δ (ppm)

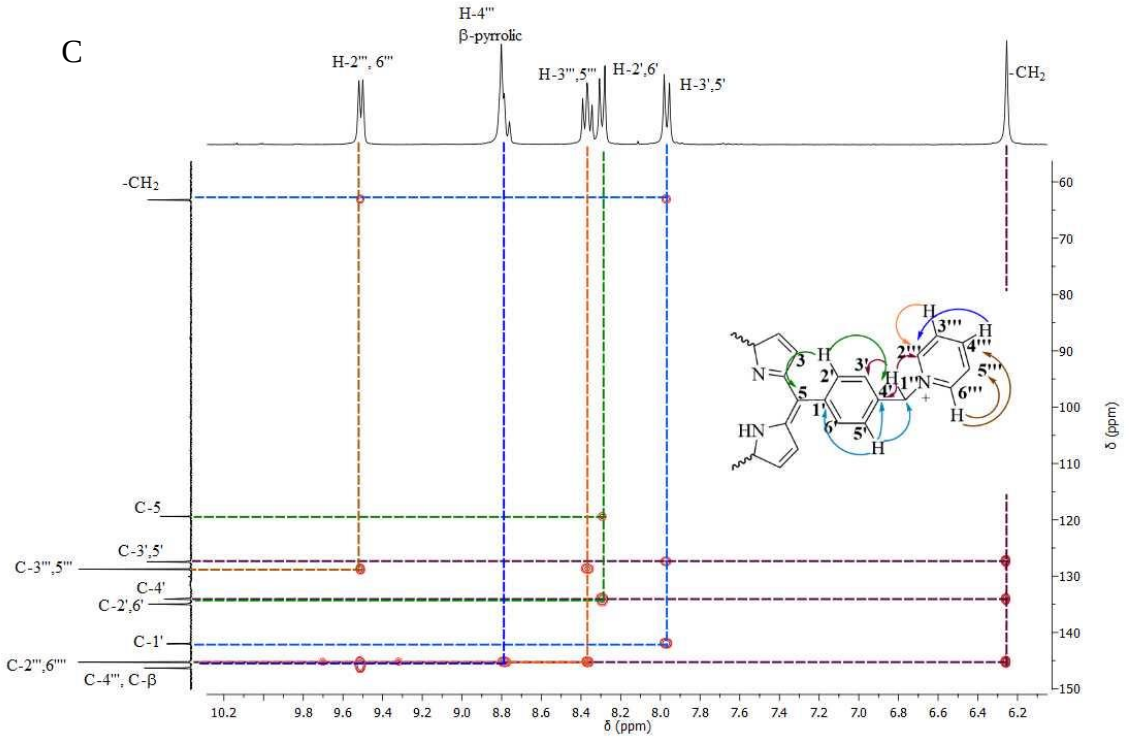

Figure 20. Expansion of COSY (A), HSQC (B) and HMBC (C) spectra of porphyrin 6 in DMSO-d_6 (500 MHz).

The ESI(+) mass spectrum for compound **6** shows a peak at *m/z* 245.9 corresponding to $[M]^{4+}$ ion. Also, the presence of two peaks at *m/z* 225.6 and *m/z* 274.5 corresponding to $[M\text{-Py-H}]^{4+}$ and $[M\text{-2Py-2H}]^{3+}$, respectively, helped to confirm the structure of compound **6**.

Considering the identification of compound **2** by NMR, it was very difficult to acquire a good spectrum even after trying different conditions. The best spectrum was obtained in DMSO at 50ºC, although the quality was not very good (**Figure 21**). However, the signals in the ^{1}H NMR spectrum are in accordance with the literature for this compound[102] and it was possible to detect the deviation of the multiplet due to the CH_2 resonance to δ 6.12-6.23; the signals corresponding to the H-pyridinium units were also detected at δ 8.74 ppm, δ 8.30-8.34 ppm and δ 9.40-9.49 ppm.

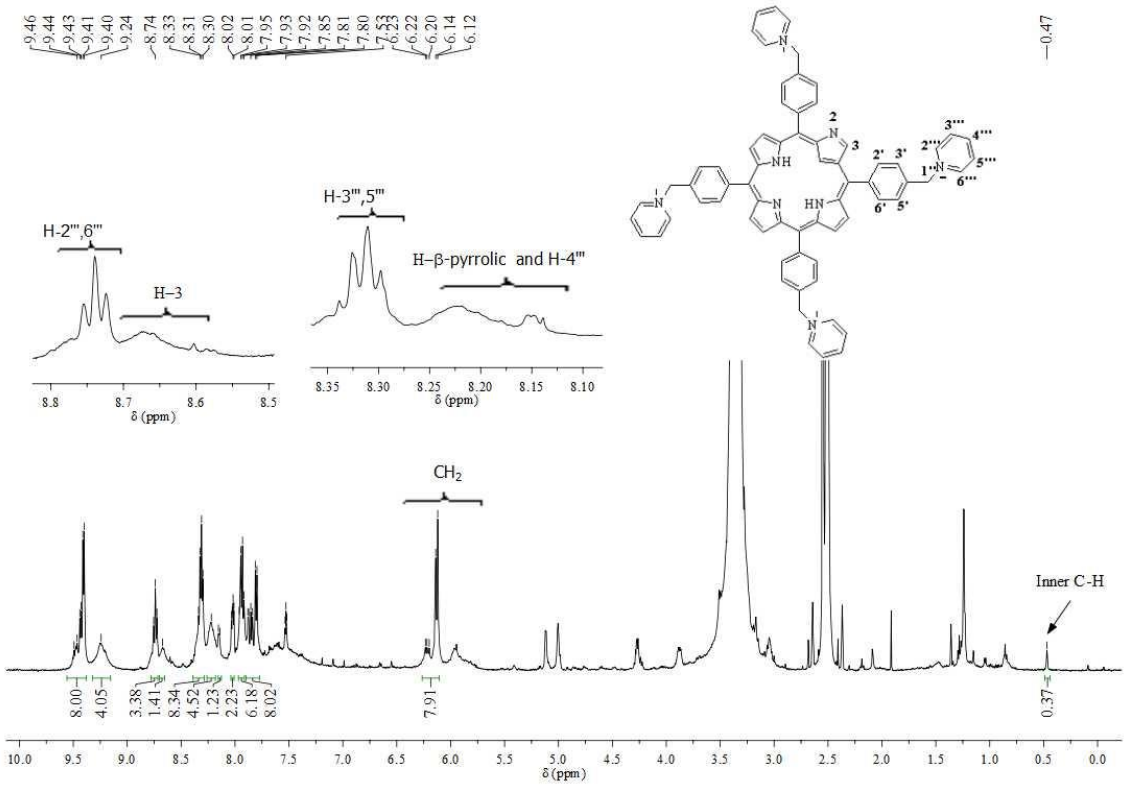

Figure 21. ^{1}H NMR spectrum of porphyrin 2 (300MHz, DMSO-d_6 at 50ºC).

The mass spectrum of compound **2** in ESI (+) shown two peaks at *m/z* 274.5 and at *m/z* 225.8 which corresponds to $[M\text{-}2Py\text{-}H]^{3+}$ and $[M\text{-}Py\text{-}H]^{4+}$ ions, respectively.

2.2 Photophysical Characterization

In order to know the effect of the insertion of the pyridinium groups in the photophysical properties of compounds **2** and **6**, their coefficients of absorptivity molar (ε) and the fluorescence quantum yields were compared with the ones of compounds **1** and **5**. In **Figure 22** are shown the absorption spectra of all porphyrins recorded in DMF and the coefficient of absorptivity molar of each band is summarized in **Table 2.** The UV-Vis spectrum of the regular porphyrin **5** (**Figure 22**) shows a typical ethio-type spectrum with a strong Soret band at 419 nm and four Q bands between 516 and 647 nm. No significant changes were detected in the UV-Vis spectrum of the cationic porphyrin **6**

when compared with its neutral precursor **5;** the Soret band is also localized at 419 nm and the Q bands appear between 515 and 647 nm (**Figure 22**).

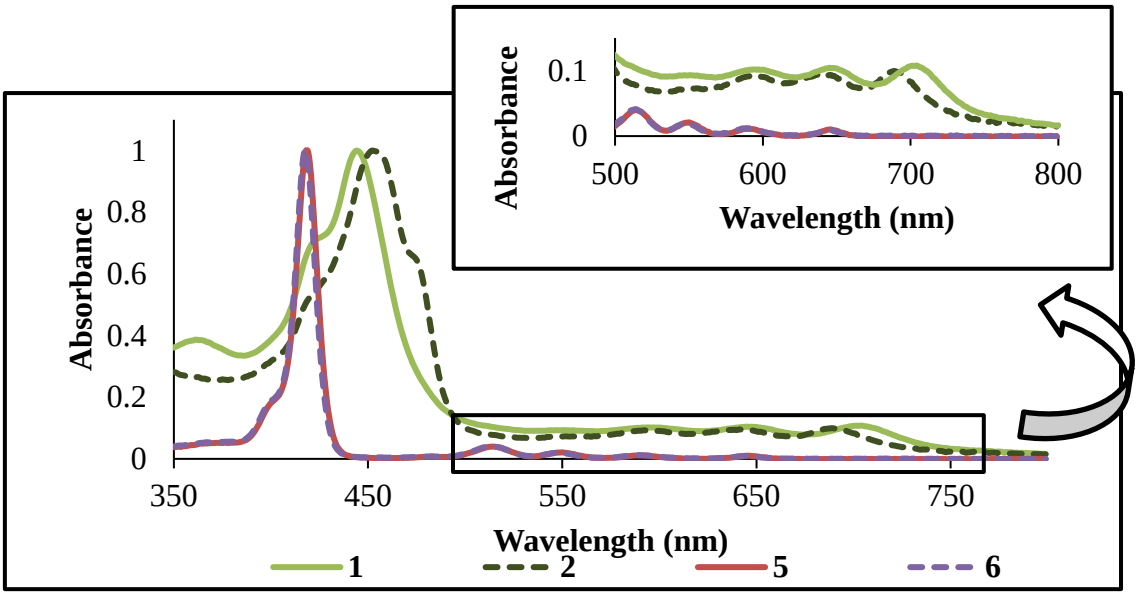

Figure 22. Normalized UV-Vis spectra in DMF of porphyrin 1, 2, 5 and 6.

The inversion of one pyrrole ring change the macrocycle conjugation and the absorption properties of compounds **1** and **2** were strongly affected when compared with the ones of the regular porphyrins **(Figure 22** and **Table 2)**. Therefore, for compound **1** it is possible to observe a red-shifted spectrum with the Soret band at 445 nm and the four Q bands between 548 and 705 nm. The UV-Vis spectrum of porphyrin **2** shows also the spectrum of a typical *N*-confused derivative but the Soret band suffered a red-shift of 8 nm when compared with the one of the neutral porphyrin **1.** In the Q band region, it was observed a small blue-shift (15 nm) for the last Q band, but no significant changes were observed for the remaining bands.

The emission spectrum of each compound was also performed in DMF and it was measured under normal conditions (open air) at 298 K. The fluorescence quantum yield (Φ_{Flu}) of each porphyrin was calculated by using a fluorescence standard and was made through the formula:

$$\Phi_{Flu} = \Phi_{St} \frac{\eta^2}{\eta_{St}^2} \frac{I}{A} \frac{A_{St}}{I_{St}}$$

where Φ_{St} is the fluorescence quantum yield of the standard compound, η is the refractive index of the solvent, I is the integrated fluorescence intensity (area underneath the spectrum) and A is the absorbance at the excitation wavelength λ= 425 nm. In this

work, the standard reference used was **TPP** in DMF (Φ_{Flu} = 0.11).[104] The absorbance of each compound at 425 nm was kept between 0.0414-0.0540 in order to avoid inner filter effects and ensure linear response on the fluorescence intensity.

The studied compounds shown different emission profile. The *N*-confused porphyrin derivatives **1** and **2** did not show any fluorescence emission in DMF while porphyrins **5** and **6** have an emission spectrum characteristic of porphyrins (**Figure 23**). The spectra of **5** and **6** are characterized by a strong emission band with a maximum intensity around 650 nm and a less strong band at 715 nm (**Figure 23**). The fluorescence quantum yield obtained is similar for both porphyrins (**Table 2**) and to the reference **TPP (0.11);** it is worth to refer that the fluorescence emission was not significantly affected by the insertion of the pyridine units.

Table 2. Photophysical parameters of porphyrins 1, 2, 5 and 6 in DMF. The fluorescence parameters of TMPyP were done in DMF and the others were done in DMSO.[105]

Photophysical properties	**1**	**2**	**5**	**6**	**TMPyP**
Soret and Q bands (log (ε))	445 (4.96)	453 (4.92)	419 (5.87)	419 (5.63)	425 (5.43)
	548 (3.91)	549 (3.79)	516 (4.42)	515 (4.49)	516 (4.29)
	595 (3.95)	598 (3.89)	551 (4.15)	551 (4.16)	549 (3.77)
	646 (3.96)	643 (3.90)	592 (3.90)	590 (3.96)	588 (3.84)
	705 (3.98)	690 (3.93)	647 (3.85)	647 (3.87)	642 (3.30)
λ_{em} (nm)	--	--	652, 717	651, 716	652, 714
Φ_{Flu}	--	--	0.11	0.10	0.12

Concerning the *N*-confused derivatives, it is reported in the literature a very low fluorescence emission for 5,10,15,20-tetraphenyl-2-aza-21-carbaporphyrin (Φ_{Flu} =0.036 – 0.0016) and it is dependent on which is the preferential tautomer (see chapter 1, **Scheme 1).** So, the results obtained for these derivatives are in accordance with the ones described in the literature.[106,107]

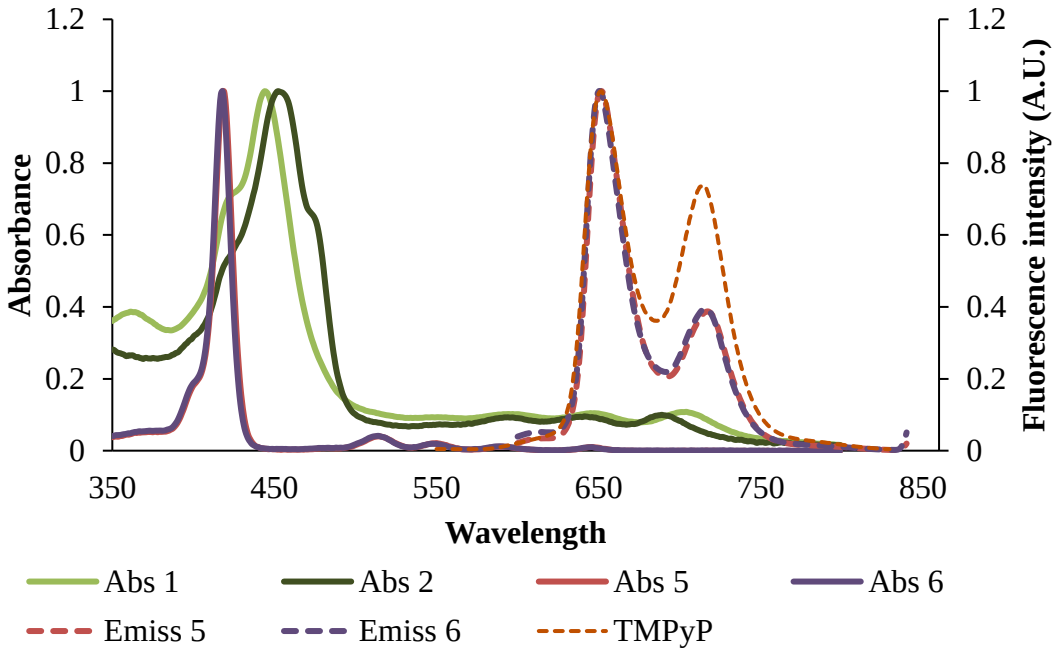

Figure 23. Normalized UV-Vis and normalized fluorescence spectra of porphyrin 1, 2, 5 and 6 with λexc= 424 nm and OD = 0.05 in DMF.

Since the main aim of this work was to evaluate the ability of the synthesized compounds to act as photosensitizers and also to assess their influence on alternative splicing, it was important first to study their capacity to generate singlet oxygen.[108]

The method used in this work to determine the $^1O_2$ generation involves the 1,3-diphenylisobenzofuran quencher (**DPiBF**). **DPiBF** is a furan and can be used to qualitatively determine the $^1O_2$ generation. This compound absorbs in the visible region of the spectrum, namely at 415 nm. However, in the presence of $^1O_2$, the **DPiBF** undergoes a cycloaddition [4+2] with $^1O_2$ and it is converted into an intermediate **7** which is subsequently degraded in 1,2-dibenzoylbenzene (1,2-DBB) (**Figure 24**). As the 1,2-DBB formed does not absorb in the visible region of the electromagnetic spectrum, a decrease in the absorbance of a **DPiBF** solution allows to evaluate the amount of $^1O_2$ produced by the porphyrinic derivative in study. Thus, this reaction was the base to perform a qualitative test to determine if the previous synthesized derivatives and potential PSs can generate $^1O_2$ when activated by light.

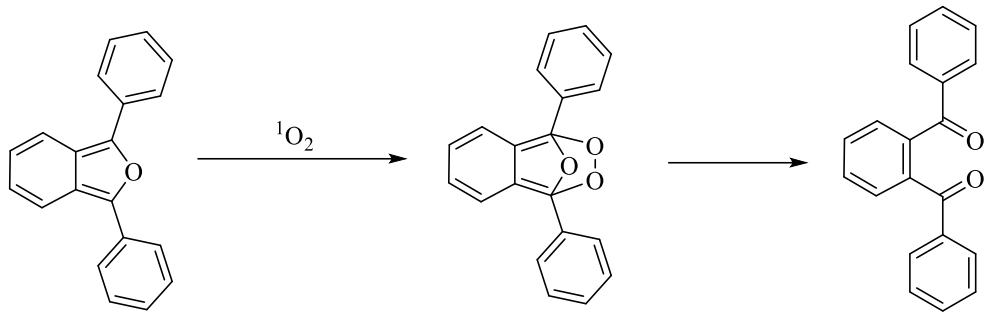

Figure 24. Degradation of the DPiBF in 1,2-DBB in the presence of $^1O_2$.

In order to determine qualitatively the production of $^1O_2$, the PS and the **DPiBF** are dissolved in a solvent which does not interfere with the $^1O_2$ generation and its quantification. The concentration of the **DPiBF** must be about 100 times higher than the PS concentration because the PS also absorbs in the visible region where it was monitored the **DPiBF** degradation. If the photosensitizer is able to generate $^1O_2$, by illuminating the solution with light above 550 nm, a decreasing in absorbance of the **DPiBF** will happen. The **DPiBF** absorbance monitoring is done at 415 nm. The results enable us to correlate the absorbance of the **DPiBF** with the $^1O_2$ production.

In a quartz cuvette, a solution with a PS concentration of 0.5 and 50 µM of **DPiBF** in DMF was prepared. The solution was irradiated with a light of wavelength 640 ± 20 nm and with an irradiance of 9 mW/cm^2 and the absorbance was measured. The neutral **TPP** and the cationic **TMPyP** were selected as controls because it is known that they are good photosensitizers.[68]

Since the reaction of **DPiBF** with $^1O_2$ follows a first order kinetics, the [$^1O_2$] is proportional to $Ln\frac{A_0 DPiBF}{ADPiBF}$, where A is the absorbance of **DPiBF** in each minute and A_0 the initial absorbance of the **DPiBF**.

The results obtained for neutral (**1** and **5**) and cationic (**2** and **6**) porphyrinic derivatives (**Figure 26**) are represented in **Figure 25** and **Figure 26.** Structure of porphyrin 1, 2, 5, 6, TPP and TMPyP.

Table 3. The decay of **DPiBF** absorbance in the presence of each compound confirms that only the regular porphyrins have high efficiency to generate $^1O_2$.

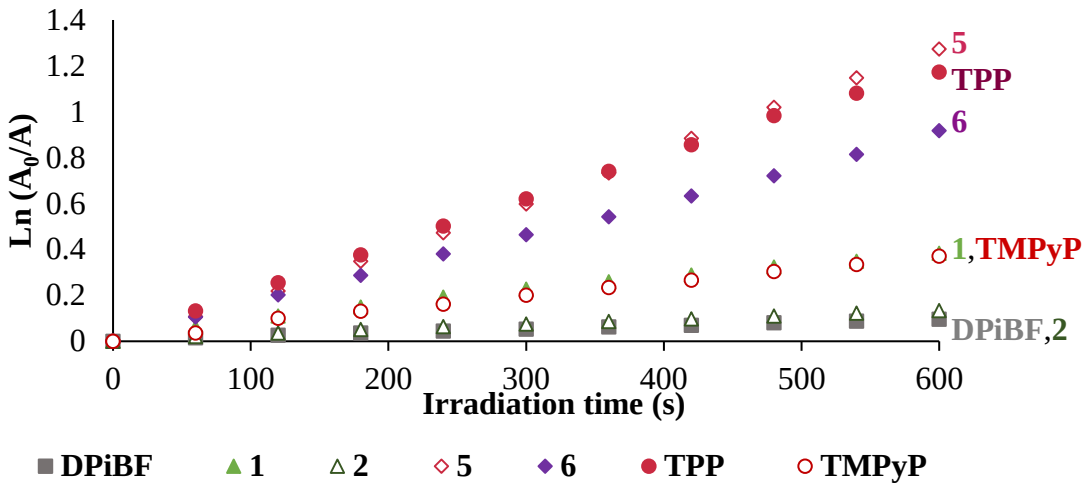

Figure 25. Comparative degradation of DPiBF (50µM) in DMF for 10 min with or without photosensitiser (0.5 µM); red light (9mW/cm^2).

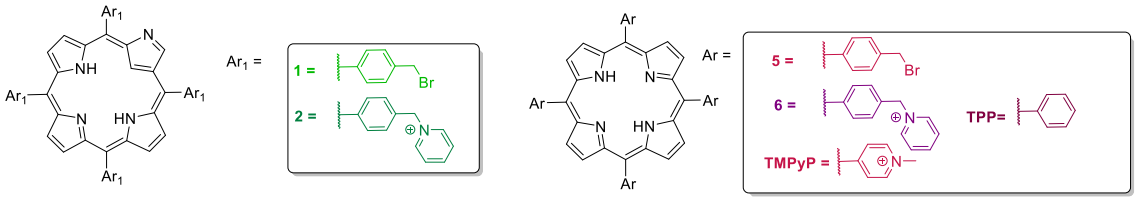

Figure 26. Structure of porphyrin 1, 2, 5, 6, TPP and TMPyP.

Table 3. Slopes of the degradation of DPiBF (50 µM) in DMF for 10 min with or without photosensitizer (0.5 µM) by using red light (9mW/cm^2)

COMPOUND	SPLOPE
DPIBF	1.67×10^{-4}
1	6.82×10^{-4}
2	2.33×10^{-4}
5	2.09×10^{-3}
6	1.52×10^{-3}
TPP	2.02×10^{-3}
TMPYP	6.36×10^{-4}

Regarding the synthesised derivatives, the regular porphyrin **5** is the best $^1O_2$ generator being slightly better than **TPP**, known as a good singlet oxygen generator (Φ_Δ = 0.65 in DMF). In contrast, the cationic *N*-confused derivative **2** does not show any ability to generate singlet oxygen. In fact, the **DPiBF** photodegradation in the presence of **2** is comparable to its own photodegradation in absence of a PS. On the other hand, regarding the cationic porphyrin derivative **6** is ability to produce $^1O_2$ is much higher than the one of the well-known cationic PS **TMPyP.** However, the insertion of the pyridinium

moieties was responsible by a decrease in the ability of compound **6** to generate $^1O_2$ when compared with porphyrin **5**. As far as we know, there are no records in the literature regarding the ability of the compounds synthesised to generate singlet oxygen. However, it was reported that the *meso*-tetrakis(*p*-sulfonatophenyl)-*N*-confusedporphyrin tetrasodium salt was a highly efficient singlet oxygen generator.[100] This seems to indicate that the singlet oxygen generation is dependent of the substituents in the *meso* positions.

The results above mentioned indicate that among the synthesized porphyrins only **5** and **6** shown to be good PS candidates.

2.3 Material and methods

2.3.1 Chemicals and equipment

The commercial chemicals were used without any further purification and the solvents used in synthesis or purification process were analytical pure or distilled when needed. Pyridine was dried by refluxing it in the presence of adding sodium hydroxide and then distilled.

The evolution of chemical reactions was controlled by analytical TLC carried out on precoated sheets with silica gel (Merck 60, 0.2 mm thick for coloured compounds and with F_{254} for uncoloured compounds). The compounds purification was done in general by column chromatography with silica gel 60 with 0.063-0.200 nm (Merck). The preparative thin layer chromatography purifications were performed in glass plates (20x20 cm), previous coated by a layer of silica gel 60 of Merck with 0.5 mm of thick and further activation at 100ºC for 12 h. All of the fractions were monitored by TLC and UV-Vis (between λ = 350 and λ = 800 nm). The Celite ® used for reaction purification was Celite® S (Sigma-Aldrich).

The ^{1}H NMR spectra were recorded in a Bruker AMX 300 NMR spectrometer at 300.13 MHz. $CDCl_3$ was used as a solvent but in some cases other solvents were used and that it is indicated. TMS was used as internal reference. The chemical shifts are expressed in δ (ppm) and the coupling constants (*J*) in Hertz (Hz).

The electrospray ionization mass spectra (ESI^+) were recorded in a mass spectrometer Q-TOF [1µg of sample was dissolved in chloroform or tetrahydrofuran (THF) in 200 µL of 0.1% of formic acid/methanol solution. Nitrogen was used as nebulization gas and argon as collision gas. The needle voltage was set to 3000 V with

an ion source of 80ºC and a desolvation temperature of 150ºC. The cone voltage was 35 V]. The data obtained from the mass spectra are represented in mass/charge of the correspondent ions. These mass spectra were done by the mass spectroscopy group of the chemistry department of University of Aveiro.

Absorption and fluorescence spectra were recorded in DMF using a Shimadzu UV-2501-PC and FluoroMax3 (in 1 cm × 1 cm quartz optical cells), respectively. As reference for measurements of fluorescence quantum yield, Φ_{Flu}, the *meso*-tetraphenylporphyrin (**TPP**) in DMF (Φ_{Flu} =0.11) was used.[104]

2.3.2 Synthesis of 4-bromomethylbenzaldehyde (4)

Manganese oxide (IV) (2.25 g, 25.9 mmol) was added to a solution of 1,4-bis(bromomethyl)benzene **3** (1.5 g, 5.6 mmol) in chloroform (18.0 mL) and the mixture was heated at reflux for 72 h. After this time the reaction mixture was filtered on Celite®. The crude material was taken into CH_2Cl_2 and directly chromatographed by silica column using hexane/CH_2Cl_2 (2:1) as eluent. The first fraction was identified as **3**. The second fraction eluted with hexane/CH_2Cl_2 (1:1) gave the desired aldehyde **4** (212 mg,19%).

1,4-bis(bromomethyl)benzene (**3**). **Aspect**: white solid. **Yield**: 28% (63.3 mg). **^{1}H NMR** (300 MHz, $CDCl_3$): δ (ppm) 4.48 (s, 4H, -CH_2); 7.57 (s, 4H, H-2,6 and H-3,5) ppm.

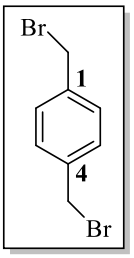

4-Bromomethylbenzaldehyde (**4**). **Aspect**: white crystals. **Yield**: 19% (212 mg). **^{1}H NMR** (300 MHz, $CDCl_3$): δ (ppm) 4.52 (s, 2H, -CH_2); 7.56 (d, 2H, *J* = 8.2 Hz, H-3,5); 7.87 (d, 2H, *J* = 8.2 Hz, H-2,6); 10.02 (s, 1H, CHO) . **MS (ESI (+)):** *m/z* 199 $[M+H]^+$.

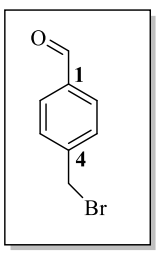

2.3.3 Synthesis of 5,10,15,20-tetrakis(4-bromomethylphenyl)-2-aza-21-carbaporphyrin (1) and 5,10,15,20-tetrakis(4-bromomethylphenyl)porphyrin (5)

Pyrrole (0.18 mL, 2.5 mmol) and aldehyde **4** (500.0 mg, 2.5 mmol) were added to CH_2Cl_2 (250.0 mL) under nitrogen atmosphere protected from light. The reaction started with the addition of methanesulfonic acid (MSA) (0.12 mL, 1.87 mmol). The reaction mixture was stirred for 30 min at room temperature. After this period, it was added DDQ (500.0 mg, 2.2 mmol) to the reaction mixture and it was maintained under stirred for more 30 min at room temperature. The reaction was monitored by TLC and UV-Vis. Then, the reaction was stopped by quenching it with water saturated with Na_2CO_3. The organic layer was separated, dried under Na_2SO_4 anhydrous and the solvent was evaporated under reduced pressure. The crude mixture was purified by column chromatography (silica gel), using CH_2Cl_2/MeOH (95:5) as eluent. The reddish less polar fraction isolated was identified as the porphyrin **5** (141.00 mg, 23%) and the more polar fraction with a green colour, corresponded to compound **1** (56.3 mg, 9%).

5,10,15,20-tetrakis(4-bromomethylphenyl)porphyrin (**5**). **Aspect**: purple solid. **Yield**: 23% (98.95 mg). **^{1}H NMR** (300 MHz, $CDCl_3$): δ -2.82 (s, 2H, *N*-H); 4.86 (s, 8H, -CH_2); 7.80 (d, 8H, *J* = 8.1 Hz, H-2',6'); 8.19 (d, 8H, *J* = 8.1 Hz, H-3',5'); 8.84 (s, 8H, β-H) ppm. **MS (ESI (+))**: *m/z* 987.1 $[M+H]^+$. **UV-Vis** λ_{max} nm (log ε) in DMF: 419 (5.87), 516 (4.42), 551 (4.15), 592 (3.90), 647 (3.85). **Fluorescence** λ_{max} nm in DMF: 652, 717; Quantum Yield (Φ_{Flu}): Φ_{Flu} = 0.11.

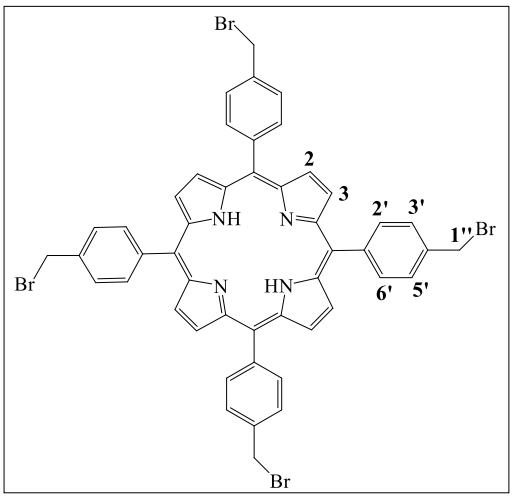

5,10,15,20-tetrakis(4-bromomethylphenyl)-2-aza-21-carbaporphyrin (**1**). **Aspect**:

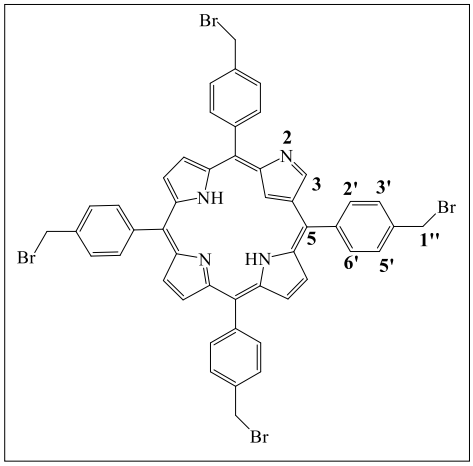

dark green solid. **Yield**: 9% (38.6 mg). **^{1}H NMR** (300 MHz, $CDCl_3$): δ (ppm) -5.0 (s, 1H, inner-CH); 4.82 (s, 4H, -CH_2); 4.84 (s, 4H, -CH_2); 7.80 (d, *J* = 9.2 Hz, 4H, H_m-ph); 7.87-7.91 (m, 4H, H_m-ph); 8.11-8.15 (m, 4H, H_o-ph); 8.22-8.36 (m, 4H, H_o-ph); 8.50-8.65 (m, 4H, β-H); 8.71 (s,1H, H-3); 8.95 (d, *J* = 4.7 Hz, 1H, β-H); 9.0 (d, *J* = 5.1 Hz, 1H, β-H).**MS ((ESI(+))** : *m/z* 987.1 $[M+H]^+$.**UV-Vis** λ_{max} nm (log ε) in DMF: 445 (4.96), 548 (3.91), 595 (3.95); 646 (3.96); 705 (3.98). **Fluorescence** λ_{max} nm; in DMF: 650, 716 Quantum Yield (Φ_{Flu}): Φ_{Flu} = 0.03.

2.3.4 Synthesis of 5,10,15,20-tetrakis(4-(pyridinium-1-yl-methyl)phenyl) porphyrin tetraiodide (6)

Sodium iodide (NaI) (6.55 equiv., 20.0 mg, 0.133 mmol) was added to a mixture of porphyrin **5** (20.0 mg, 0.0203 mmol) in pyridine (3.0 mL). The reaction mixture was stirred for 5 min at room temperature. Then it was filtered with hexane and washed with diethyl ether and a purple solid of **6** (27 mg, 90%) was obtained.

5,10,15,20-tetrakis(4-(pyridinium-1-yl-methyl)phenyl)porphyrin tetraiodide (**6**).

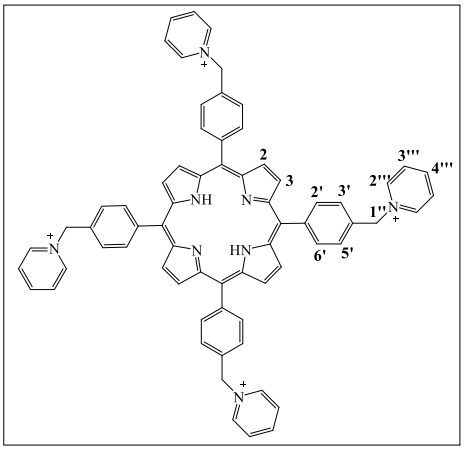

Aspect: purple solid. **Yield**: 90% (27 mg). **^{1}H NMR** (300 MHz, DMSO-d_6): δ (ppm) -3.0 (s, 1H, inner C-H), 6.25 (s, 8H, -CH_2), 7.97 (d, *J* = 8.1Hz, 8H, H-2',6'), 8.29 (d, *J* = 8.1 Hz, 8H, H-3',5'), 8.37 (dd, *J* = 6.7 Hz and *J* = 7.8 Hz, 8H, H-3''', 5'''), 8.76-8.80 (m, 12H, H4''', β-H), 9.51 (d, J = 5.6 Hz, 8H, H- 2''',6'''). **^{13}C NMR** (126 MHz, DMSO-d_6): δ (ppm) 63.22 (-CH_2), 119.38 (C-5), 127.45 (C-3', 5'), 128.46 (C-3''', 5'''), 134.08 (C-4'), 134.95 (C-2', 6'), 141.99 (C-1'), 145.27 (C-2''', 6'''), 146.30 (C-4''', C-β). **MS ((ESI(+))** : *m/z* 245.9 $[M]^{4+}$; 225.6 $[M\text{-}Py\text{-}H]^{4+}$. **UV-Vis** λ_{max} nm (log ε) in DMF: 419

(5.63), 515 (4.49), 551 (4.16); 590 (3.96); 647 (3.87). **Fluorescence** λ_{max} nm in DMF: 651, 716; Quantum Yield (Φ_{Flu}): Φ_{Flu} = 0.10.

2.3.5 Synthesis of 5,10,15,20-tetrakis(4-(pyridinium-1-yl-methyl)phenyl)-2-aza-21-carbaporphyrin tetraiodide (2)

NaI (6.0 equiv. 20 mg, 0.133 mmol) was added to a stirred solution of porphyrin **1** (20 mg, 0.0203 mmol) in pyridine (3 mL). After 30 min at room temperature the reaction was ended. This was confirmed by TLC and the reaction mixture was filtered with hexane and wash with diethyl ether. Then a green dark solid was obtained (24.8 mg, 82%).

5,10,15,20-tetrakis(4-(pyridinium-1-yl-methyl)phenyl)-2-aza-21-carbaporphyrin tetraiodide (2). Aspect: green dark solid. **Yield**: 82% (24.8 mg). **^{1}H NMR** (300MHz, DMSO-d_6 at 50ºC) : δ (ppm) 6.12-6.23 (m, 8H, -CH_2); 7.80-8.03 (m, 16H, H-Ph); 8.11-8.15 (m, 2H, β-H, H-Py); 8.30-8.36 (m, 8H, H-Py); 8.67 (s, 1H, H-3); 8.74(t, J = 7.6, 4H, H-Py); 9.24 (s, 4H, β-H); 9.40-9.49 (m, 8H, H-Py). **MS ((ESI (+))**: *m/z* 274.5 $[M\text{-}2Py\text{-}H]^{3+}$; *m/z* 225.8 $[M\text{-}Py\text{-}H]^{4+}$. **UV-Vis** λ_{max} nm (log ε) in DMF: 453 (4.92), 549 (3.79), 598 (7.89); 643 (3.90); 690 (3.93). **Fluorescence** λ_{max} nm in DMF: 650, 714; Quantum Yield (Φ_{Flu}) : Φ_{Flu} = 0.04.

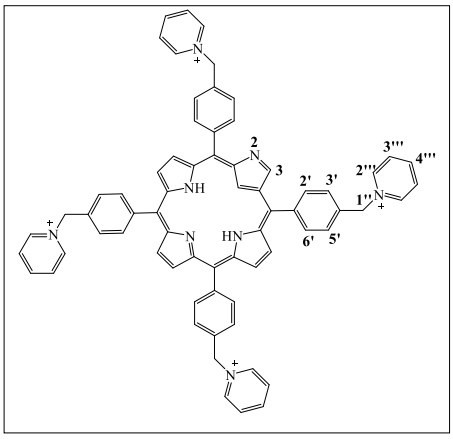

2.3.6 Irradiation conditions for $^1O_2$ generation

A LED array composed by a matrix of 5x5 LED making a total of 25 light sources with an emission peak centred at 640 nm ± 20 nm was used. The irradiance of the LED was 9 $mW.cm^{-2}$ (measured with a light meter LI-COR model LI-250, LI-COR inc., USA)

2.3.7 Singlet oxygen generation

The singlet oxygen production was qualitatively evaluated through absorbance decay of **DPiBF**, a singlet oxygen quencher. Stock solution of each porphyrin at 0.1 mM in DMF was prepared.

A solution of 50 µM of **DPiBF** and 0.5 µM of a porphyrin in DMF in glass cuvette (3 mL) at room temperature and under gentle magnetic stirring was irradiated with a LED array at 640 nm ± 20 nm (red light) with an irradiance of 9 $mW.cm^{-2}$. The absorbance decay of **DPiBF** at 415 nm was measured 1 min irradiation intervals up to 10 min. The solution of **DPiBF** (50 µM) without PS was used to evaluate the **DPiBF** photodecomposition under the irradiation conditions. The graphic reporting Ln (A/A0) for 10 min of irradiation was done, being A the absorbance of the **DPiBF** at 415 nm and A0 the absorbance at 0 min.

CHAPTER 3

Can photodynamic therapy interfere with alternative splicing of mRNA ?

3.1 General remarks

Before doing any assays with the synthesized porphyrins to verify if their ability to induce mRNA alternative splicing in MCF-7 cells under PDT conditions, it is important to establish the experimental conditions (concentration and light dose) to reach 50% of mortality. This is the ideal mortality for the RNA splicing assays in this breast cancer cell line. For that reason, three different methods (WST-1, ATPlite^{TM} and Trypan Blue) to check the MCF-7 cells viability were effectuated. The subcellular localization and cellular uptake was also investigated.

After checking the cell viability, it is also important to know which type of cell death the studied compounds induce after PDT treatment. As it was discussed in chapter 1, there are four main types of cell death: apoptosis, necrosis, necroptosis and autophagy. Cell death type was determined by Western blotting. Protein extracts from MCF-7 cells after the photodynamic treatment were analysed with different antibodies according to the type of cell death under evaluation.

Finally, the possibility of alternative splicing was assessed in MCF-7 cells by extracting the total RNA from cells previous submitted to photodynamic treatment. A reverse transcriptase polymerase chain reaction (RT-PCR) was performed in the total RNA with specific primers. The PCR products were separated by electrophoresis.

All the results presented in this chapter were obtained in GIGA-Institute of University of Liège with the collaboration of Drs Jacques Piette and Yvette Habraken.

3.2 Viability assays

3.2.1 Measurement of cell viability using the Cell Proliferation Reagent WST-1

WST-1 (Water soluble Tetrazolium, sodium (4-[3-(4-Iodophenyl)-2(4-nitrophenyl)-2H-5-tetrazolium)-1,3-benzene disulphate) reagent was selected for spectrophotometric quantification of cell proliferation growth, viability, and chemosensitivity in cell populations using a 96 well-plate. This reagent was chosen because it can be used to analyse the cytotoxicity of certain compounds such as anti-cancer drugs or other pharmaceutical compounds.[109]

The principle of this assay is based on the reduction of tetrazolium salt into formazan by cellular enzymes (**Scheme 12**).[110] So, if the cells are dead there is a decrease in the overall activity of mitochondrial dehydrogenases in the sample.[110] The

diminishment of enzyme activity leads to a decrease in the amount of formazan dye formed, which is directly correlated with the number of deceased (metabolically inactive) cells in culture. The quantification of the formazan dye produced by metabolically active cells is done by a spectrophotometer where the absorbance at 450 nm is measured against the background control at 690 nm.[109]

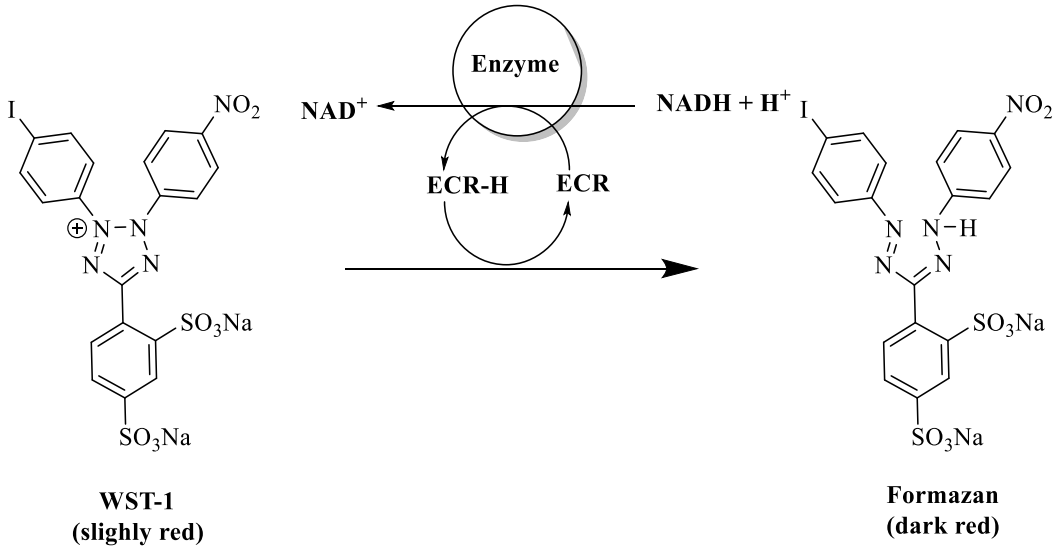

Scheme 12. Cleavage of the tetrazolium salt WST-1 by its reduction to formazan. The enzyme involved is the mitochondrial succinate-tetrazolium-reductase system. ECR: Electron coupling reagent.

3.2.1.1 Cell viability assay with WST-1 in HeLa Cells

In the first assays HeLa cells were used. First, after plating the cells in 96-well plates each compounds **1**, **2**, **5**, **6** and **TMPyP** was added at a concentration of 5.0 μM. **TMPyP** was used as a positive control for the synthesized compounds because it is known that it is a good PS in PDT.[99] Camptothecin (**CPT**) was also added as a positive control at a concentration of 20 μM. Light and dark controls were also included. The cells were incubated with each compound for 3 h and then irradiated with red light for 15 min with a wavelength >640 nm and an irradiance of 23.70 mW/cm^2. After 24 h of dark incubation, 10.0 μL of WST-1 was added for 30 min to each well. Then, the absorbance at 450 nm was measured as well as at 690 nm for the background. The "corrected" absorbance was calculated by subtracting the absorbance at 450 nm from the absorbance at 690 nm. The cell survival was calculated by doing the relationship between the treated and the control cells both in presence of light. The results are summarized in **Figure 27** and **Table 4**

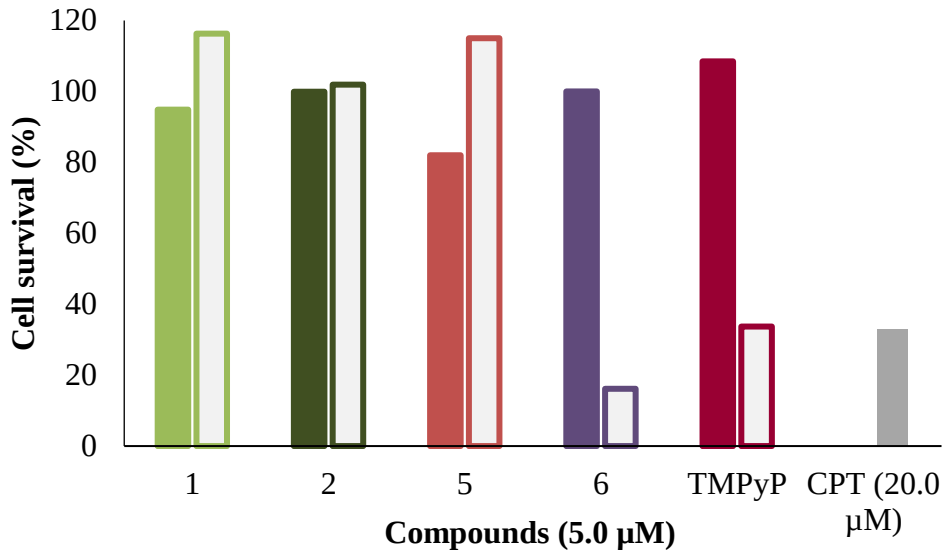

Figure 27. Survival rates of HeLa cells incubated with 5.0 µM of each PS and 20 µM of CPT for 3 h, then irradiated for 15 min (contoured bars) with red light (λ > 640 nm) at an irradiance of 23.70 mW/cm^2 or kept in the dark (full coloured bars).

Table 4. Percent survival of HeLa cells incubated with 5.0 µM of each PS and 20 µM of CPT for 3 h, then irradiated for 15 min with red light (λ >640 nm) at an irradiance of 23.70 mW/cm^2 or kept in the dark.

Compound	Cell Survival in the dark (%)	Cell survival after PDT (%)
1 (5.0 µM)	94.9	116.3
2 (5.0 µM)	99.9	101.9
5 (5.0 µM)	82.0	115.0
6 (5.0 µM)	100.0	16.2
TMPyP (5.0 µM)	108.5	33.7
CPT (20 µM)	_____	32.8

The results obtained in **Figure 27** and **Table 4** show that the phototoxic effect is more pronounced with compound **6** (16.2%), being even higher than the positive controls **CPT** (32.8%) and **TMPyP** (33.7%) used.

3.2.1.2 Cell Viability assay with WST-1 in MCF-7 Cells

After the preliminary results, MCF-7 cells (human breast adenocarcinoma cell line) were selected to perform the experiments as they exhibit strong AS with numerous chemotherapeutic drugs. Different concentrations of derivatives **1**, **2**, **5** and **6** (1.0 and 5.0 µM) were administrated to cell cultures and the cells were submitted to the photodynamic treatment. A light and dark controls were also included. After 24 h the WST-1 reagent

was added and the absorbance was measured after 1 h. The survival rates obtained (**Figure 28** and **Table 5**) show that no significant dark cytotoxicity was observed at concentrations up to 5.0 µM. (**Figure 28-B**)

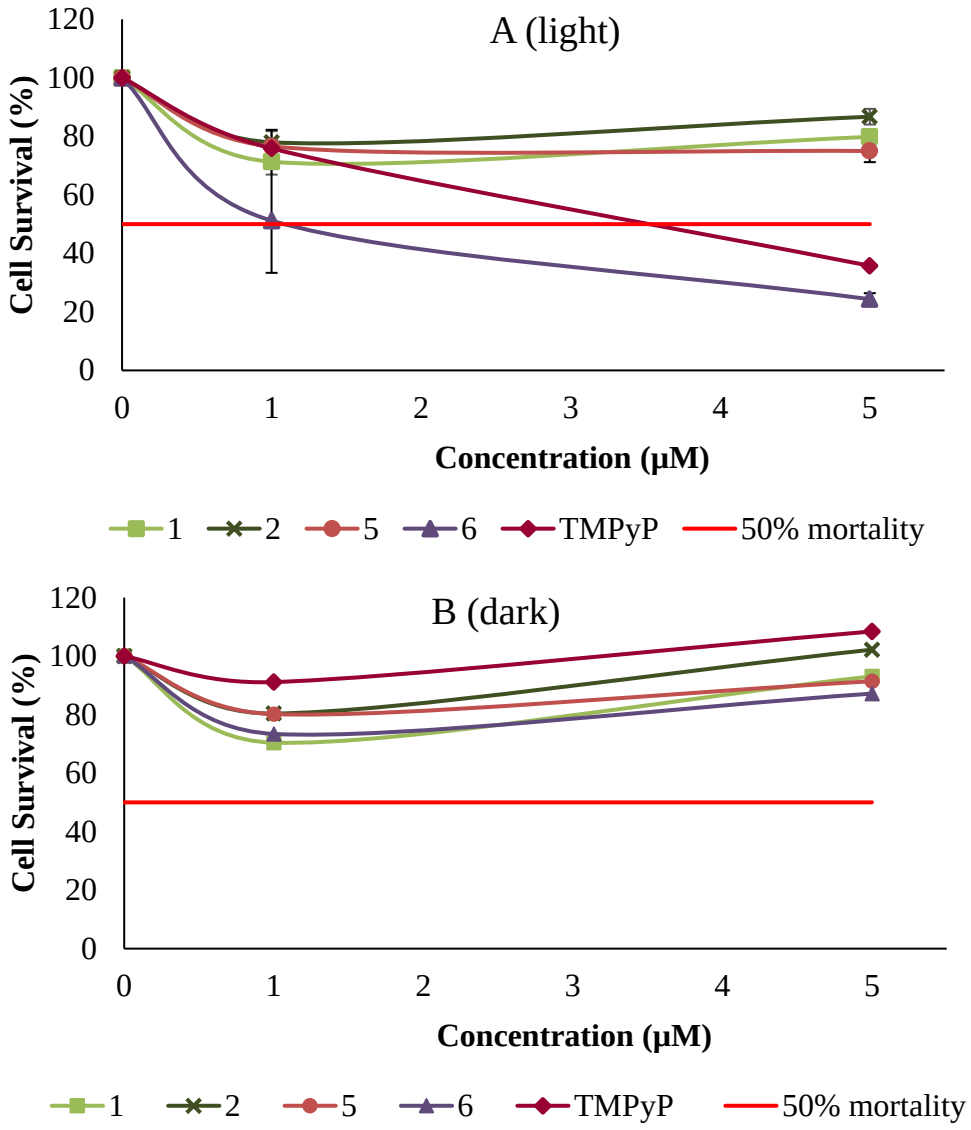

Figure 28. Survival rates of MCF-7 cells incubated with 1.0 µM and 5.0 µM of each PS for 3 h, then irradiated for 15 min (A) with red light (λ > 640 nm) at an irradiance of 23.70 mW/cm^2 or kept in the dark (B)

Table 5. Percent survival of MCF-7 cells incubated with 1.0 µM and 5.0 µM of each PS for 3 h, then irradiated for 15 min with red light (λ > 640 nm) at an irradiance of 23.70 mW/cm^2 or kept in the dark.

Compound	1.0 µM		5.0 µM	
	Dark	Light	Dark	Light
1	70.40	71.32 ± 4.39	93.07	79.83 ± 0.92
2	80.36	77.97 ± 3.80	102.19	86.72 ± 2.68
5	80.16	76.58 ± 2.38	91.40	74.99 ± 3.80
6	73.40	51.20 ± 17.85	87.16	24.34 ± 2.06
TMPyP	91.11	75.88 ± 6.37	108.42	35.8
CPT	20 µM			
	Dark		Light	
	69.01 ± 0.98		79.83	

Regarding the irradiated cells, it is possible to observe that only compound **6** and **TMPyP** can kill more than 50% of the cells after 15 min of irradiation and at a concentration of 5.0 µM. However, porphyrin **6** at a concentration of 1.0 µM was able to kill almost 50% of cells (cells survival 51.20 %). It is important to highlight that the cell photokilling is not cell line dependent.

After this assay, only compound **6** and **TMPyP** were selected to proceed with the photodynamic therapy assays in order to assess if the cell killing is dose-dependent and/or light-dependent. So the cell cultures were incubated for a period of 3 h in the presence of non-cytotoxic concentrations of each porphyrin (0.1 µM-5.0 µM) and then submitted to different times of irradiation (5, 10 and 15 min) with a wavelength >640 nm and an irradiance of 23.70 W/m^2. After 24 h, WST-1 reagent was added and the absorbance measured after 1 h. The results obtained for the cell survival (see **Table 6** and **Figure 29**) show that the synthesized derivative **6** seems to be a better PS than the well-known **TMPyP** selected as positive control.

Table 6. Percent survival of MCF-7 cells incubated with 0.1, 0.25, 0.5, 1.25, 2.5 and 5.0 µM of porphyrin 6 and TMPyP for a period of 3 h, then irradiated for 15 min with red light (λ > 640 nm) at an irradiance of 23.70 mW/cm^2 or kept in the dark.

Porphyrin 6				
Concentration (µM)	**Dark control**	**Irradiation time (min)**		
		5	**10**	**15**
0.10		110.6 ± 6.2	105.3 ± 5.6	109.1 ± 10.5
0.25		110.0 ± 4.6	93.2 ± 21.4	99.0 ± 17.3
0.50		105.8 ± 5.6	108.8 ± 5.1	67.2 ± 13.7
1.25		97.1 ± 6.6	70.6 ± 11.4	27.5 ± 6.15
2.50	103.5 ± 10.7	87.0 ± 7.5	33.5 ± 10.7	22.5 ± 3.9
5.0	104.3 ± 10.7	55.9 ± 19.7	28.0± 4.3	26.3 ± 7.8
Porphyrin TMPyP				
Concentration (µM)	**Dark control**	**Irradiation time (min)**		
		5	**10**	**15**
0.10		11.23 ± 7.68	106.97 ± 9.82	116.95 ± 18.17
0.25		117.17 ± 5.71	117.9 ±4.16	119.95 ± 23.83
0.50		116.63 ± 10.06	109.73 ± 11.21	117.85 ± 23.26
1.25		114.70 ± 11.88	109.77 ± 10.35	85.35 ± 9.97
2.50	127.57 ± 17.25	119.73 ± 14.66	114.73 ± 9.87	51.00 ± 12.73
5	141.47 ± 17.68	125.70 ± 20.30	97.60 ± 20.88	39.15 ± 5.87

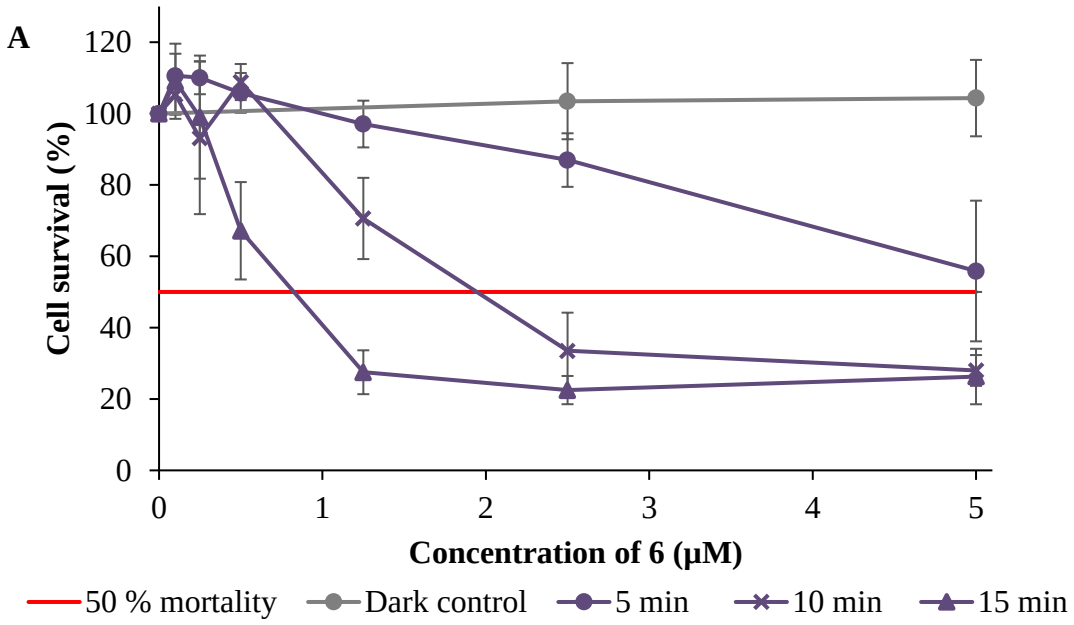

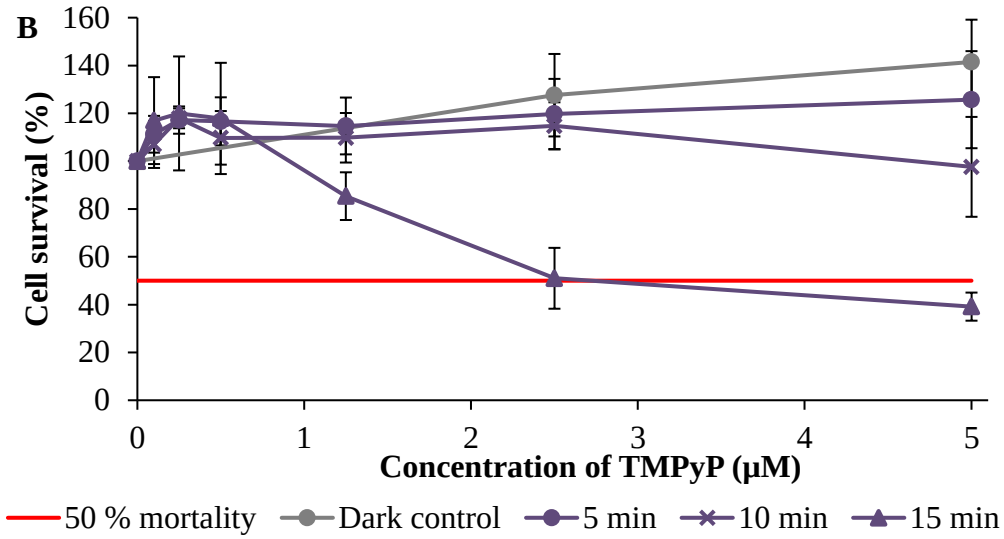

Figure 29. Survival rates of MCF-7 cells incubated with 0.10, 0.25, 0.50, 1.25, 2.5 and 5.0 µM of porphyrin 6 (A) and TMPyP (B) for 3 h, then, irradiated for 15 min with red light (λ >640 nm) at an irradiance of 23.70 mW/cm^2 or kept in the dark.

These results show that the cell photokilling is dependent in both cases of PS concentration and irradiation time (**Figure 29** and **Table 6**).

Regarding porphyrin **6**, for concentration of 1.25 µM there is a difference between the mortality using 10 or 15 min of irradiation with a significance level of 0.07. (95% of confidence). On the other hand, for concentrations of 2.5 µM the difference between the mortality by using 10 or 15 min of irradiation is not statistically significant (p = 0.24). It is important to highlight that a high photocytotoxicity (survival fractions of about 20%) can be observed when using porphyrin **6** at concentration 2.5 µM and after 15 min of irradiation. However, there is no significant difference between concentrations 2.5 and 5.0 µM at 10 and 15 min of irradiation because the mortality is already too high (p = 0.53).

As it can be seen in **Figure 29** and **Table 6**, **TMPyP** only can induce approximately 50% mortality with 15 min of irradiation and only with a concentration of 2.5 µM. The maximum mortality (39.15% of cell survival) is achieved with 15 min of irradiation at a wavelength of 640 nm and an irradiance of 23.70 mW/cm^2 and at a PS concentration of 5.0 µM.

However, it was proved that due to their colour both porphyrin **6** and **TMPyP** could interfere with the absorbance of WST-1 reagent. It is to be noted that the interference of the **TMPyP** is more pronounced. For this reason, another cell viability test called ATPlite^{TM} assay was used to see if the results with this new test are concordant with the ones obtained with WST-1 reagent.

3.2.2 Cell viability assay using ATPlite™ kit

ATP (adenosine triphosphate) is a molecule responsible for energy storage in every living cell. For this reason, its monitorization can be an alternative for the usual cell survival assays. That is the case of the ATPlite™ kit which is an ATP monitoring system based on firefly (*Photinus pyralis*) luciferase (**Figure 30**). This luminescence assay can be used as an alternative to colorimetric and quantitative evaluation of proliferation due to its advantages regarding high sensitivity and excellent linearity.[111,112]

This method is based on production of light induced by the reaction of ATP luciferase and D-Luciferin (the last two added).

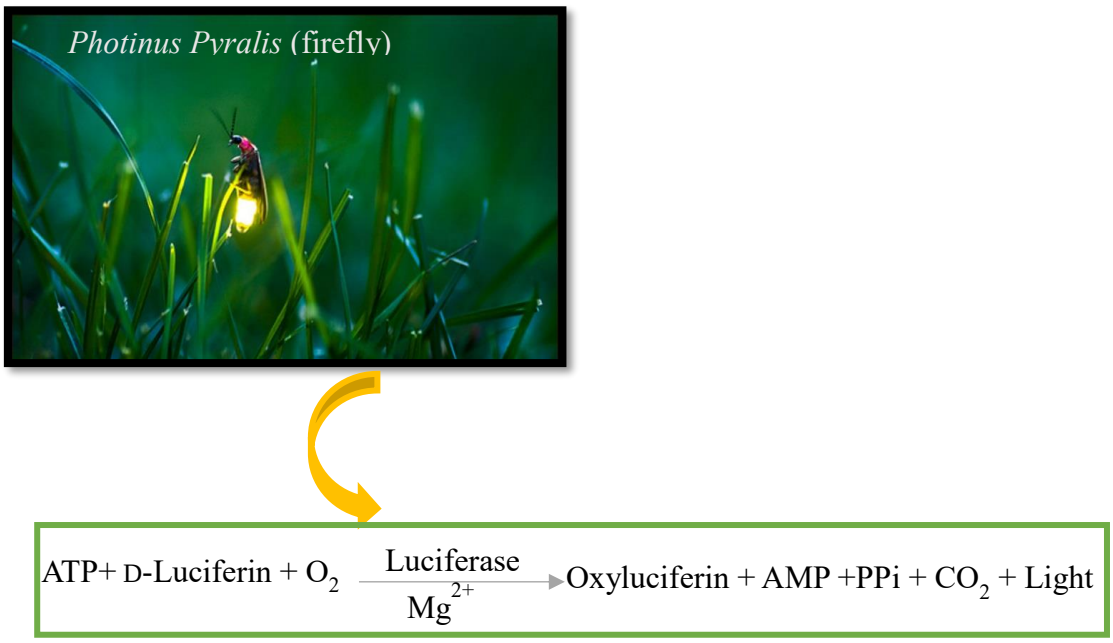

Figure 30. ATPlite™ method basis

It is known that the concentration of ATP declines when cells die. So, the concentration of ATP can be estimated because it is proportional to the light emitted and by measuring the light emitted it is possible to calculate the percentage of cell death.

4.2.2.1 Dose dependence assay

Porphyrin **6** and **TMPyP** were added to MCF-7 cell cultures and then incubated for 3 h in the dark. Concentrations of 1.25 µM, 2.5 µM and 5.0 µM were selected for porphyrin **6** and 5µM and 10 µM for **TMPyP**. This concentrations selection was based on the percentages of survival detected by WST-1. That range of concentration should give more or less 50% survival. All the cells were incubated with the studied PS at the

selected concentrations but a group of cells was irradiated for 15 min with a wavelength of >640 nm and an irradiance of 23.70 mW/cm^2 and another group was kept in dark. After 24 h the ATPlite^{TM} cell viability test was done and the results are shown in **Figure 31** and **Table 7**.

Table 7. Percent survival of MCF-7 cells using ATPlite^{TM} incubated with 1.25, 2.5 and 5.0 µM of porphyrin 6 and 5 µM and 10 µM TMPyP in the dark for a period of 3 h and kept in the dark or irradiated for 15 min with red light (λ >640 nm) at an irradiance of 23.70 mW/cm^2. The cell survival was analysed after 24 h.

Compound	Concentration (µM)	Irradiation time (min)	Dark controls	Cell Survival (%)
6	1.25	15	88.14 ± 3.83	82.81 ± 12.46
	2.5		87.43 ± 4.19	68.81 ± 17.20
	5.0		96.66 ± 19.92	38.80 ± 11.49
TMPyP	5.0		100.69 ± 16.63	77.52 ± 7.24
	10		91.25 ± 18.28	76.28 ± 32.20

Porphyrin **6** shown higher phototoxic activity than **TMPyP** at the same concentration (5.0 µM) after 15 min of irradiation reaching a cell survival of 38.80% and 77.52%, respectively. Even at 10 µM, **TMPyP** was not able to reach 50% of mortality. Although, these results were different from the WST-1 assay the main conclusion is that porphyrin **6** has a higher photokilling effect on MCF-7 cells than **TMPyP**.

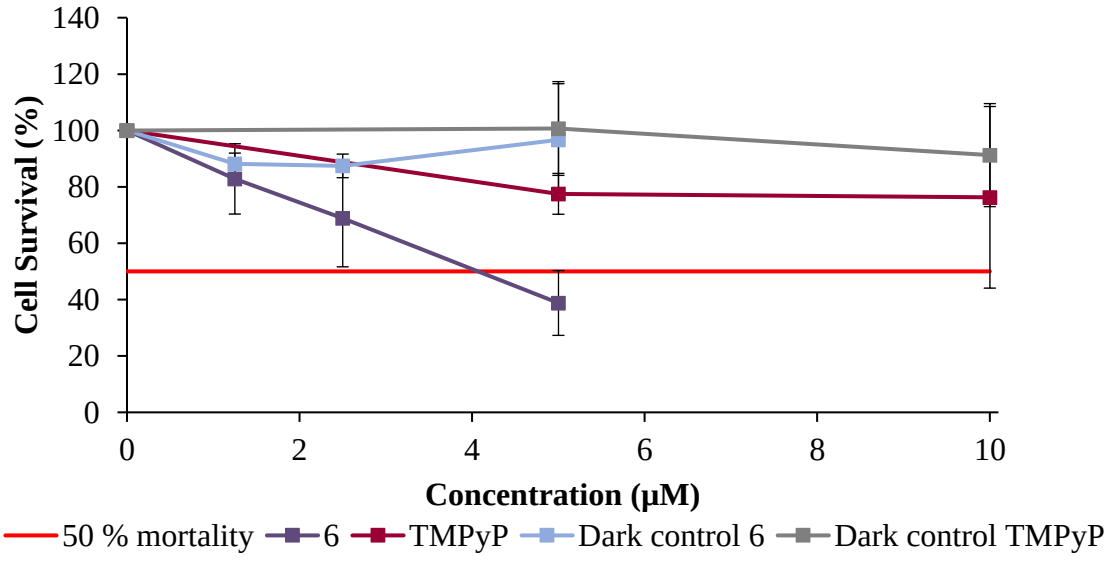

Figure 31. Survival rates of MCF-7 cells using ATPlite^{TM} incubated with 5.0 µM of porphyrin 6 and 10 µM of TMPyP in the dark for a period of 3 h and kept in the dark or irradiated for 15 min with red light (λ >640 nm) at an irradiance of 23.70 mW/cm^2.

4.2.2.2 Time post-PDT dependence assay

A time-dependence assay was conducted to see if the photocytotoxicity effect increases with time after irradiation. So, after a 3h incubation with compounds **6** and **TMPyP** at concentrations of 5.0 µM and 10 µM, respectively, MCF-7 cells were irradiated for 15 min with a wavelength >640 nm and an irradiance of 23.70 mW/cm^2. Then, the ATPlite™ assay was performed at 0, 3, 6 and 19 h after irradiation. The concentrations used were selected according to the dose-dependence assay results. The results obtained are shown in **Figure 32** and **Table 8** .

Table 8. Percent survival of MCF-7 using ATPlite^{TM} cells incubated with 5.0 µM of porphyrin 6 and 10 µM of TMPyP in the dark for a period of 3 h and kept in the dark or irradiated for 15 min with red light (λ >640 nm) at an irradiance of 23.70 mW/cm^2. Different times of incubation after PDT were used to calculate the cell survival percentages.

6 (5.0 µM)			**TMPyP (10 µM)**	
Dark controls	**Cell Survival (%)**	**Time after irradiation (h)**	**Dark controls**	**Cell Survival (%)**
74.33	105.32 ± 12.94	0	75.15	73.00 ± 8.45
86.80	77.78 ± 31.06	3	98.25	71.54 ± 23.55
63.22	73.19 ± 18.85	6	74.87	82.29 ± 18.73
108.25	27.20 ± 13.63	19	137.36	78.09 ± 18.55
96.66 ± 19.92	38.80 ± 11.49	24	91.25 ± 18.28	76.28 ± 32.20

The results show that after 3 h after irradiation, both compounds do not induce significant cell death. However, 19 h post-irradiation a significant photocytotoxicity effect appears for porphyrin **6**, being the cell survival percentage of 27.20%. Regarding **TMPyP**, 19 h or 24 h are not sufficient for reaching 50% of cell mortality.

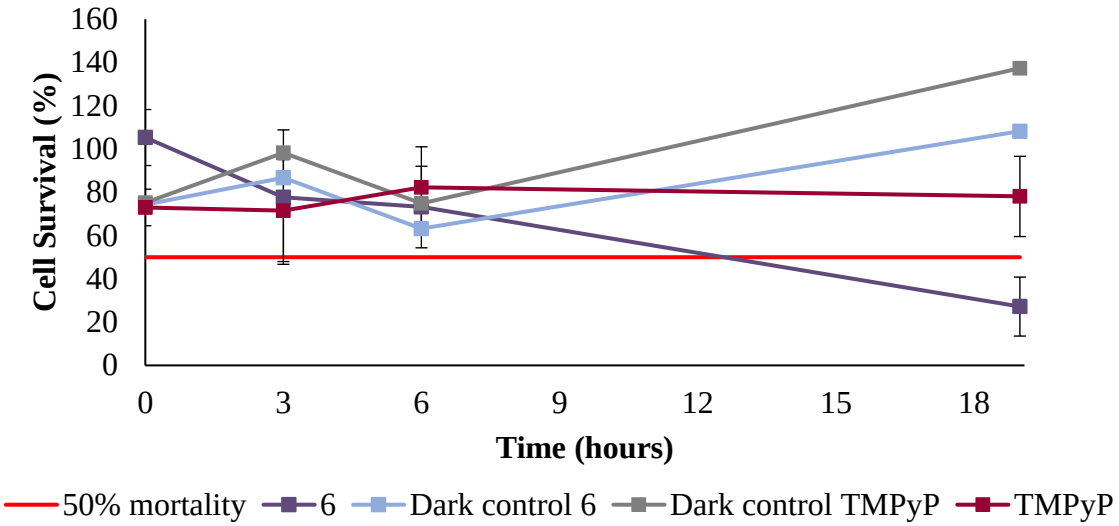

Figure 32. Survival rates of MCF-7 cells using ATPlite™ incubated with 5.0 μM of porphyrin 6 and 10 μM of TMPyP in the dark for a period of 3 h and kept in the dark or irradiated for 15 min with red light (λ >640 nm) at an irradiance of 23.70 mW/cm^2. Different times of incubation after PDT were used to calculate the cell survival percentages.

Regarding time-dependence assay, it is better to leave the cells for 24 h (more than the 19 h used) in the incubator before doing the assay in order to get a low cell survival percentage for porphyrin **TMPyP**. Despite of having already a low cell survival percentage within 19 h samples (27.20 ±11.49 %), porphyrin **6** should be in the incubator for the same time as **TMPyP** in order to be able to compare each other's cell mortality.

Concerning the dose dependence assay, the difference between the two methods is statically significant (p = 0.013) and for that reason is not possible to compare both methods or even to know which one is better. The only conclusion that is possible to take is that **6** is a better PS than **TMPyP**.

3.2.3 Cell viability assay using Trypan Blue

A third assay named trypan blue exclusion was also used, in order to confirm the cell viability results obtained by ATPlite™ and WST-1 assays. This type of assay is currently used in PDT field, so it was considered important to validate the previous results.

Trypan blue is a dye used for dye exclusion procedures for viable cell counting. The method is based on a simple principle: live/viable cells actively excluded certain dyes while death/non-viable cells do not.[113]

Different concentration of porphyrin **6** (0.75; 1.25; 2.5 and 5.0 µM) and **TMPyP** (2.5; 5 and 10 µM) were administrated to MCF-7 cell cultures which was followed by a incubation period in the dark for 3 h. Then, one set of cells was irradiated for 15 min with red light with a wavelength of 640 nm and an irradiance of 23.70 mW/cm^2 and the other was kept in the dark. After irradiation, the cells were placed in the incubator for 24 h. Then the trypan blue was added and pictures of the cells were taken after washing. The results are represented in **Figure 33** and **Figure 34**.

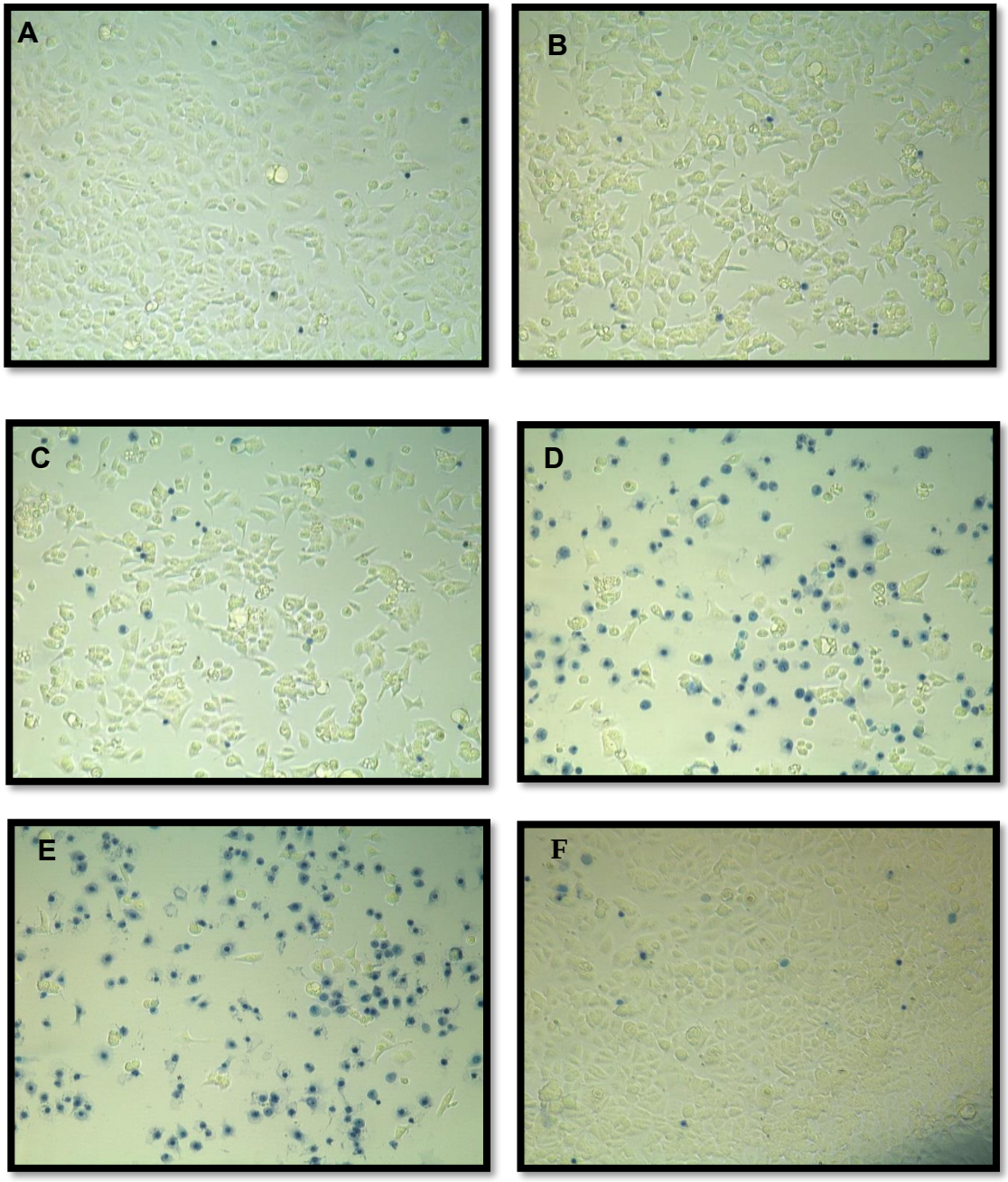

Figure 33. Cell mortality using trypan blue in MCF-7 cells after 3 h incubation with porphyrin 6, then irradiated for 15 min with a wavelength >640 nm and an irradiance of 23.70 mW/cm^2 or kept in the dark. The concentrations used are 0 µM (A); 0.75 µM (B); 1.25 µM (C); 2.5 µM (D); 5.0 µM (E) and dark control 5 (F)

In **Figure 33** are shown the results obtained with porphyrin **6**, and it is clear that there is an increase in the mortality when the concentration was increased from 0 µM (A) to 5.0 µM (E); at the highest concentration, almost every cell is dead (**E**). Nor light nor the PS **6** at the highest concentration (5.0 µM) without irradiation affect the mortality of MCF-7 cells. These results are consistent with ATPlite^{TM} and WST-1 assays where with 5.0 µM and 15 min irradiation it was observed 38.8% and 24.34% of cell survival, respectively.

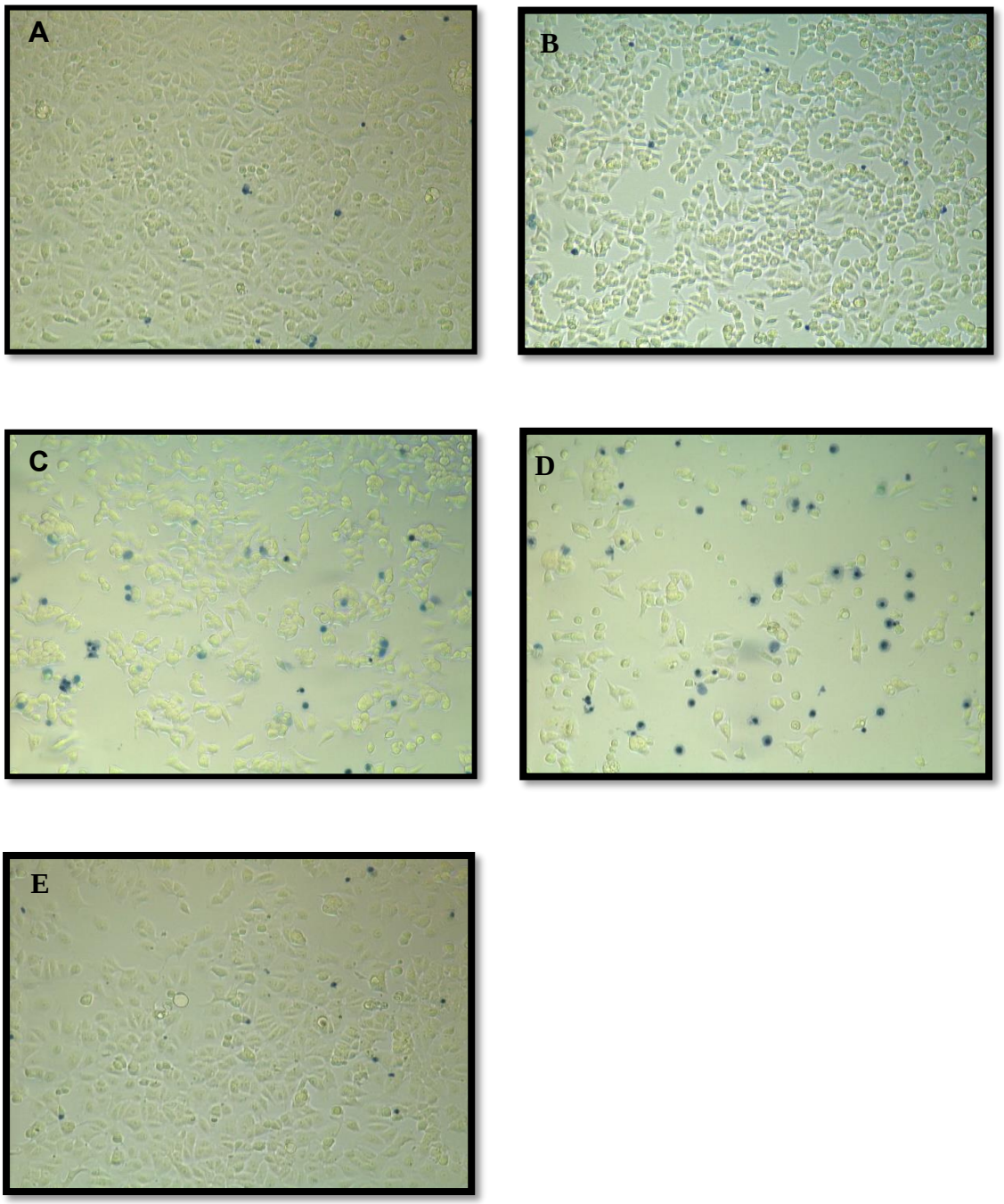

Figure 34. Cell mortality using trypan blue in MCF-7 cells after 3 h incubation with porphyrin TMPyP, then irradiated for 15 min with a wavelength >640 nm and an irradiance of 23.70 mW/cm^2 or kept in the dark. The concentrations used are 0 µM (A); 2.5 µM (B); 5.0 µM (C); 10 µM (D) and dark control 10 µM (E).

Regarding **TMPyP** (**Figure 34**) similar results were observed although the cell death was not so extensive as with porphyrin **6** (**Figure 33**). These results can illustrate the percentages obtained with ATPlite^{TM} assays where with 15 min of irradiation and at 5 μM it was observed 77.52% of cell survival. However, with the same conditions and using WST-1 assay the percentage obtained for cell survival was 39.15% which is not in agreement with the results represented in **Figure 34-C** picture.

3.3 Cellular uptake

The cellular uptake in MCF-7 cells was monitored through intracellular fluorescence using only the fluorescent regular porphyrins **5**, **6** and **TMPyP.** In these experiments the fluorescence spectrum was taken and compared with the one of the correspondent porphyrin. The cells were incubated with each porphyrin for 4 h at 10 μM. Then, they were washed with PBS for 1 min and DMSO was added for 10 min under gentle stirring. Finally, the fluorescence was read at different wavelengths according to each porphyrin's absorption spectrum. A negative (MCF-7 cells by itself) control and a fluorescence spectrum of the compound after washing were made and the results are presented in **Figure 35**.

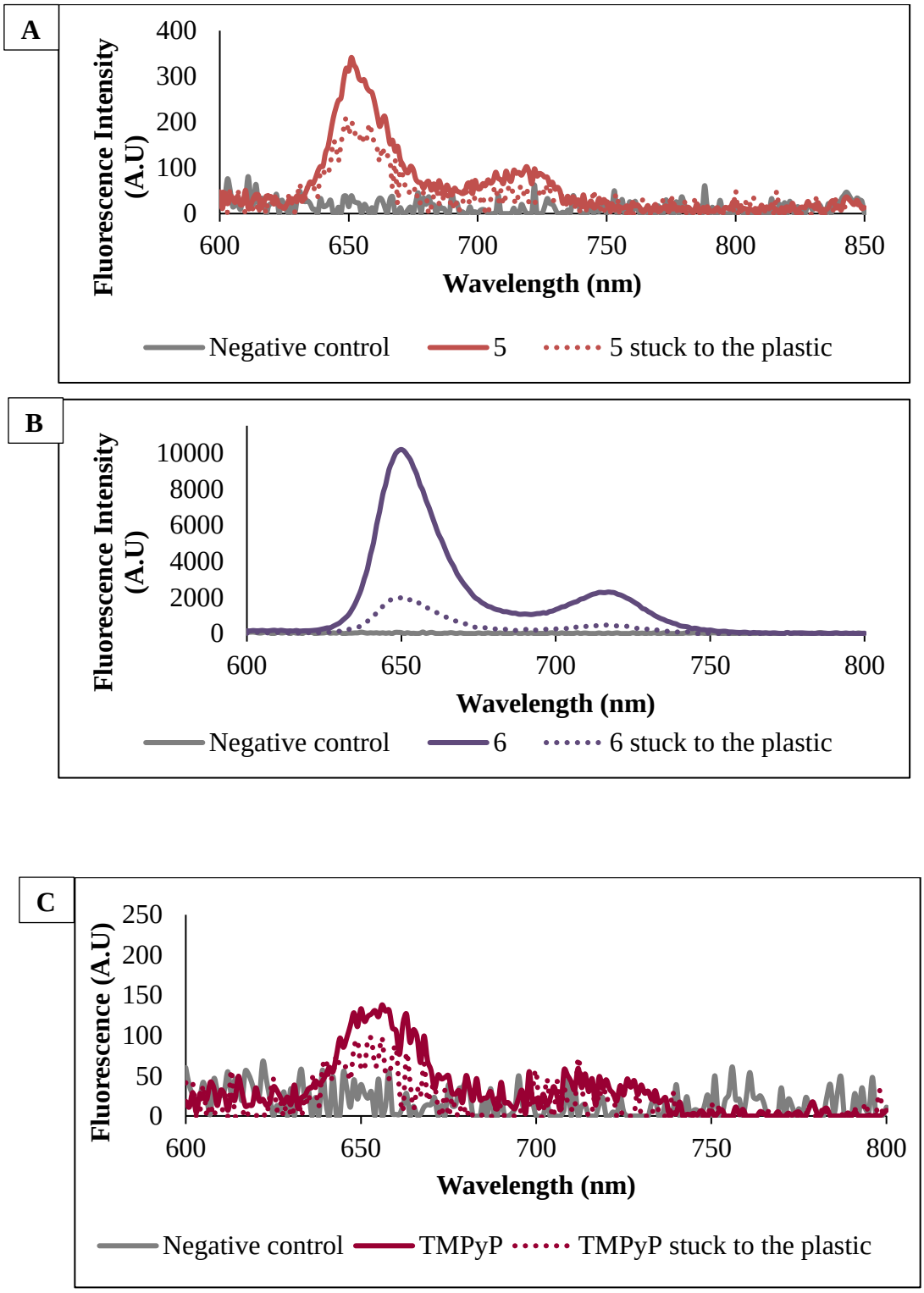

Figure 35. Fluorescence spectra of porphyrins 5 (C- λ_{exc}= 425 nm), 6 (D- λ_{exc}= 425 nm) and TMPyP (E- λ_{exc}= 425 nm) in DMSO/DMEM. Negative control represents MCF-7 cells by itself and the positive control just porphyrin.

In **Figure 35** is clear that the highest uptake by MCF-7 cells was attained with porphyrin **6** (**B**), followed by porphyrin **5** (**A**) despite its neutral character. There was a

very limited uptake of **TMPyP** (**C**) by MCF-7 cells. This can be seen when comparing the spectrum of **TMPyP** with the **TMPyP** that stuck to the plastic.

3.4 Subcellular localization

The efficiency of a photosensitizer depends on its subcellular localization. Moreover, the lifetime and diffusion length of $^1O_2$ are very short (0.5 and 0.1 μs respectively).[114] Thus, the initial oxidative reaction will occur in subcellular organelles in which the PS are located.[115] The subcellular localization of porphyrins **5**, **6** and **TMPyP** in MCF-7 cells was determined by considering the red fluorescence emission (λ= 607-708 nm) after being excited with violet radiation (λ=448 nm). The subcellular localization of porphyrins **1** and **2** was not determined since they are not fluorescent.

The previous results confirmed that porphyrins **5**, **6** and **TMPyP** enter in the cells. From literature it is known that **TMPyP** accumulates in the nucleus,.[116] So, in this assay the cells were stained with Hoescht, a fluorescent marker for the nucleus in order to verify this possibility.

So, MCF-7 cells were incubated for 3 h with all porphyrins, using a concentration of 10 μM for **TMPyP** and 5.0 μM for porphyrins **5** and **6**. The results are shown in **Figure 36**.

In the cell controls no PS was added, but the fluorescence was measured in the same conditions in order to see if the cell or the medium fluorescence interferes with the compound.

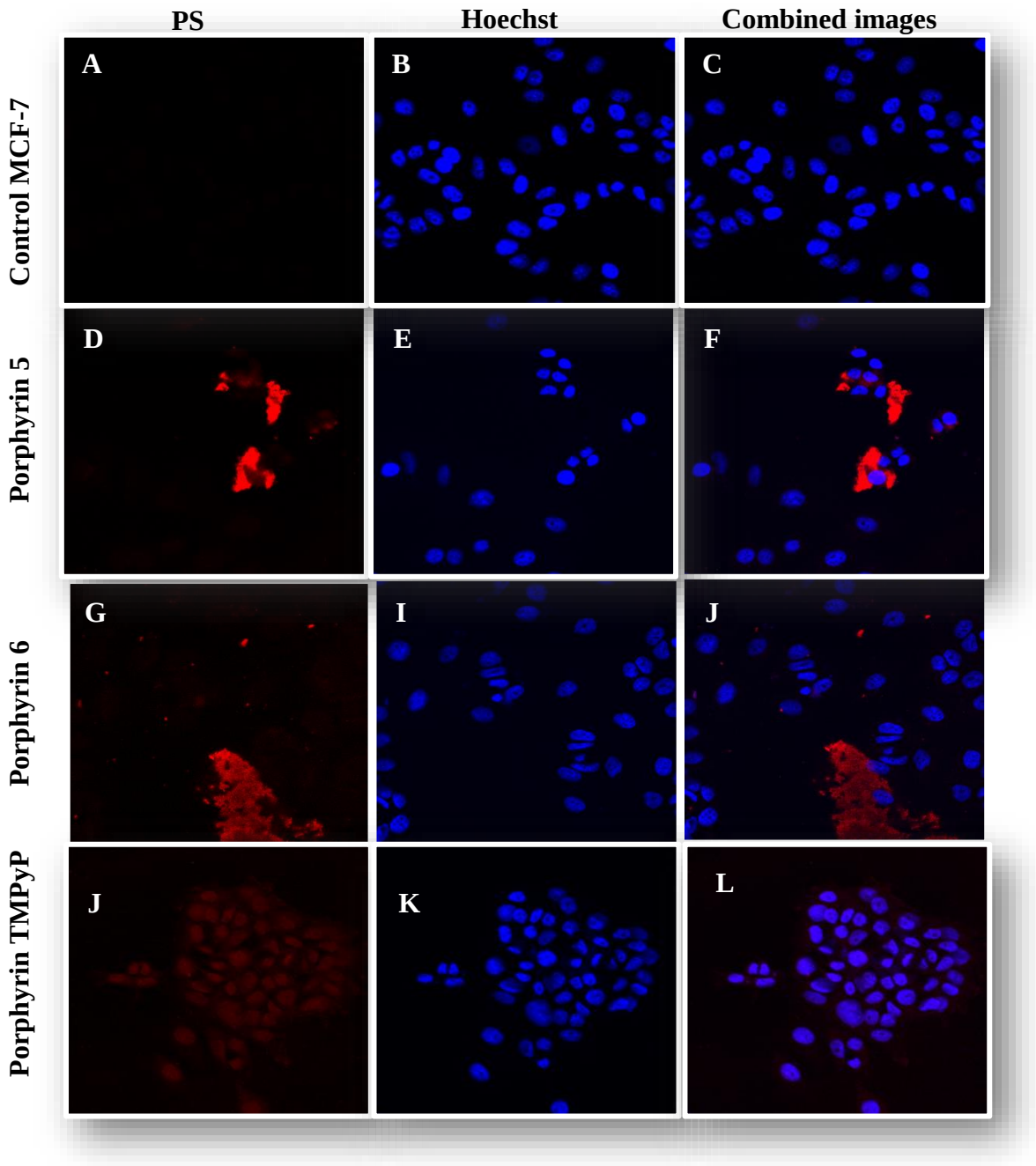

Figure 36. Intracellular localization of porphyrin 5 (D-F), 6 (G-J) and TMPyP (J-L) in MCF-7 cells after incubation with each derivative for 3 h at 5.0 μM in Dulbecco's Modified Eagle's Medium (DMEM). A, D and G concerns the fluorescence of porphyrins, B, E, I the Hoechst fluorescence and C, F, J the overlay images. Controls were also made (A-C).

It is described in literature that the sub-localization of the PS is dependent mainly of its charge. For example, cationic porphyrins have high affinity to the nucleus, particularly **TMPyP** which can induce apoptosis after PDT due to DNA damage.[116]

Porphyrin **TMPyP** was clearly localized in the nucleus, as seen in (**Figure 36 J-L)**. A different situation was observed with the neutral porphyrin **5 (Figure 36 D-F)** and

also with the charged porphyrin **6** (**Figure 36 G-J)** where no porphyrin localization was detected in the nucleus

These results show that porphyrin **6,** despite of being cationic and inducing the highest mortality after PDT, does not accumulate in the nucleus. However, the accumulation in other organelles can be considered as it is described in the literature for other cationic porphyrins.[116]

3.5 Type of cell death induced by photodynamic therapy with porphyrin 6 and TMPyP

3.5.1 General background

There are three main types of cell death: apoptosis, autophagy and necrosis/necroptosis. So, it was decided to study and assess the type of cell death induced by PDT with porphyrin **6** and **TMPyP.**

As it was said before, DNA damage can induce programmed cell death like apoptosis. There are several markers for this type of cellular death such as caspase-3, -7 or PARP-1. The antibodies for these proteins can be used in a western blot in order to detect if the apoptosis process is present. Given that MCF-7 cells do not have caspase-3, PARP-1 cleavage was followed as an apoptosis marker. This is the most common marker used for study this type of cell death and has good results regarding camptothecin (**CPT**) that was also used as a positive control for this study. It is known that during apoptosis process the cleavage of full length PARP-1 (116 kDa) is generated by caspase-3 and 7 into two fragments of 89 kDa and 24 kDa (**Figure 37**).[117]

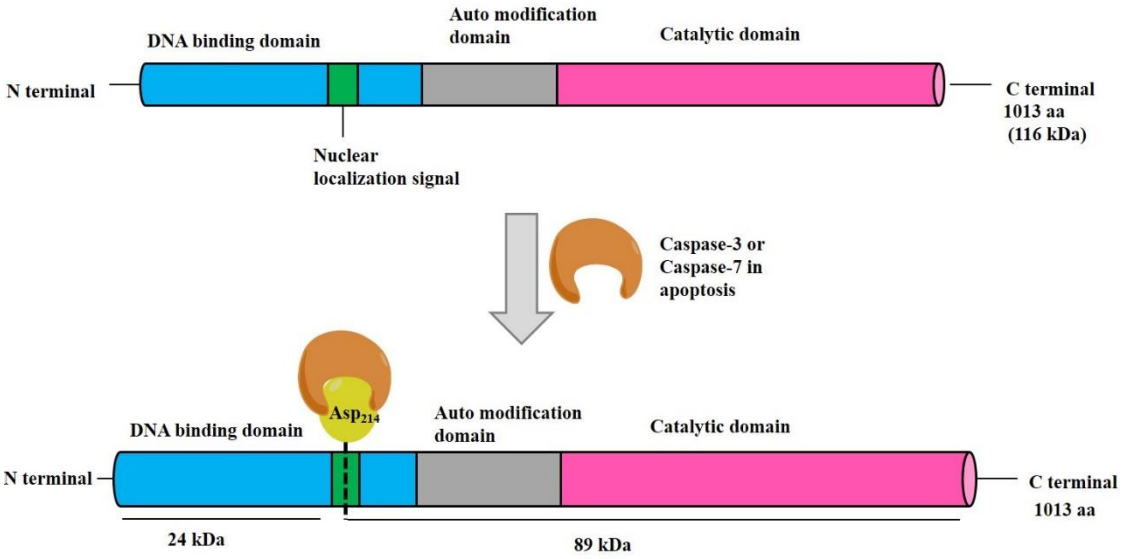

Figure 37. PARP-1 (116 kDa) cleavage between Asp214 and Gly215 by caspase-3 or -7 in apoptosis into two fragments with 24 kDa and 89 kDa.[118]

There are several ways to monitor if the cells undergo necrosis including a cleavage of PARP-1. However, in this case there are two main enzymes responsible for this cleavage: cathepsins and papains. If the first type of enzymes cleaves PARP-1, it can origin the formation of the fragments with 42 kDa and 55 kDa or 62 kDa and 55 kDa. On the other hand, the fragments derived from PARP-1 cleavage with papains have 42 kDa and 72 kDa or 42 kDa and 55 kDa (**Figure 38**).[118] So, in order to have a single membrane with the results for the apoptotic and necrotic pathway, a primary PARP antibody that can recognize both the necrotic and apoptotic fragments was used.

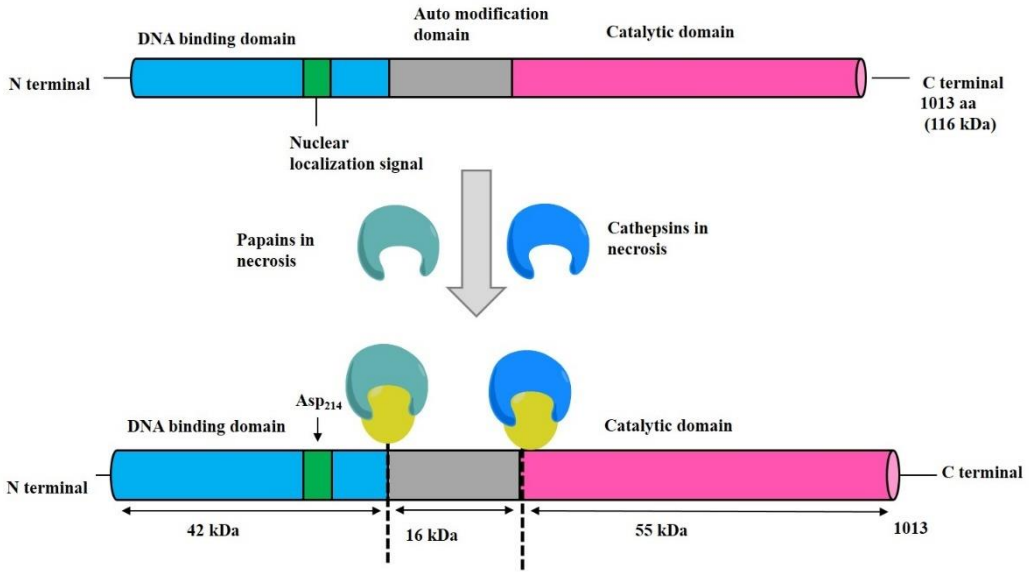

Figure 38. PARP-1 (116 kDa) cleavage by cathepsins in necroptosis into two fragments with 42 kDa and 55 kDa.[118]

Autophagy is essential for cell maintenance and cell viability. There are many proteins involved in the formation of the autophagossome including LC3-II. This protein can be used as a marker for autophagy due its location in the autophagossome. LC3-II is originated from the modification of LC3-I. So when the autophagic flux is activated, it is expected to appear in the western membrane a band representing LC3-II while there is a disappearance of LC3-I (**Figure 39**).[119,120]

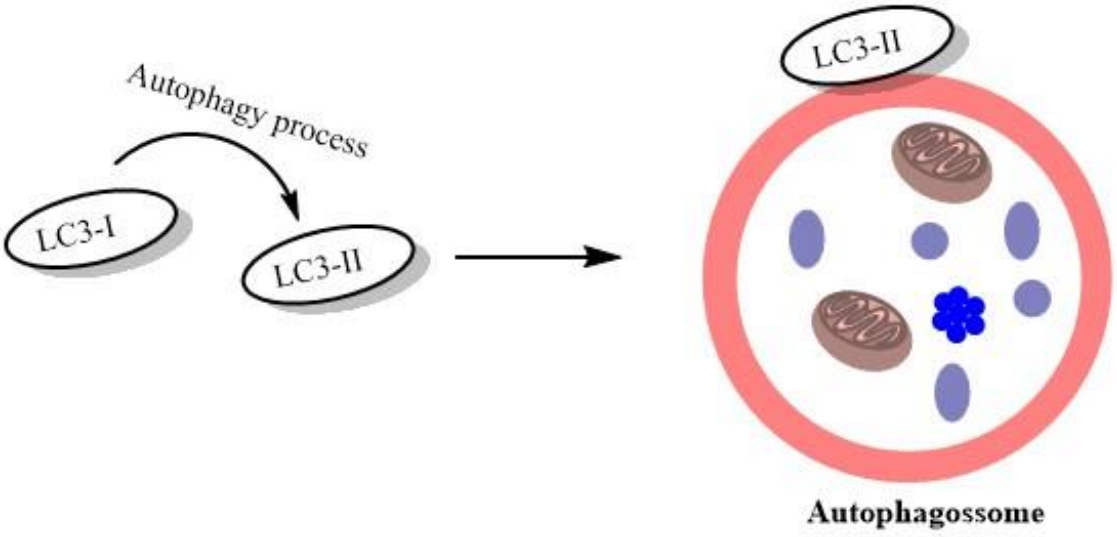

Figure 39. Formation of the autophagossome in the presence of LC3-II (14 kDa) which derived from LC3-I (16 kDa).[120]

When the necrosis process occurs, there is a permeabilization of the cytoplasmic membrane in the early process. This causes the release of several proteins to outside the cell such as cyclophilin A, as it can be seen in **Figure 40**.[121]

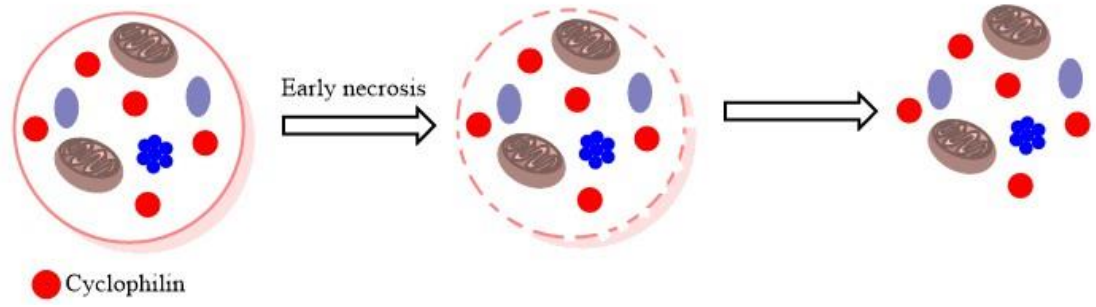

Figure 40. Permeabilization of the cytoplasmic membrane and release of several organelles and proteins including Cyclophilin A.[121]

3.5.2 General procedure to access type of cell death

MCF-7 cells were incubated with porphyrin **6** (2.5 µM and 5.0 µM) and **TMPyP** (5.0 µM and 10 µM) for 3 h. Then, the cells were irradiated for 15 min with red light at

an irradiance of 23.70 mW/cm^2. Cells irradiated or not were incubated at 3, 6 and 20 h post-irradiation and lysed to prepare protein crude extracts. The presence of cell type specific proteins or fragments of protein was assessed by wester blotting. Different positive controls and primary antibodies were used depending on which cell type of death we intended to study. In order to have the same amount of protein in each well of the polyacrylamide gel, a protein dosage was effectuated. The amount of protein deposited in each well is referred in every western membrane image's subtitle and which primary antibody was used is referred in the introductory text of the next subsections. HSP60 was used as a loading control for PARP and LC3.

3.5.3 Apoptosis and necroptosis pathway - the cleavage of PARP-1

The positive control used to study if the cells undergo apoptotic deathy was **CPT** 20 µM for 18 h. The western membrane was incubated with an antibody that recognizes the 42 kDa, 62 kDa, 116 kDa (full length) and 89 kDa PARP fragments. The results are represented in **Figure 41**.

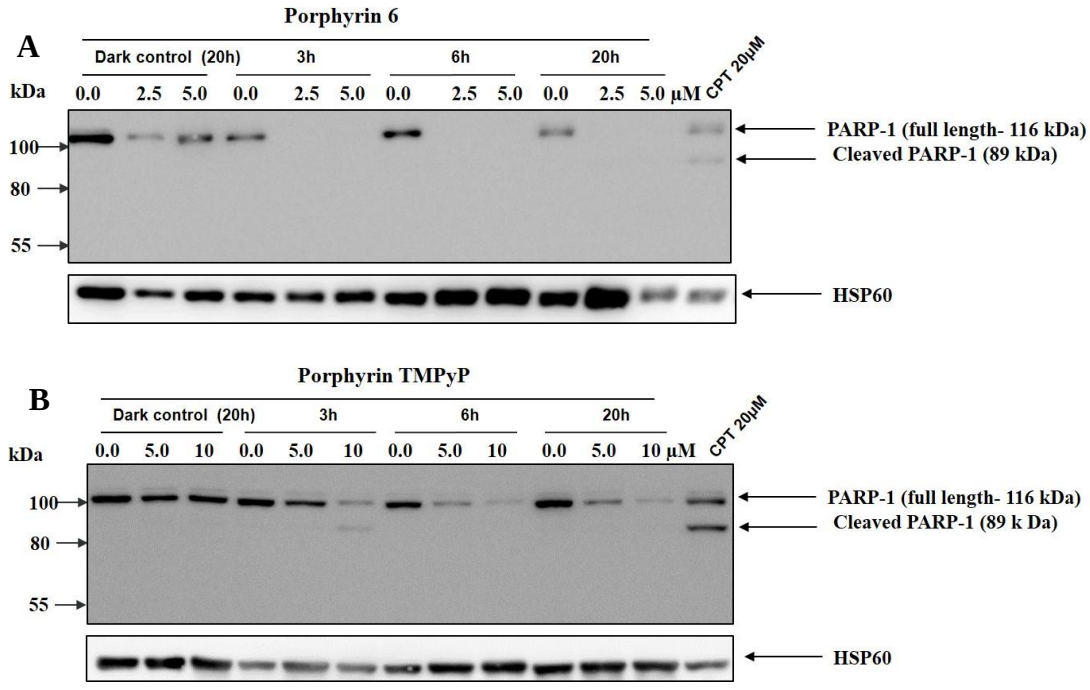

Figure 41. Western blot analysis to detect PARP-1 cleavage in MCF-7 cells treated 3 h with PS 6 (A) and TMPyP (B) with different concentrations 2.5 µM; 5 µM and 5.0 µM; 10 µM, respectively. After, they were irradiated for 15 min and all proteins were extracted after 0, 3, 6 and 20 h post irradiation or mock treatment. 5.7 µg (A) or 20 µg (B) of each sample were deposited in the well and the PVDF membrane probed with anti-PARP antibody. HSP60 was used as a loading control.

As it can be seen in **Figure 41-A**, after PDT treatment with porphyrin **6** at 2.5 µM and 5.0 µM, there is a disappearance of full length PARP-1 (116 kDa) without the appearance of smaller fragments (89 kDa, 62 kDa or 42 kDa). Even with longer incubation periods there is no appearance of the 89 kDa, 62 kDa or 42 kDa fragment. So, neither apoptosis or necrosis is responsible for the death of porphyrin **6**-treated MCF-7 cells. Regarding **TMPyP** (**Figure 41-B**) there is a slight cleavage of PARP-1 related to apoptosis at 3 h with 10 µM but there is still a loss of full length PARP without the presence of the smaller fragments (89 kDa, 62 kDa or 42 kDa). So, **TMPyP** does not induce the apoptosis or the necrosis pathway.

3.5.4 Autophagy – Transformation of LC3-I into LC3-II

The western blot was made with an anti-LC3 antibody that could recognize both forms (I and II). The C-terminal glycine of LC3-I is modified by addition of phosphatidyletanolamine (PE) to form LC3-II. **CPT** 20 µM was used as a positive control as in the previous assay. The results are shown in **Figure 42 .**

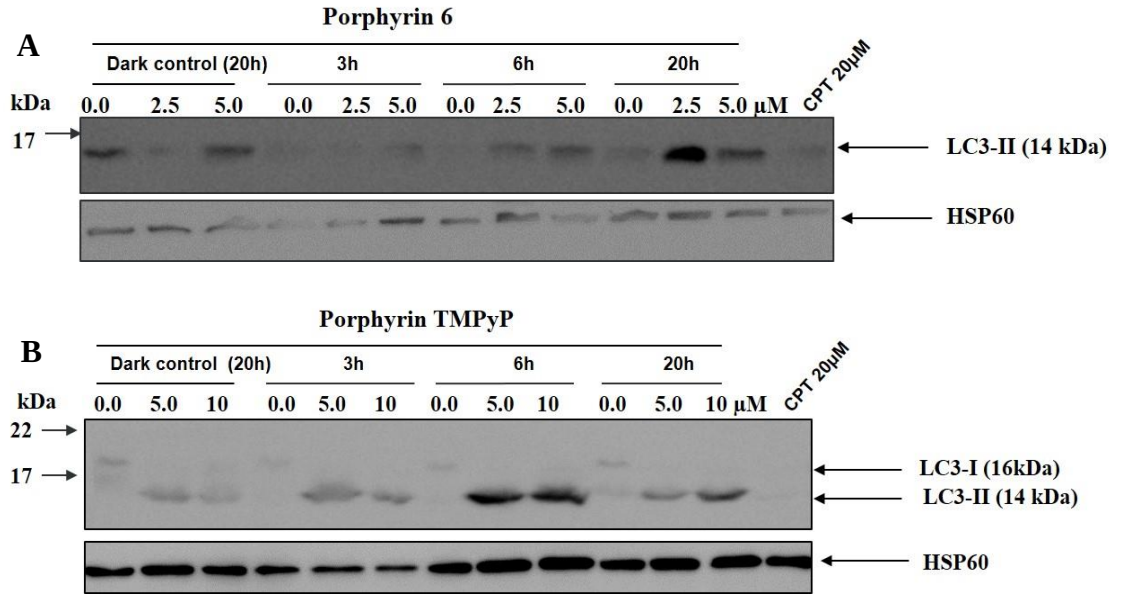

Figure 42. Western blot analysis to detect the two LC3 forms (LC3-I and LC3-II) in MCF-7 cells treated 3 h with PS 6 (A) and TMPyP (B) with different concentrations 2.5 µM; 5 µM and 5.0 µM; 10 µM, respectively. After, they were irradiated for 15 min and then all proteins were extracted after 0, 3, 6 and 20 h. 5.7 µg (A) or 20 µg (B) of protein were deposited in each well and the PVDF membrane probed with anti-PARP antibody. HSP60 was used as a loading control.

Regarding **6**, as seen in **Figure 42**, it is not possible to conclude if the concentration or time of protein extraction after irradiation influences the activation of the autophagy. However, there is an appearance of LC3-II with all the samples. Regarding

TMPyP there is an autophagic flux and the compound by itself seems to induce some autophagy. So, the cells seem to undergo autophagy after PDT with porphyrin **6** and **TMPyP**. However, the autophagic flux does not long until the 20 h samples and the appearance of LC3-II is visible in the dark controls. So, the appearance of LC3-II is does not mean that autophagy is responsible of the death after PDT.

It was previous reported that autophagy can block the apoptotic pathway in cancer cells, protecting them against cancer treatment. This is called "protective autophagy". These facts can be related to the results shown above when there is autophagy but the apoptotic process is absent (loss of PARP) (**Figure 41** and **Figure 42**).

3.5.5 Necroptosis- Release of Cyclophilin A

Methyl methanesulfonate (**MMS**) 25 mM was chosen as positive control. There is no need to harvest the cells, instead it is necessary to collect the medium (DMEM) because, as said before, when necroptosis occurs Cyclophilin A is released to the extracellular medium. However, the cells were harvested and used for PARP and LC3 westerns, described before. The results from incubation with Cyclophilin primary antibody are shown in **Figure 43**. It was not used a loading control because HSP60 is localized inside the cell and cyclophilin outside it.

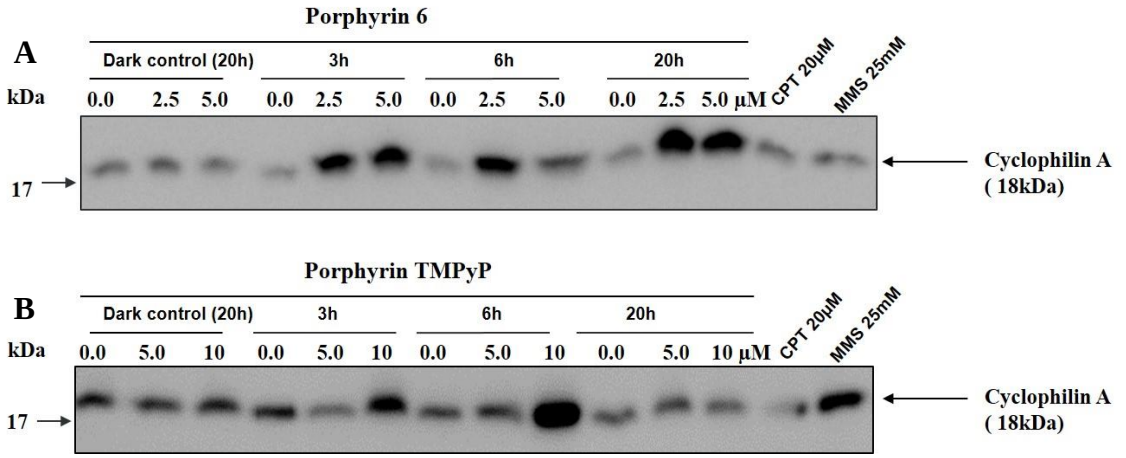

Figure 43. A - Western blot analysis to detect the release of Cyclophilin A after photodynamic therapy with synthesized porphyrins in by MCF-7 cells. MCF-7cells were incubated with porphyrin 6 (A) and TMPyP (B) with different concentrations 2.5 µM; 5 µM and 5.0 µM; 10 µM, respectively, for 3 h. After they were irradiated for 15 min and the presence of Cyclophylin detected in 18 µL of cell supernatant 0. 3. 6 and 20 h later. The PVDF membranes were probed with anti-Cyclophilin A antibody

As it can be seen in **Figure 43**, there is an accumulation of Cyclophilin A caused by PDT with each porphyrin derivative. Moreover, porphyrin **6** shows this accumulation

when there is the disappearance of the full-length PARP-1. So, the cells may undergo necrosis.

It was said before, when the apoptotic machinery is damaged, another cell type of death can occur after PDT. So, when comparing **Figure 41** and **Figure 43**, it is possible to conclude that when PARP-1 disappears there is an accumulation of Cyclophilin A regarding **6**. This can mean that instead of undergo apoptosis, these cells suffer necrosis besides autophagy. Regarding **TMPyP**, the accumulation of Cyclophilin A is visible and indicates that after PDT there is also necrosis and autophagy. Both compounds show the accumulation of Cyclophilin A after PDT at the maximum concentration. A stable low level cyclophilin release is detected in the non-treated and in the treated non-irradiated cells that probably reflects a permanent low level necrosis in these cancerous cell line.

3.6 Influence assessment of photodynamic therapy in alternative splicing of mRNA

CoASY synthase is a bio-functional enzyme that plays and important role in cellular metabolism because it carries the two final stages of CoA (coenzyme A) biosynthesis. *In vitro* several isoforms of this enzyme were previously identified. The design of the correct primers allows to observe the respective isoform (**Figure 44).** In case of COASY gene the mRNA can be with the full-length form having 350 bp or the two spliced isoforms with 150 bp and 100 bp. The first one regards the skipping of exon 4 and the second one the loss of exon 4 and 5. [122]

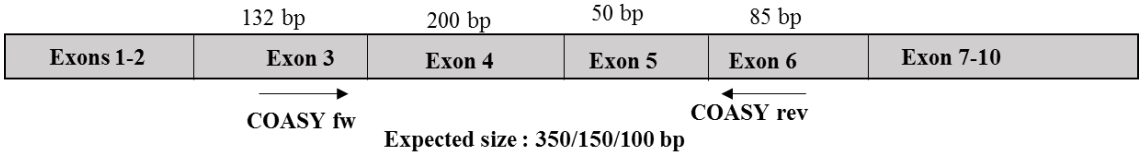

Figure 44. Primer designed and its location in the CoASY gene. Based on GenBank® [123]

Archaemetzincin-2 (AMZ2) is a metalloprotease and it is codified by the gene with the same name. Proteases are very important because they mediate several key processes such as, for example, cell cycle progression, apoptosis and autophagy. The design of the correct primer allows to recognize the mRNA for the full length form (452 bp) and the spliced isoform without exon 3 (ΔE3) with 278 bp (**Figure 45**).[124]

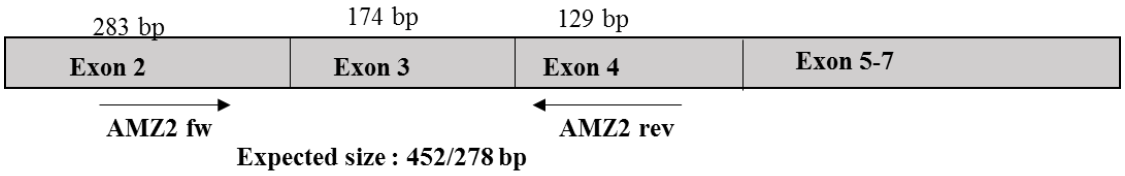

Figure 45. Primer designed and its location in the AMZ2 gene. Based on GenBank® [123]

The cyclic AMP-dependent transcription factor ATF-3 is a protein coded by ATF3 gene which has an important function such as binding to DNA to promote transcription. There two spliced isoforms of the full length mRNA (546 bp) identified as ATF3ΔZip2a (858 bp) and ATF3ΔZip2b (767 bp). It is possible to observe these isoforms, with a primer design for that purpose. (**Figure 46**).[124]

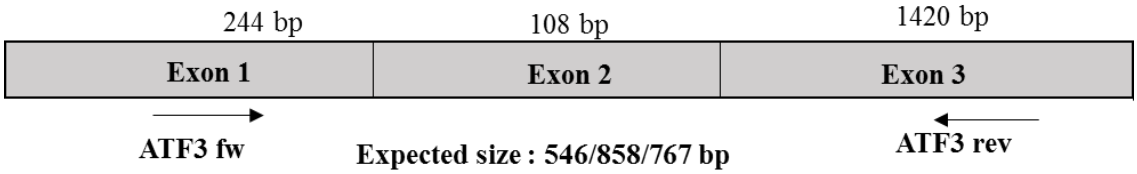

Figure 46. Primer designed and its location in the ATF3 gene. Based on GenBank® [123]

p53 is a tumour suppressor due to its crucial function in preventing cancer formation. This protein is codified by the gene TP53. There are several isoforms of these protein and some of them are highly expressed in cancer cells. Its mRNA can be identified by designing the correct primer as it can be shown in **Figure 47**. Depending on which primer we choose; it is possible to detect different fragments [125] as it can be seen in **Figure 47.**

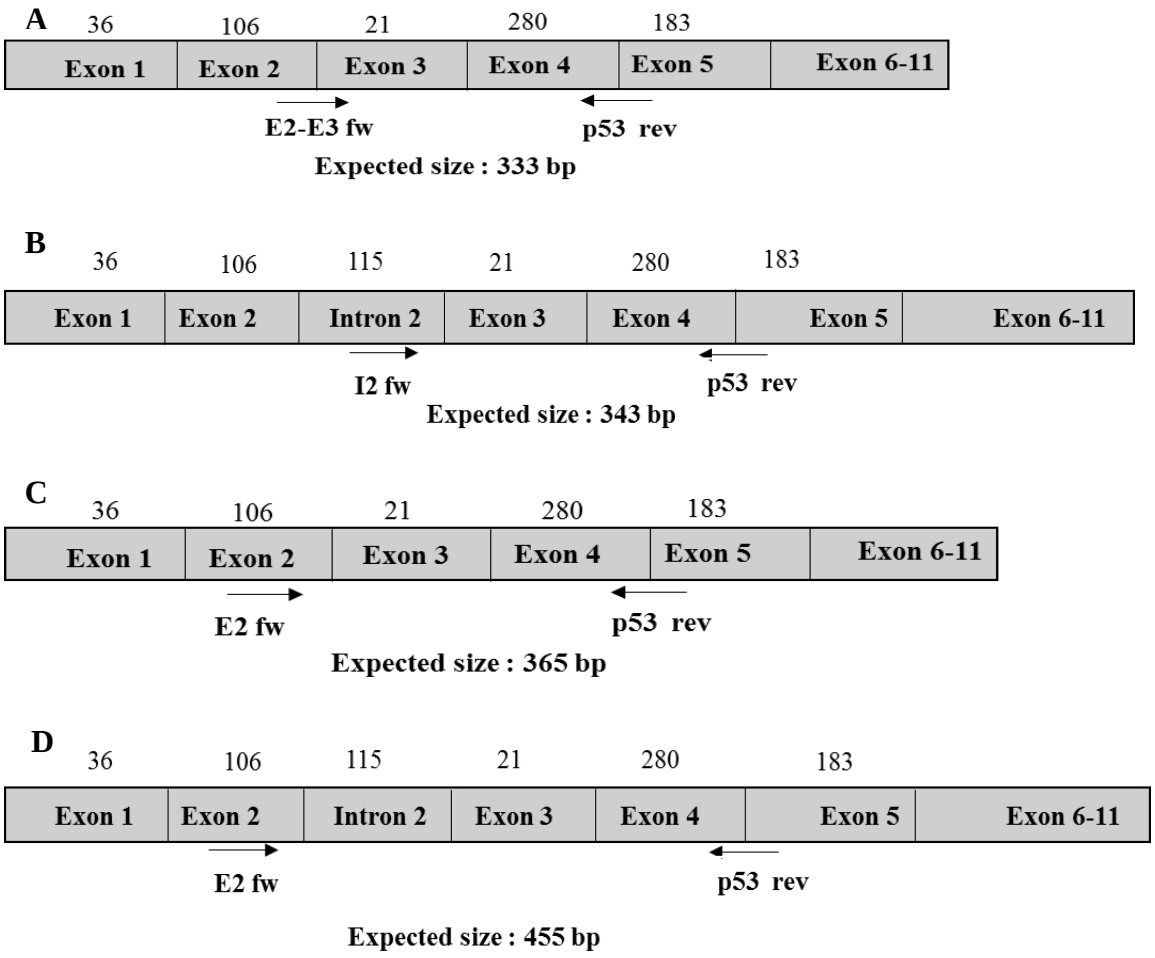

Figure 47. Different primers designed for the p53 gene and its location. Based on GenBank® [123]

MCF-7 were treated with the same conditions as described in section 3.5.2. Twenty-four hours post-irradiation the RNA was extracted according to the instructions given by the manufacturer of the RNA purification kit used (Roche). The RT-PCR was done with different primers depending on which gene was under evaluation.

The results for CoASY are represented in **Figure 48.** In order to have alternative splicing, the two smaller isoforms must exist in higher percentage than the full length one.

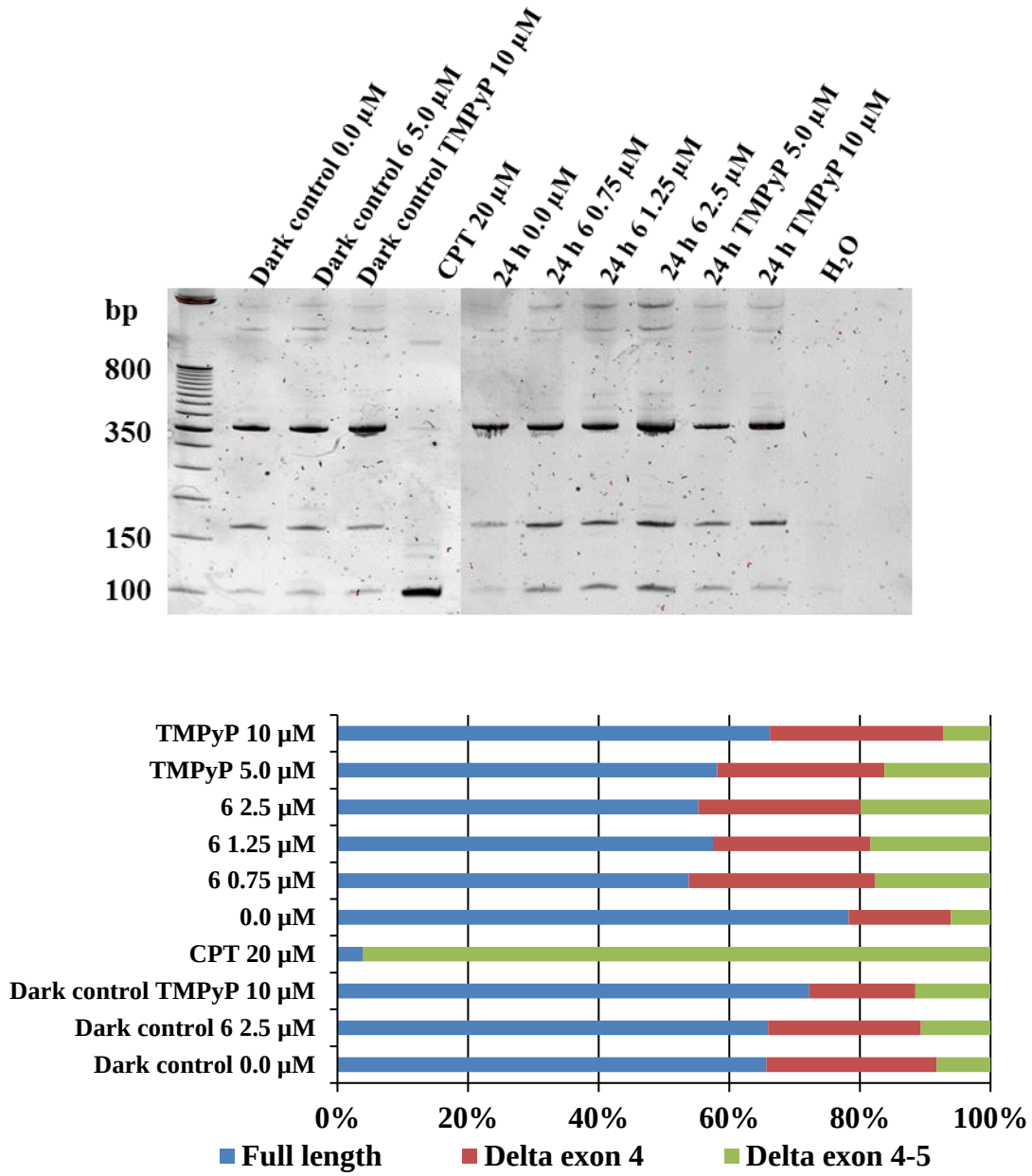

Figure 48. Alternative splicing induced by photodynamic therapy with TMPYP, 6 and treatment with CPT. Top image: MCF-7 cells were checked to find alternative splicing of CoASY. The cells exposed or not to compound 6 and TMPyp were irradiated or not. They were analysed 24 h after treatment. RT-PCR was performed with specific primers for endogenous CoASY. Negative control (no compound) as well as a positive control (CPT) were done. The PCR products were revealed in an acrylamide gel (10%). The size of the markers is shown on the left side and the RT-PCR products are marked on the right side of the image. Bottom: Rates of alternative splicing regarding the CoASY gene.

As it can be seen compound **6** and **TMPYP** seem to induce a small alternative splicing. However, this influence does not seem to be dose-dependence.

Regarding this assay, it was possible to detect an instability in the dark controls that is statically significant ($p = 0.37$). For this reason, it is necessary to repeat and adjust the experimental conditions in order to improve these results.

The results for AMZ2 are presenting in **Figure 49**. As it can be seen there is the appearance of the 278 bp isoform but it is not higher in percentage than the 452 bp (the full-length form).

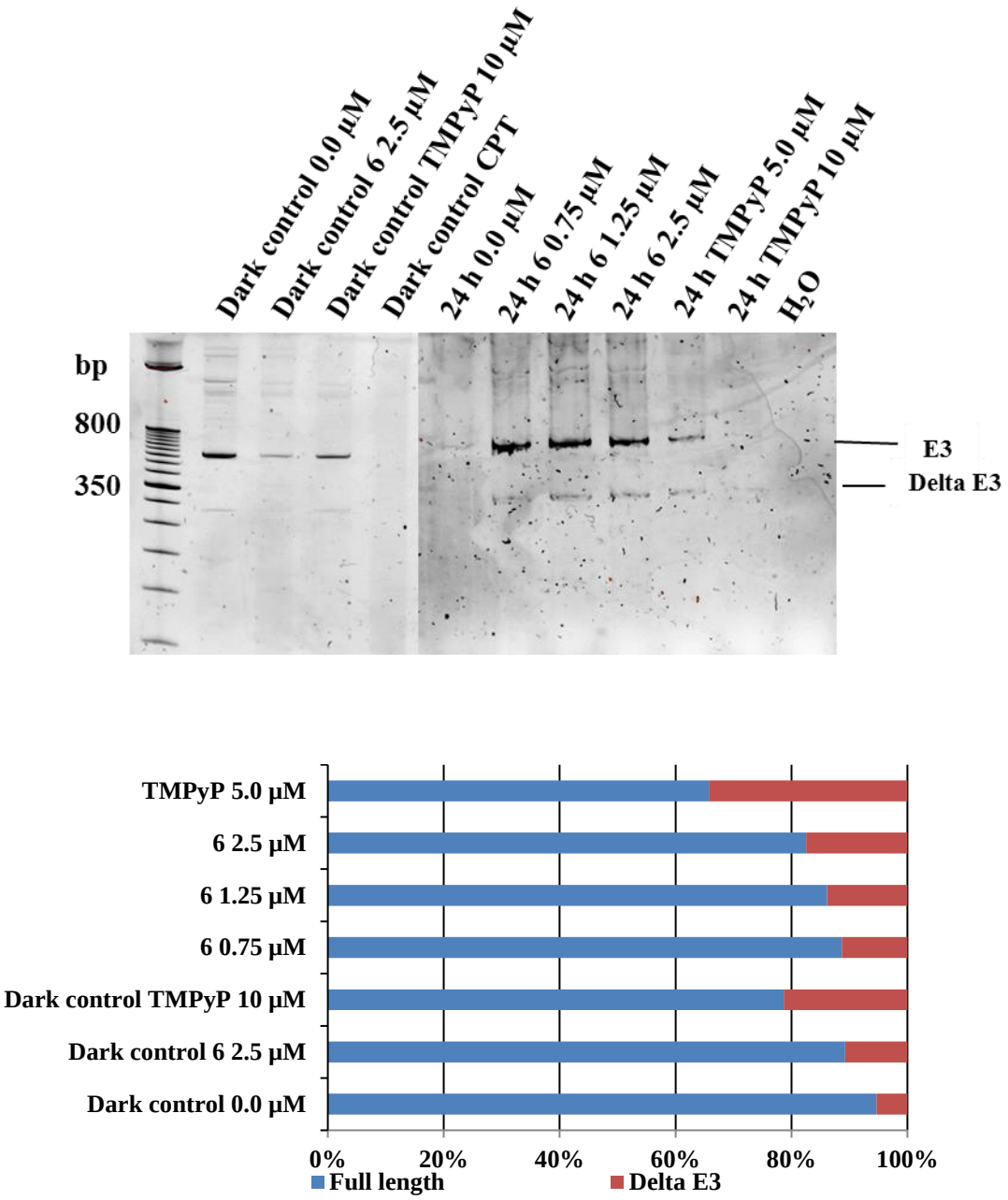

Figure 49. Alternative splicing induced by photodynamic therapy with TMPYP, 6 and treatment with CPT. Top image: MCF-7 cells were checked to find alternative splicing of AMZ2. The cells underwent a photodynamic treatment with each compound and they were analysed 24 h after treatment. RT-PCR was performed with specific primers for endogenous AMZ2. Negative control (no compound or compound without irradiation. The PCR products were revealed in an acrylamide gel (10%). The size of the markers is shown on the left side and the RT-PCR products are marked on the right side of the image. Bottom: Rates of alternative splicing regarding the AMZ2 gene..

In **Figure 49** it is possible to observe that the alternative splicing does not occur because the spliced isoform analysed is lower than 50%. However, regarding **6**, the spliced isoform has higher percentages with increased concentration being dose-dependent.

Regarding the other genes ATF3 and p53 the gel did not show any PCR products. This can result from bad adjustments during the PCR conditions such as temperature and/or time. These conditions were adapted from other genes but considering each melting point. Several conditions were tried without success. Concerning p53, in addition to try different conditions maybe designing another primer for another p53 isoform since there is several of them.

The previous results show that CoASY seem to under AS derived from PDT but the same did not happened to AMZ2 gene. PDT can cause oxidative stress and by inducing alternative spicing, new protein isoforms can be formed. Cancer cells are characterized by having several protein isoforms which avoid cell death while the canonical form promotes it. So, if PDT seems to induce AS, maybe the isoforms formed can induce the cell death showed earlier in this chapter. However further tests should be done in order to identify which isoform of a promoting cell death protein is present in MCF-7 after PDT.

There are several studies about new alternative spliced isoforms caused by genotoxic agents.[67,91–93] However, it is important to highlight that regarding the effect of PDT on alternative splicing, there is not any study exploring this theme. So, this work becomes relevant for its novelty and its continuation can be important to find new chemotherapeutic approaches.

3.7 Material and methods

3.7.1 Solutions and buffers

PBS (phosphate buffer saline): NaCl 140 mM; KCl 2.7 mM; Na_2HPO_4 8 mM; KH_2PO_4 1.8 mM; pH 7.4. The PBS used for cell culture was purchase from Lonza, Verviers, Belgium.

Trypsin/EDTA: 0.025%, pH 7.6-7.8 purchase from Lonza, Verviers, Belgium

PageRuler™ Prestained Protein Ladder: (2.3 to 250 kDa) (New England Biolabs® inc., France).

Lysis buffer for total protein extraction (Myamato): HEPES 25 mM pH 7.50; NaCl 150 mM; Triton X-100 0.5%; Glycerol 10%.

Lysis mix for total protein extraction containing protease and phosphatase inhibitors: 500 µL of Myamato buffer; 1 µL of 1,4-Dithiothreitol (DTT) 1 mM; 5 µL of PMSF (phenylmethylsulfonyl fluoride) 1 mM; 40 µL of cOmplete™ (Roche, Switzerland); 6.7 µL of NaF 3.3 mM; 10µL of Na_3VO_4 1 mM; 5 µL of β-glycerophosphate 25 mM; 10 µL of NPP (Nitrophenyl-phosphate) 10 mM; 442.3 µL of H_2O.

Loading buffer 4x (TR4x): Tris-HCl 25 mM pH 6.80; SDS 8%; Glycerol 40%; β-glycerolmercaptoetanol 10%; bromophenol blue

Migration buffer used to SDS-PAGE: Tris-HCl 20 mM pH 8.00; Glycine 200 mM; SDS 10%.

Transfer buffer used in the western's transference: Tris 25 mM; glycine 192 mM; methanol 10%.

TBST-Tween (Tris buffer Saline): Tris-HCl 20 mM pH 7.50; NaCl 15 mM, Tween-20 0.1%

TBST-milk: TBST + 5% (m/v) of skimmed milk powder.

TBE 5 x buffer (electrophoresis gel): Tris-HCl 50 mM pH 8.00; Boric acid 50 mM; EDTA 1mM.

Acrylamide/bisacrylamide gel (DNA electrophoresis gel) 10%: 2.0 mL Acrylamide/bisacrylamide 40% 29:1 (v/v); 1.5 mL of TBE 5x buffer; 3.9 mL of Water-nuclease free; 37.5 µL of APS 10%; 7.5 µL of TEMED.

Polyacrylamide/bisacrylamide gel (SDS-PAGE):

a) Stacking gel: 519 µL of acrylamide/bisacrylamide 40% 37.5:1 (v/v); 1.25 mL of Tris 0.5 M pH 6.80; 3.2 mL of H_2O; 50 µL of SDS 10%; 50 µL of APS 10%; 5 µL of TEMED.
b) Gel concentration 6%: 1.87 mL of acrylamide/bisacrylamide 40% 37.5:1 (v/v); 3.0 mL of Tris 1.5 M pH 8.8; 7.0 mL of H_2O; 120 µL of SDS 10%; 90 µL of APS 10%; 6 µL of TEMED.
c) Gel concentration 8%: 2.49 mL of acrylamide/bisacrylamide 40% 37.5:1 (v/v); 3.0 mL of Tris 1.5 M pH 8.8; 6.33 mL of H_2O; 120 µL of SDS 10%; 90 µL of APS 10%; 6 µL of TEMED.
d) Gel concentration 10%: 3.11 mL of acrylamide/bisacrylamide 40% 37.5:1 (v/v); 3.0 mL of Tris 1.5 M pH 8.8; 5.6 mL of H_2O; 120 µL of SDS 10%; 90 µL of APS 10%; 6 µL of TEMED.
e) Gel concentration 12%: 3.68 mL of acrylamide/bisacrylamide 40% 37.5:1 (v/v); 3.0 mL of Tris 1.5 M pH 8.8; 5.1 mL of H_2O; 120 µL of SDS 10%; 90 µL of APS 10%; 6 µL of TEMED.
f) Gel concentration 15%: 4.67 mL of acrylamide/bisacrylamide 40% 37.5:1 (v/v); 3.0 mL of Tris 1.5 M pH 8.8; 4.15 mL of H_2O; 120 µL of SDS 10%; 90 µL of APS 10%; 4 µL of TEMED.

Nuclear lysis buffer: Tris-HCl 50 mM pH 8.00; NaCl 280 mM; NP40 0.5%; EGTA 2mM; EDTA 10mM; Glycerol 10%.

"Wash buffer": HEPES 10mM pH 7.90; KCl 20 mM; $MgCl_2$ 2mM; EDTA 0.1 mM.

DNA ladder sample (for 10 gels): 80µL of TBE 1x; 18 µL of glycerol blue; 2 µL of DNA ladder of 50 bp (Invitrogen).

Reaction mix reverse transcription: 10 ng/ml total RNA, 10 µM of dNTPs, 10x rTth Reverse Transcriptase Buffer, 10 mM $MnCl_2$ solution, rTth polymerase, 20 µM reverse initiator primer, water nuclease-free for total volume reaction of 5 µL.

PCR reagents: 10x PCR buffer, EGTA 7.5 mM, forward initiator primer 20 µM water nuclease-free for total volume reaction of 20 µM.

3.7.2 Statistical analysis

All the statistical analysis was done with ANOVA analysis with Microsoft Excel 2016.

3.7.3 Eukaryotic cell line and cell culture

MCF-7 (human breast adeno-carcinoma cell line) and HeLa cells (human epithelial cervix carcinoma) were grown in Dulbecco's Modified Eagle's Medium (DMEM, Lonza, Verviers, Belgium), supplemented with foetal bovine serum (FBS 10%, Gibco, Carlsbad California, USA), non-essential amino acid (NEAA, 1%) and antibiotics penicillin 100 U/mL and streptomycin 100 µg/mL. DMEM supplemented with FBS, amino acids and antibiotics will be referred to as media. Cells were grown in a HERAcell incubator (Heraeus, Kendro, Germany) with 5% of CO_2 atmosphere, 95% relative humidity and a constant temperature of 37ºC. The cells used for all the assays were plated 24 h prior to the experimental to be at about ~80% confluence at the time of the drug addition.

3.7.4 Photodynamic treatments

MCF-7 cells were grown overnight in the respective plates until they reach ~80% confluence and incubated with an appropriate volume of PS. The synthesised compounds were diluted in DMSO at 10mM and further diluted in DMEM just prior to cell contact. After 3 h of incubation, the cells were irradiated (0, 5, 10 or 15 min) with red filter allowing the passage of wavelengths superior to 640 nm and with an irradiance of 23.70 mW/cm^2. The assays were performed at different times after irradiation. After irradiation, the cells were incubated in the dark at the indicated time (0, 3, 6 and 19 or 24 h). The treatment with **CPT** 20 µM was adding it for 24 h. **MMS** 25 mM was added to the cells for 15 min at 37ºC,wash with PBS before addition of fresh media for 18 h. Porphyrins were previous synthesized but **CPT** and **MMS** were purchased from Sigma-Adrich. Stock solutions of **CPT** dissolved in DMSO were prepared with concentration of 5.0 mM. **MMS** was prepared from a 200 µL of a stock solution in DMSO in order to have 25 mM of final concentration.

The dark controls correspond to cells incubated with the compounds without irradiation. The light controls are irradiated cells without compound. This last control is the one used to calculate the survival rates in the survival assays.

3.7.5 Light source

Four fluorescent tubes aquarelle TLD-15W (Philips) with an irradiance of 23.70 W/m^2. Two red filters with a cut off at 640 nm that were used for all the assays.

3.7.6 WST-1 assay

Cells plated in a 96-well plate were exposed to synthetic compound and irradiated or not. 24 h post-irradiation or mock treatment, WST-1 (Roche, Switzerland) reactive diluted 1/30 was added to cells. After 30-60 min at 37ºC, the absorbance was measured at 450 nm and 690 nm as recommended by the manufacture on a Multiskan MS Plate Reader (LabSystems). Each experimental point is the mean of three independent experiments. The percentage of viable cells treated with the drugs was calculated assuming that the control cells had 100% of viability.

3.7.7 ATPlite™ kit assay

The ATPlite™ kit was purchased from PerkinElmer® (Massachusetts, USA). The cells were grown in a black bottom 96-well plate and each compound was added in order to have a final volume of 100 µL per well. After 3 h of incubation, the cells were irradiated for 15 min. After 24 h, 50 µL of mammalian cell lysis buffer were added to each well and the plate was shaken for 5 min. Subsequently, 50 µL of substrate solution was added to each well and the plate was shaken for 5 min. Then the plate placed in the dark for 10 min and the luminescence between 400-650 nm measured. Multiskan MS Plate Reader (LabSystems) was used to shake the plates with the "fast" velocity selected. The luminescence was measured in the EnSpire® 2300 multilabel reader (PerkinElmer, Massachusetts, USA). The percentage of viable cells treated with the drugs was calculated assuming that the control cells had 100% of viability.

3.7.8 Trypan Blue assay

For the pictures with the trypan blue, the cells were plated in small circular dishes and after the photodynamic treatment the media was removed and 400 µL of trypan blue 0.4% in PBS (AMRESCO®) plus 400 µL of PBS were added. Finally, the pictures were taken directly from the plate with a camera Leica DFC 420C.

3.7.9 Cellular uptake

MCF-7 cells were incubated for 3 h with each porphyrin at 10 µM in a 96 well-black plate with clear bottom (Greiner). Then the wells were washed with PBS for 1 min and DMSO 99% (Sigma-Aldrich) was added. The plates were shacked for 10 min and the fluorescence measured at the appropriate wavelength (**Table 9**). The fluorescence measurements were done by using EnSpire® Alpha Plate Reader (PerkinElmer, Massachusetts, USA).

Table 9. Excitation wavelengths (nm) and the spectrum window (nm) for each PS.

Porphyrin	**λ_{exc} (nm)**	**Spectrum window (nm)**
5	425	600-850
6	425	600-800
TMPyP	425	600-800

Several washing conditions (**Table 10**) were tried but it did not influence the results.

Table 10. Washing conditions used in the cellular uptake.

Assay No.	**1**	**2**	**3**	**4**	**5**	**6**
Volume of PBS (µL)	150	200	250	300	300	300
No. of washings	3	3	3	3	4	5

3.7.10 Subcellular localization

MCF-7 cells were seeded on coverslips placed into 24-well plates and allowed to grow for 24 h. After that the cells were incubated for 3 h with each PS at defined concentrations. The cells were fixed for 20 min with 4% *p*-formaldehyde-PBS, washed

with PBS 3 times for 5 min and then incubated with Hoechst 33342 (Fisher) for 10 min. After 3 additional PBS washes the coverslips were mounted on glass slides with Mowiol (Sigma-Aldrich). The pictures of subcellular localization were taken with a Leica TCS SP5 confocal microscope using a 63×/1.30 GLYC objective. Hoechst was excited at 405 nm and the fluorescence detected from 417 nm to 446 nm. Porphyrins were excited at 488 nm with a detection reading from 608 to 699 nm. The photographs were processed using Adobe Photoshop CS software (Adobe systems, San Jose, USA).

3.7.11 The Western Blot Technique

Western blot, also called immunoblotting is a technique used very often to detect specific proteins in a sample extract. First it is necessary to extract all proteins from the cell cytosol and to do a protein dosage in order to load the same amount of protein in each well of the electrophoresis gel. The proteins are denatured before loading in a Tris buffered solution containing SDS (an anionic detergent) that covers and unfold the protein, Beta mercaptoethanol that reduces disulfide bounds, glycerol (to sink easily into the wells) and bromophenol dye (to check how the proteins concentrate in the concentrating gel due to different pH in both gels.). The sample is heated in order to denature the proteins structure. This denaturation process allows the protein to acquire negative charge allowing the proteins to have the same charge and move in an electrical field. The proteins are then separated according to size by gel electrophoresis.[126,127]

There are two types of gels (stacking and separating gel). The first one concentrates the proteins due to its pH and low acrylamide concentration which leads to a porous gel. The separating gel has higher pH and concentration in polyacrylamide which makes the pores narrower and the proteins are separated by their size. The smaller proteins will travel faster.[127,128] (**Figure 50**)

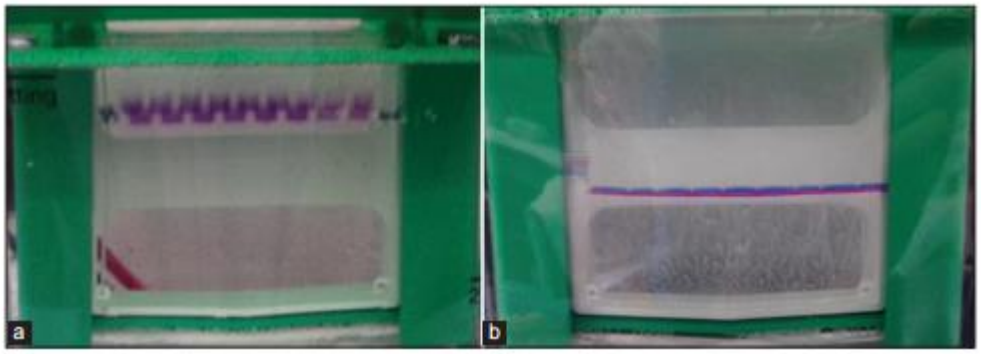

Figure 50. a- Samples running through the stacking gel (lower voltage) and b- samples running through the separation gel (higher voltage). [127]

After separation of the proteins, they are transferred to a membrane.[129,130] The transfer is done by using an electric field oriented perpendicular to the surface of the gel leading to the movement of the proteins to the membrane. This type of transfer is called electrophoretic transfer. The membranes can be nitrocellulose or polyvinylidene fluoride (PVDF). The last is used more often because it allows to reprobing and storage, unlike the first one.[127,128] (**Figure 51** and **Figure 52**)

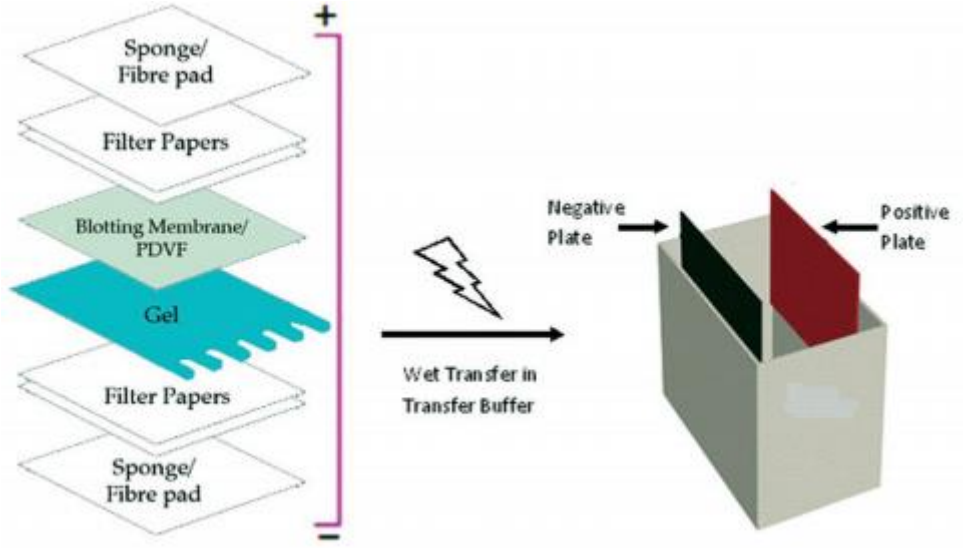

Figure 51. The constitution of the sandwich in the western blot. [127]

Figure 52. PVDF membrane after transfer. [127]

Before incubation with the antibody, it is necessary to wash the membrane and block the non-specifically bound between the antibodies and the membrane.[128] Usually, this blockage is done with 5% skimmed milk or BSA diluted in TBST. Skimmed milk is preferred over BSA due to its cheaper price and readily availability.[127]

The membranes are first incubated with primary antibodies and then with a horseradish peroxidase coupled secondary antibody. The concentration of the antibody depends on the manufacturer instructions. After incubation with the primary and secondary antibody, the membrane should be washed with TBST. The membrane are revealed by chemiluminescence with a luminol-based substrate (ECL detection from Amersham). This signal is captured with a camera.[127,130]

Usually, the uniformity of the loading is verified by checking the level of a reference protein which is not affected by the study (like HSP60, α-tubulin) in each sample.[131]

3.7.12 Protein extraction

3.7.11.1 Harvest

MCF-7 cells were plated in individual dishes of 20 cm^2. After the photodynamic treatment, the cells were washed in cold PBS and collected with a scraper. Following harvesting, they were suspended in PBS, washed and centrifuged at 1000 rpm at 4ºC for 30 s.

3.7.11.2 Total Protein extraction

The pellets were suspended in lysis buffer. After an incubation period of 15 min on ice, the extracts were centrifuged at 1000 rpm at 4ºC. Then, the supernatants containing the total protein extracts were stored at -80ºC.

3.7.11.3 Protein Dosage

The concentration in protein of each cellular extracts was determined by the Bio-Rad Protein Assay based on the method ofBradford. It is a colorimetric assay relying on a dye which changes of absorbance in presence of proteins. The readings are effectuated at 595 nm in a multiskan MS plate reader. The calibration curved is obtained with BSA (bovine serum albumin) standard.

3.7.11.4 SDS-Page and Immuno-detection (Western Blotting)

The appropriate volume of loading buffer (TR4x) was added to each extracts and boiled at 100ºC for 3 min. Then, 5-30 µgr of denatured proteins were loaded onto the gel. The same protein amount was added in each well to allow comparison. 4 µL of a prestained protein ladder (New England Biolabs® inc., France) was loaded.

Proteins were separated by SDS-PAGE and the percentage of polyacrylamide/bisacrylamide used for each protein is given in **Table 11**. The electrophoresis was run at 90 V until each sample enters the gel and then for 120 V with migration buffer 1x until the tracking dye reaches the bottom. After the separation, the proteins were electrotransfered on a PVDF membrane (GEHealth Care, Belgium) overnight at 45 V in transfer buffer.

Table 11. Percentage in polyacrylamide/bisacrylamide used in this study.

Protein analysed	**Gel Percentage (%)**
PARP	8%
LC3	15%
Cyclophilin	15%

In order to block the non-specific interacting sites, the membranes were incubated with TBST-milk 5% for 1 h at room temperature. Then the membranes were incubated with the respective primary antibody for 2 h which detects the desired specific proteins (the concentration was optimized for each antibody) (**Table 12**).

Table 12. List of antibodies and its properties used.

Antibody	**Company**	**Reference**	**Dilution**	**Solvent**	**Source**
PARP-1	Cell signalling, Netherlands	9542	1/1000	Milk-TBST 5%	Rabbit
LC3-I and II	Axxor (enzolife sciences), USA	0231-100/LC3-5f10	1/500	Immunoboost	Mouse
Cyclophilin	Cell signalling, Netherlands	2175s	1/1000	Milk-TBST 5%	Rabbit
HSP60	Enzo life sciences, USA	SPA-806	1/1000	Milk-TBST 5%	Mouse

After washing the membranes with TBST, they were incubated with the secondary antibody-HRP (House radish peroxidase) (1/1000 dilution) (Dako Cytomation, Denmark or cell signalling). After washing, ECL (enhanced chemiluminescence) western blotting substrate was added. The membranes were revealed using a LAS4000 Biomolecular Imager system (GE Healthcare Life Sciences) . The molecular weight of the fragments was estimated by comparison with PageRuler^{TM} Prestained Protein Ladder. The loading control of each membrane (except for Cyclophilin) was anti-HSP60

3.7.13 Total RNA extraction

Cells were plated in a 6-well plate and the photodynamic treatment was applied. The total RNA extraction was done with the "high Pure RNA isolation kit" (Roche, Switzerland). The cells were washed with PBS and 600 µL of Lysis buffer solution (Lysis buffer+ water 2:1) was added to each well. Then the cells were scrapped and placed on top of the filter tube and centrifuged for 30 s at 12.000 rpm at 20ºC. After discarding the content of the collection tube, each sample was incubated with 100 µL of DNase I incubation buffer + DNase I (9:1) for 15 min at room temperature. Then three washes followed by 30 s centrifugation at 12.000 rpm at room temperature with 500 µL of Wash Buffer 1, 500 µL and 200 µL of Wash Buffer 2 were performed. At the end, the purified RNA was eluted by adding 100 µL of elution buffer atop the filter tube and centrifugating 1 min at 12.000 rpm at room temperature. The eluates were stored at -80ºC

3.7.14 RNA dosage

The extracted RNA was quantified on a spectrometer ND-1000 Nanodrop (Thermo Fisher Scientific, Massachusetts, USA) by measuring the absorbance at 260 nm. Stock solutions were prepared in order to have a concentration of 4 ng/µL.

3.7.15 Generation of cDNAs by reverse transcriptase and amplification by PCR

10 ng/µL of total RNAs was used as a template for cDNA synthesis. RT was performed using thermostable rTth reverse transcriptase (from Thermus Thermophilus H-8) (RNA PCR kit) (Roche, Switzerland) by incubating it with the RNA samples at 70ºC. RT was carried out by preparing the reverse transcription reaction mixes with transcript-specific-reverse primer (**Table 13**). Primers were obtained from Eurogentec (Liège, Belgium). The cDNAs fragments obtained were later amplified by PCR in the amplification buffer with both reverse and forward primers and the same polymerase.

Table 13. Sequences of the primers used for RT-PCR analysis.

Target mRNA	Target exon/ intron	Primers	Length (bp)
COASY	E4-5	Fwd: 5' TTC-CGC-CAG-CGA-ATG-TTG-GG 3'	FL: 355 bp/ ΔE-4 150 bp / ΔE4-5:100 bp
		Rev: 5' CTC-GGG-CCA-GCT-TTG-CGA-TA 3'	
AMZ2	E3	Fwd: 5' GCC-AGT-GAT-CTC-TTT-GGA-CCC-ATT 3'	FL:452bp/ ΔE3:278 bp
		Rev: 5' GTC-AAA-GAG-GCC-TGT-CCA-AAG-ACA 3'	
P53	E2-3	Fwd: 5' CCT-ATG-GAA-ACT-ACT-TCC-TG 3'	333 bp
		Rev: 5' AGG-GGA-CTA-CGT-GCA-AGT 3'	
P53	E2	Fwd: 5' CGA-AAC-ATT-TTC-AGA-CCT-ATG-G 3'	365 bp
		Rev: 5' AGG-GGA-CTA-CGT-GCA-AGT 3'	
P53	I2	Fwd: 5' ATG-GGA-CTG-ACT-TTC-TGC-TCT 3'	343 bp
		Rev: 5' AGG-GGA-CTA-CGT-GCA-AGT 3'	
P53	E2 (bis)	Fwd: 5' CCC-TCT-GAG-TCA-GGA-AAC 3'	455 bp
		Rev: 5' AGG-GGA-CTA-CGT-GCA-AGT 3'	
ATF3		Fwd: 5' ATG-ATG-CTT-CAA-CAC-CCA-GGC 3'	FL: 546 bp / ATF3ΔZip2a: 858 bp / ATF3ΔZip2b: 767 bp
		Rev: 5' TTA-GCT-CTG-CCA-TGT-TCC-TTC 3'	

PCR program was carried out for 35 cycles. The temperature of annealing and length of the elongation steps depended in which mRNA we were targeting. (**Table 14**)

Table 14. Conditions for each phase of a PCR cycle

Gene	Phase	Temperature (ºC)	Time
COASY AMZ2	Initial denaturation	94	5 min
	Melting	94	15 s
	Annealing	66	20 s
	Extension	72	30 s
	Final polymerization	72	5 min
P53 I2	Initial denaturation	94	5 min
	Melting	94	30 s
	Annealing	54	30 s
	Extension	72	75 s
	Final polymerization	72	5 min
P53 E2 (bis) P53 E2/3	Initial denaturation	94	5 min
	Melting	94	30 s
	Annealing	58	30 s
	Extension	72	75 s
	Final polymerization	72	5 min
ATF3 P53 E2	Initial denaturation	94	5 min
	Melting	94	30 s
	Annealing	50	30 s
	Extension	72	75 s
	Final polymerization	72	5 min

3.7.16 Analysis on polyacrylamide gel 10%

10 µL of each PCR product was separated by electrophoresis on a 10% acrylamide/bisacrylamide gel in TBE 1x buffer and 10 µL of DNA ladder sample was added to estimate the bp of each PCR product. The gel ran for 180 V for 1 h. Then the PCR products were revealed by staining of each gel with 13 mL TBE 1x + 1.3 µL of gelstar^{TM} (Invitrogen, California, USA) for 20 min. The fluorescence was monitored by the LAS4000 Biomolecular Imager and the bands quantified by the Image Quant Las 4000 software (GE Healthcare Life Sciences)

CHAPTER 4

Conclusion and future perspectives

4. Conclusion and future outcomes.

In this work were synthesized and characterized the *N*-confused and the regular porphyrins **1** and **5** (**Figure 53**), that were used as templates to obtain the correspondent cationic derivatives **2** and **6** (**Figure 53**). The synthesis of the neutral porphyrins occurred with a yield of 9% and 23% for porphyrin **2** and **5**. The access to the neutral derivatives required the previous preparation of 4-bromomethylbenzaldehyde that was obtained in 19% yield by oxidation of 1,4-bis(bromomethyl)benzene with MnO_2. The protocol selected to prepare the neutral macrocycles was based on the condensation of that benzaldehyde with pyrrole in the presence of MSA, under Lindsey conditions. This strategy allowed to obtain both neutral derivatives in the same reaction, porphyrin **1** in 9% yield and porphyrin **5** in 23%. The lower yield of the *N*-confused porphyrin is probably associated with some self-autopolymerisation involving the nitrogen of the inverted pyrrole and the bromomethyl substituent in the aryl groups during the work-up. The cationization of the neutral templates with pyridine allowed to obtain compounds **2** (82%) and **6** (90%) in excellent yields. So, considering the protocol selected it will be important to improve the experimental conditions in order to obtain in better yields the aldehyde and the neutral porphyrin derivatives.

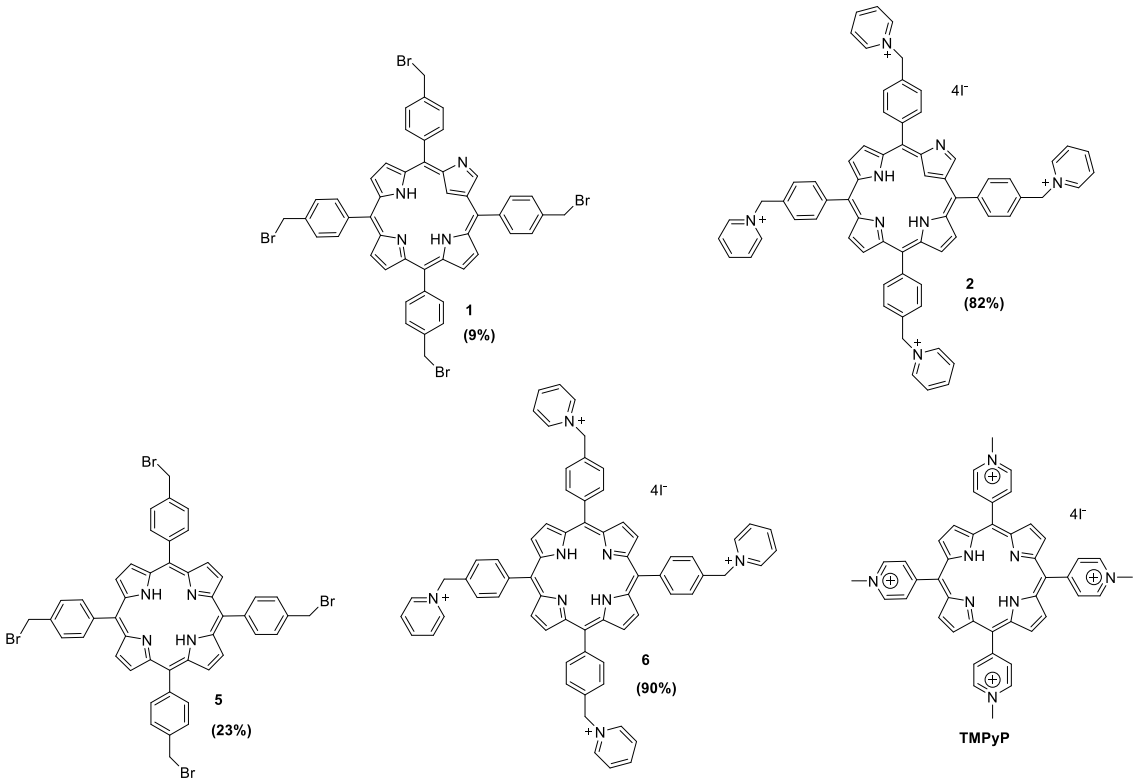

Figure 53. All synthesized porphyrin derivatives used in this work.

The photophysical characterization of the synthesized derivatives showed that only the regular porphyrin **5** and **6** are fluorescent. When the capacity of the different derivatives in generating $^1O_2$ was evaluated, it was verified that the best PSs were the regular porphyrin **5** (even better than TPP), followed by **6;** this cationic derivative, under the conditions used, showed a much higher efficiency to generate known $^1O_2$ than the conventional TMPyP. The presence of an inverted pyrrole ring in the *N*-confused porphyrins seems to reduce their ability to generate $^1O_2$, being the worse performance observed for derivative **1** (similar to **TMPyP**) followed by **2**. Although it is described in literature that some *N*-confused porphyrins with different substituents in *meso* positions can generate high amounts of singlet oxygen,[100] our results suggest that this efficiency must be strongly related with those *meso*-substituents. So, it would be interesting in future work to try the cationization of **1** and even **5** with different groups in order to verify if the performance of these cationic *N*- confused derivatives to generate singlet oxygen can be improved; probably even more efficient $^1O_2$ generator than the cationic regular porphyrin **6** would be obtained.

In the second part of this work, where it was evaluated photodynamic action of the synthesized derivatives to kill breast cancer MCF-7 and HeLa cells, the PDT results were compared with the ones obtained with **TMPyP**, one of the most studied PS in this field.

In the preliminary assays, the results obtained showed that the cationic regular porphyrin **6** was the one that has the highest photo-killing action, even higher than the positive control **TMPyP**. The high photo-killing effect also observed with **TMPyP** confirms the results reported in literature.[69] It is important to highlight that these first PDT studies involving porphyrin **6** seem very promising and merits to be developed.

The studies concerning the cellular uptake and subcellular localization studies were only performed with the fluorescent derivatives **5**, **6** and **TMPyP** and it was verified that their uptake by the MCF-7 cells was efficient; however, only **TMPyP** accumulates in the nucleus. Although porphyrin **5** is the best $^1O_2$ generator and is able to enter in the cells, probably the subcellular localization is not ideal to promote photokilling. A different situation was observed with porphyrin **6** which showed the highest photokilling effect; future studies are required in order to clarify its localization in the cell. Since only this cationic porphyrin and **TMPyP** showed relevant cell mortality (more or less 50%), they were selected to clarify the type of cell death involved after PDT and the studies of alternative splicing.

The cell death studies, both cationic PSs **6** and **TMPyP** seem to induce an autophagic flux and the disappearance of full length PARP without the appearance of the known apoptosis related cleaved forms. Moreover, there is an accumulation of cyclophilin for both porphyrins which suggest that beyond autophagy the cells undergo necrosis as well.

It is also necessary to repeat the alternative splicing assays with ATF3 and p53 genes, adjusting the PCR conditions such as temperature and/or time or in case of p53 gene, trying to design more primers since there are several isoforms of this gene.

PDT can cause oxidative stress and by inducing alternative splicing, new protein isoforms can be formed. Cancer cells are characterized by having several protein isoforms which avoid cell death but the canonical form promotes it. So, if PDT seems to induce AS, maybe the isoforms formed can induce the cell death shown earlier in this chapter. However further tests should be done in order to identify which isoform of a promoting cell death protein is present in MCF-7 after PDT.

There are several studies about new alternative spliced isoforms caused by genotoxic agents.[67,91–93] However, it is important to highlight that regarding the effect of photodynamic therapy on alternative splicing, there is not any study exploring this theme. So, this work becomes relevant for its novelty and its continuation can be important to find new chemotherapeutic approaches.

5. References

(1) Moss, G. P. Nomenclature of Tetrapyrroles (Recommendations 1986). *Pure. Appl. Chem.* **1987**, *59*, 779.

(2) Milgrom, L. R. *The Colours of Life*; Oxford University Press: Oxford, Inglaterra, 2000.

(3) Smith, A.; Witty, M. *Heme, Chlorophyll, and Bilins: Methods and Protocols*; Humana Press, 2001.

(4) Nelson, D. L.; Lehninger, A. L.; Cox, M. L. *Lehninger, Principles of Biochemistry*; W. H. Freeman, 2008.

(5) Zanardi, F. B.; Barbosa, I. A.; de Sousa Filho, P. C.; Zanatta, L. D.; da Silva, D. L.; Serra, O. A.; Iamamoto, Y. Manganese Porphyrin Functionalized on Fe_3O_4@nSiO_2@MCM-41 Magnetic Composite: Structural Characterization and Catalytic Activity as Cytochrome P450 Model. *Micropor. Mesopor. Mat.* **2016**, *219*, 161–171.

(6) Babbitt, S. E.; Sutherland, M. C.; Francisco, B. S.; Mendez, D. L.; Kranz, R. G. Mitochondrial Cytochrome c Biogenesis: No Longer an Enigma. *Trends. Biochem. Sci* **2015**, *40* (8), 1–10.

(7) Fan, J.-R.; Zheng, Q.-C.; Cui, Y.-L.; Li, W.-K.; Zhang, H.-X. Investigation of Ligand Selectivity in CYP3A7 by Molecular Dynamics Simulations. *J. Biomol. Struct. Dyn.* **2015**, *33* (11), 2360–2367.

(8) Vázquez-Torres, A.; Bäumler, A. J. Nitrate, Nitrite and Nitric Oxide Reductases: From the Last Universal Common Ancestor to Modern Bacterial Pathogens. *Curr. Opin. Microbio.* **2016**, *29*, 1–8.

(9) Fischer, H. *Nobel Lecture Chemistry 1922-1941*; Elsevier Publishing Company: Amesterdam, 1966.

(10) Furuta, H.; Asano, T.; Ogawa, T. " *N*-Confused Porphyrin": A New Isomer of Tetraphenylporphyrin. *J. Am. Chem. Soc.* **1994**, *116*, 767–768.

(11) Falk, J. . *Porphyrins and Metalloporphyrins : A New Edition Based on the Original Volume*; Smith, K. M., Ed.; Elsevier Scientific Pub: Liverpool, 1975.

(12) Sternberg, E.; Dolphin, D.; Brückner, C. Porphyrin-Based Photosensitizers for Use in Photodynamic Therapy. *Tetrahedron* **1998**, *54*, 4151–4202.

(13) Baker, E. W.; Palmer, S. E.; Dolphin, D. *The Porphyrins Structure and Synthesis*; Dolphin, D., Ed.; Academic Press: Canada, 1978; Vol. II.

(14) Collman, J.; Wagenknecht, S. P.; Hutchison, J. Molecular Catalysts for

Multielectron Redox Reactions of Small Molecules: The "Cofacial Metallodiporphyrin" Approach. *Angew. Chem. Int.* **1994**, *33*, 1537–1554.

(15) Huang, X.; Nakanishi, K.; Berova, N. Porphyrins and Metalloporphyrins: Versatile Circular Dichroic Reporter Groups for Structural Studies. *Chirality* **2000**, *12*, 237–255.

(16) Zabardasti, A. Molecular Interactions of Some Free Base Porphyrins σ- with and π-Acceptor Molecules. In *Molecular Interactions*; Meghea, A., Ed.; Iran, 2012; pp 49–78.

(17) Senge, M. O. *The Chemistry of Organozinc Compounds*; Rappoport, Z Marek, I., Ed.; John Wiley & Sons, Ltd, 2007.

(18) Chou, J.-H.; Kosal, M. E.; Nalwal, H. S.; Rakow, N. A.; Suslick, K. S. The Porphyrin Handbook-Applications: Past, Present and Future. In *The Porphryin Handbook*; Academic Press: New York, 2000; pp 44–128.

(19) Sakashita, R.; Ishida, M.; Furuta, H. Spectroscopic and Theoretical Studies of Acid–Base Behaviors of *N*-Confused Porphyrins: Effects of *Meso*-Aryl Substituents. *J. Phys. Chem. A* **2015**, *119*, 1013–1022.

(20) Toganoh, M.; Yamamoto, T.; Hihara, T.; Akimaru, H.; Furuta, H. Regulation of NH-Tautomerism in *N*-Confused Porphyrin by *N*-Alkylation. *Org. Biomol. Chem.* **2012**, *10*, 4367–4374.

(21) Furuta, H.; Ishizuka, T.; Osuka, A.; Dejima, H.; Nakagawa, H.; Ishikawa, Y. NH Tautomerism of *N*-Confused Porphyrin. *J. Am. Chem. Soc.* **2001**, *123*, 6207–6208.

(22) Mamardashvili, G. M.; Mamardashvili, N. Z.; Berezin, B. D. Solubility of Alkylporphyrins. *Molecules* **2000**, *5*, 762–766.

(23) Chmielewski, P. J.; Latos-Grażyński, L. *N*-Methyltetraphenylporphyrin with an Inverted *N*-Methylpyrrole Ring: The First Isomer of *N*-Methyltetraphenylporphyrin. *J. Chem. Soc. Perkin Trans. 2* **1995**, No. 3, 503–509.

(24) Golubchikov, O.; Ageeva, T. Symposium on Applications of Porphyrins in Medicine and the Fourth School for Young Scientists on the Chemistry of Porphyrins and Related Compounds Ivanovo 2000. *Molecules* **2000**, *5*, 1461–1514.

(25) Muhammad, Y.; Seen; Mukhtar, A.; Na, M. Microwave-Assisted Synthesis, Metallation and Duff Formylation of Porphyrins. *J. Heteroyclic. Chem.* **2009**, *46*,

251–255.

(26) Liu, W.; Groves, J. T. Manganese Catalyzed C–H Halogenation. *Acc. Chem. Res.* **2015**, *48*, 1727–1735.

(27) Li, J.; Raabe, G.; Yang, G.; Duan, M.; Mele, G.; Zhang, F. Regiospecific Naphthyl Nitration of 5,10,15,20-Tetranaphthylporphyrin. *J. Phys. Org. Chem.* **2011**, *24*, 1030–1038.

(28) Cabrer, A.; Ribó, J. M.; El-Hachemi, Z.; Crusats, J. 5,10,15,20-Tetrasulfonatophenylporphyrin Regioisomers: How the Location of the Sulfonato Groups Determines the Formation of Their Supramolecular Aggregates. *J. Porphyr. Phthalocya.* **2015**, *19*, 852–857.

(29) Thompson, S. J.; Dong, G. Alkylation of Rhodium Porphyrins Using Ammonium and Quinolinium Salts. *Organometallics* **2014**, *33*, 3757–3767.

(30) Jeandon, C.; Ruppert, R.; Callot, H. J. Acylation of Nickel *Meso*-Tetraarylporphyrins: Porphyrin to Corrole Ring Contraction and Formation of Seco-Porphyrins. *J. Org. Chem.* **2006**, *71*, 3111–3120.

(31) Latos-Grazynski, L.; Rachlewicz, K.; Wojaczyński, J. Novel Routes for the Modification of Iron Porphyrins. *Coord. Chem. Rev.* **1999**, *190–192*, 109–125.

(32) Kalpana, R. Synthesis and Characterization of 2, 3, 7, 8, 12, 13, 17, 18, Octabromo 5, 10, 15, 20 Tetra Phenyl Porphyrin. *Orient. J. Chem.* **2015**, *31* (2), 1195–1200.

(33) Qu, W.; Ding, T.; Cetin, A.; Harvey, J. D.; Taschner, M. J.; Ziegler, C. J. Facile Peripheral Modification of *N*-Confused Porphyrin. *J. Org. Chem.* **2006**, *71*, 811–814.

(34) Xiao, Z. Studies Toward the Chemistry of *N*-Confused Porphyrins, University of British Columbia, 2003.

(35) Wang, Y.-C.; Chen, J.-H.; Wang, S.-S.; Tung, J.-Y. Metal Complexes of 2-Aza-2-Benzyloxycarbonylmethyl-5,10,15,20-Tetraphenyl-21-Carbaporphyrin: M(2-$NCH_2COOCH_2C_6H_5$NCTPP) ($M=Ni^{2+}$, Pd^{2+}) and Mn(2-$NCH_2COOCH_2C_6H_5$NCTPP)Br (NCTPP=*N*-Confused 5,10,15,20-Tetraphenylporphyrinate). *Polyhedron* **2014**, *68*, 23–31.

(36) Srinivasan, A.; Furuta, H.; Osuka, A. The First Bis-Rh(I) Metal Complex of *N*-Confused Porphyrin. *Chem. Commun.* **2001**, 1666–1667.

(37) Lin, W.-C.; Hsaio, D.-Z.; Chang, W.-P.; Chen, J.-H.; Wang, S.-S.; Tung, J.-Y. Molecular Structures of Cu(II), Rh(III) Complexes of 2-N Substituted *N*-

Confused Porphyrin Inner C-Oxide. *Polyhedron* **2012**, *42*, 243–248.

(38) Jiang, H. W.; Hao, F.; Chen, Q. Y.; Xiao, J. C.; Liu, S. Bin; Gu, Y. C. Electrophilic Reaction of Ag(III) *N*-Confused Porphyrin with Alcohols. *J. Org. Chem.* **2010**, *75*, 3511–3514.

(39) Furuta, H.; Youfu, K.; Maeda, H.; Osuka, A. Facile Formation of *N*-Confused Porphyrin Dimers by platinum(II) Coordination to the Outer-Nitrogen Atoms. *Angew. Chem., Int. Ed.* **2003**, *42*, 2186–2188.

(40) Furuta, H.; Ishizuka, T.; Osuka, A. Flexible Inner and Outer Coordination of Zn(II) *N*-Confused Porphyrin Complex. *J. Am. Chem. Soc.* **2002**, *124*, 5622–5623.

(41) Chmielewski, P.; Latos-Grażyński, L.; T. Reactions of Nickel (II) 2-Aza-5, 10, 15, 20-Tetraphenyl-21-Carbaporphyrin with Methyl Iodide. The First Structural Characterization of a Paramagnetic Organometallic. *J. Am. Chem. Soc* **1996**, *118*, 5690–5701.

(42) Chen, W. C.; Hung, C. H. Synthesis and Characterization of Iron *N*-Confused Porphyrins: Structural Evidences of Agostic Interaction. *Inorg. Chem.* **2001**, *40*, 5070–5071.

(43) Rothemund, P. A New Porphyrin Synthesis. The Synthesis of Porphin 1. *J. Am. Chem. Soc.* **1936**, *58* (4), 625–627.

(44) Rothemund, P. Porphyrin Studies. III. The Structure of the Porphine Ring System. *J. Am. Chem. Soc.* **1939**, *61* (10), 2912–2915.

(45) Rothemund, P. Formation of Porphyrins From Pyrrole and Aldehydes. *J. Am. Chem. Soc.* **1935**, *57* (10), 2010–2011.

(46) Adler, A. D.; Longo, F. R.; Shergalis, W. Mechanistic Investigations of Porphyrin Syntheses. I. Preliminary Studies on *Meso* -Tetraphenylporphin. *J. Am. Chem. Soc.* **1964**, *86* (15), 3145–3149.

(47) Shanmugathasan, S.; Edwards, C.; Boyle, R. W. Advances in Modern Synthetic Porphyrin Chemistry. *Tetrahedron* **2000**, *56*, 1025–1046.

(48) Adler, A. D.; Longo, F. R.; Finarelli, J. D.; Goldmacher, J.; Assour, J.; Korsakoff, L. A Simplified Synthesis for *Meso*-Tetraphenylporphine. *J. Org. Chem.* **1967**, *32* (2), 476.

(49) Gonsalves, A. M. d'A R.; Pereira, M. M. A New Look into the Rothemund *Meso*-Tetraakyl and Tetrarylporphyrin Synthesis. *J. Heterocycl. Chem.* **1985**, *22*, 931–933.

(50) Lindsey, J. S.; Schreiman, I. C.; Hsu, H. C.; Kearney, P. C.; Marguerettaz, A. M. Rothemund and Adler-Longo Reactions Revisited: Synthesis of Tetraphenylporphyrins under Equilibrium Conditions. *J. Org. Chem.* **1987**, *52*, 827–836.

(51) Gonsalves, A. M. d'A R.; Varejão, J. M. T. B.; Pereira, M. M. Some New Aspects Related to the Synthesis of *Meso*-Substituted Porphyrins. *J. Heterocycl. Chem.* **1991**, *28*, 635–640.

(52) Lindsey, J. S.; Wagner, R. W. Investigation of the Synthesis of Ortho-Substituted Tetraphenylporphyrins. *J. Org. Chem.* **1989**, *54*, 828–836.

(53) Botulinski, M. Synthesis of Tetramesitylporphyrin. *Inorg. Chem.* **1988**, *27*, 210–212.

(54) Geier, R. G.; Lindsey, J. S. *N*-Confused Tetraphenylporphyrin and Tetraphenylsapphyrin Formation in One-Flask Syntheses of Tetraphenylporphyrin. *J. Org. Chem.* **1999**, *64* (5), 1596–1603.

(55) Geier, G. R.; Haynes, D. M.; Lindsey, J. S. An Efficient One-Flask Synthesis of *N*-Confused Tetraphenylporphyrin. *Org. Lett.* **1999**, *1*, 1455–1458.

(56) Narayanan, S. J.; Sridevi, B. One Step Synthesis of Sapphyrin and *N*-Confused Porphyrin Using Dipyrromethane. *Tetrahedron. Lett.* **1998**, *39*, 7389–7392.

(57) Dolphin, D.; Liu, B. Y.; Brückner, C. A *Meso*-Unsubstituted *N*-Confused Porphyrin Prepared by Rational Synthesis. *Chem. Commun.* **1996**, 2141–2142.

(58) Latos-Grazynski, L.; Chmielewski, P. Tetra-*p*-Tolylporphyrin with an Inverted Pyrrole Ring: A Novel Isomer of Porphyrin. *Angew. Chem. Int.* **1994**, *33*, 779–781.

(59) Costentin, C.; Dridi, H.; Savéant, J.-M. Molecular Catalysis of O2 Reduction by Iron Porphyrins in Water: Heterogeneous versus Homogeneous Pathways. *J. Am. Chem. Soc.* **2015**, *137*, 13535–13544.

(60) Vitale, R.; Lista, L.; Cerrone, C.; Caserta, G.; Chino, M.; Maglio, O.; Nastri, F.; Pavone, V.; Lombardi, A. Artificial Heme-Enzyme with Enhanced Catalytic Activity: Evolution, Functional Screening and Structural Characterization. *Org. Biomol. Chem.* **2015**, *13*, 4859–4868.

(61) Pires, S. M. G.; Simões, M. M. Q.; Santos, I. C. M. S.; Rebelo, S. L. H.; Pereira, M. M.; Neves, M. G. P. M. S.; Cavaleiro, J. a S. Biomimetic Oxidation of Organosulfur Compounds with Hydrogen Peroxide Catalyzed by Manganese Porphyrins. *Appl. Catal. A-Gen.* **2012**, 51–56.

(62) Liu, Q.; Ding, Y.; Yang, Y.; Zhang, L.; Sun, L.; Chen, P.; Gao, C. Enhanced Peroxidase-like Activity of Porphyrin Functionalized Ceria Nanorods for Sensitive and Selective Colorimetric Detection of Glucose. *Mater. Sci. Eng.* **2016**, *59*, 445–453.

(63) Carvalho, C. M. B.; Brocksom, T. J.; de Oliveira, K. T. Tetrabenzoporphyrins: Synthetic Developments and Applications. *Chem. Soc. Rev.* **2013**, *42* (8), 3302.

(64) Agostinis, P.; Berg, K.; Cengel, K. a; Foster, T. H.; Girotti, A. W.; Gollnick, S. O.; Hahn, S. M.; Hamblin, M. R.; Juzeniene, A.; Kessel, D.; Korbelik, M.; Moan, J.; Mroz, P.; Nowiz, D.; Piette, J.; Willson, B. C.; Golab, J. Photodynamic Therapy of Cancer : An Update. *CA-Cancer. J. Clin.* **2011**, *61*, 250–281.

(65) Morton, C. A. Topical Photodynamic Therapy in Dermatology. *Brit. J. Dermatol.* **2004**, *150*, 1061–1069.

(66) Pratviel, G. Porphyrins in Complex with DNA: Modes of Interaction and Oxidation Reactions. *Coord. Chem. Rev.* **2016**, *308*, 460–477.

(67) Mineur, P.; Colige, A. C.; Deroanne, C. F.; Dubail, J.; Kesteloot, F.; Habraken, Y.; Noël, A.; Vöö, S.; Waltenberger, J.; Lapière, C. M.; Nusgens, B. V; Lambert, C. a. Newly Identified Biologically Active and Proteolysis-Resistant VEGF-A Isoform VEGF111 Is Induced by Genotoxic Agents. *J. Cell. Biol.* **2007**, *179* (17), 1261–1273.

(68) Serra, V. V.; Zamarrón, A.; Faustino, M. A. F.; Cruz, M. C. I. D. La; Blázquez, A.; Rodrigues, J. M. M.; Neves, M. G. P. M. S.; Cavaleiro, J. A. S.; Juarranz, A.; Sanz-Rodríguez, F. New Porphyrin Amino Acid Conjugates: Synthesis and Photodynamic Effect in Human Epithelial Cells. *Bioorg. Med. Chem.* **2010**, *18*, 6170–6178.

(69) Acedo, P.; Stockert, J. C.; Cañete, M.; Villanueva, A. Two Combined Photosensitizers: A Goal for More Effective Photodynamic Therapy of Cancer. *Cell. Death. Dis* **2014**, *5* (3), 1–12.

(70) Li, J.-W.; Wu, Z.-M.; Magetic, D.; Zhang, L.-J.; Chen, Z.-L. Antitumor Effects Evaluation of a Novel Porphyrin Derivative in Photodynamic Therapy. *Tumor. Biol.* **2015**, *36*, 9685–9692.

(71) Costa, L.; Faustino, M. A. F.; Neves, M. G. P. M. S.; Cunha, A.; Almeida, A. Photodynamic Inactivation of Mammalian Viruses and Bacteriophages. *Viruses* **2012**, *4* (7), 1034–1074.

(72) DeRosa, M.; Crutchley, R. Photosensitized Singlet Oxygen and Its Applications.

Coord. Chem. Rev. **2002**, *234*, 351–371.

(73) Photobiology, E. S. for. *Photodynamic Therapy*; Patrice, T., Hader D.P, Jori, G., Eds.; The Royal Society of Chemistry: Cambridge, 2003.

(74) Smith, K. M.; Guilard, R.; Kadish, K. *The Porphyrin Handbook. Applications: Past, Present and Future*; Academic Press: New York, 2000; Vol. 1–10.

(75) Barata, J. F. B.; Zamarrón, A.; Neves, M. G. P. M. S.; Faustino, M. A. F.; Tomé, A. C.; Cavaleiro, J. A. S.; Röder, B.; Juarranz, Á.; Sanz-Rodríguez, F. Photodynamic Effects Induced by *Meso*-Tris(pentafluorophenyl)corrole and Its Cyclodextrin Conjugates on Cytoskeletal Components of HeLa Cells. *Eur. J. Med. Chem.* **2015**, *92*, 135–144.

(76) Cardote, T. A. F.; Barata, J. F. B.; Faustino, M. A. F.; Preuß, A.; Neves, M. G. P. M. S.; Cavaleiro, J. A. S.; Ramos, C. I. V; Santana-Marques, M. G. O.; Röder, B. Pentafluorophenylcorrole-D-Galactose Conjugates. *Tetrahedron. Lett.* **2012**, *53* (47), 6388–6393.

(77) Gao, D.; Agayan, R. R.; Xu, H.; Philbert, M. A.; Kopelman, R. Nanoparticles for Two-Photon Photodynamic Therapy in Living. *Nano. Lett.* **2008**, *6* (11), 2383–2386.

(78) Liu, H.; Lv, C.; Ding, B.; Wang, J.; Li, S.; Zhang, Y. Antitumor Activity of G-Quadruplex-Interactive Agent TMPyP4 with Photodynamic Therapy in Ovarian Carcinoma Cells. *Oncol. Lett.* **2014**, *8*, 409–413.

(79) Dougherty T., Gomer C., Henderson B., Jori G., Kessel D., Korbelik M., Moan J., P. Q. Photodynamic Therapy. *J .Natl. Cancer. Inst.* **1998**, *90* (12), 889–905.

(80) Castano, A. P.; Demidova, T. N.; Hamblin, M. R. Mechanisms in Photodynamic Therapy: Part One - Photosensitizers, Photochemistry and Cellular Localization. *Photodiagn. Photodynm.* **2004**, *1* (4), 279–293.

(81) Allison, R. R.; Downie, G. H.; Cuenca, R.; Hu, X. H.; Childs, C. J. H.; Sibata, C. H. Photosensitizers in Clinical PDT. *Photodiagn. Photodyn.* **2004**, *1* (1), 27–42.

(82) Detty, M. R.; Gibson, S. L.; Wagner, S. J. Current Clinical and Preclinical Photosensitizers for Use in Photodynamic Therapy. *J. Med. Chem.* **2004**, *47* (16), 3897–3915.

(83) Kessel, D.; Luo, Y.; Deng, Y.; Chang, C. K. The Role of Subcellular Localization in Initiation of Apoptosis by Photodynamic Therapy. *Photochem. Photobiol.* **1997**, *65* (3), 422–426.

(84) Wilson, B. C.; Olivo, M.; Singh, G. Subcellular Localization of Photofrin and

Aminolevulinic Acid and Photodynamic Cross-Resistance in Vitro in Radiation-Induced Fibrosarcoma Cells Sensitive or Resistant to Photofrin-Mediated Photodynamic Therapy. *Photochem. Photobiol.* **1997**, *65*, 166–176.

(85) Kumar, V.; Abbas, A. K.; Fausto, N.; Aster, J. C. *Robbins and Cotran Pathologic Basis of Disease*, Eighth.; Saunders Elsevier: Philadelphia, 2010.

(86) Portt, L.; Norman, G.; Clapp, C.; Greenwood, M.; Greenwood, M. T. Anti-Apoptosis and Cell Survival: A Review. *Biochem. Biophys.* **2011**, *1813*, 238–259.

(87) Elmore, S. Apoptosis: A Review of Programmed Cell Death. *Toxicol Pathol* **2007**, *35*, 495–516.

(88) Id, C. R. E. F.; Ind, M. L.; Library, M. Pre-mRNA Splicing in Cancer : The Relevance in Oncogenesis , Treatment and Drug Resistance. *Expert. Opin. Drug. Metab. Toxicol.* **2015**, *11* (4), 673–689.

(89) Chen, M.; Manley, J. L. Mechanisms of Alternative Splicing Regulation: Insights from Molecular and Genomics Approaches. *Nat. Rev. Mol. Cell. Bio.* **2009**, *10*, 741–754.

(90) Keren, H.; Lev-Maor, G.; Ast, G. Alternative Splicing and Evolution: Diversification, Exon Definition and Function. *Nat. Rev. Genet.* **2010**, *11*, 345–355.

(91) Chandler, D. S.; Singh, R. K.; Caldwell, L. C.; Bitler, J. L.; Lozano, G. Genotoxic Stress Induces Coordinately Regulated Alternative Splicing of the p53 Modulators MDM2 and MDM4. *Cancer. Res.* **2006**, *66*, 9502–9508.

(92) Zheng, T.; Wang, J.; Zhao, Y.; Zhang, C.; Lin, M.; Wang, X.; Yu, H.; Liu, L.; Feng, Z.; Hu, W. Spliced MDM2 Isoforms Promote Mutant p53 Accumulation and Gain-of-Function in Tumorigenesis. *Nat. Commun.* **2013**, *4*, 1–24.

(93) Gabriel, M.; Delforge, Y.; Deward, A.; Habraken, Y.; Hennuy, B.; Piette, J.; Klinck, R.; Chabot, B.; Colige, A.; Lambert, C. Role of the Splicing Factor SRSF4 in Cisplatin-Induced Modifications of Pre-mRNA Splicing and Apoptosis. *BMC. Cancer.* **2015**, *15*, 227–241.

(94) Shkreta, L.; Michelle, L.; Toutant, J.; Tremblay, M. L.; Chabot, B. The DNA Damage Response Pathway Regulates the Alternative Splicing of the Apoptotic Mediator Bcl-X. *J. Biol. Chem.* **2011**, *286*, 331–340.

(95) Schwerk, C.; Schulze-Osthoff, K. Regulation of Apoptosis by Alternative Pre-mRNA Splicing. *Mol. Cell.* **2005**, *19*, 1–13.

(96) Boulikas, T.; Vougiouka, M. Cisplatin and Platinum Drugs at the Molecular Level. (Review). *Oncol. Rep.* **2003**, *10* (6), 1663–1682.

(97) Kelland, L. The Resurgence of Platinum-Based Cancer Chemotherapy. *Nat. Rev. Cancer* **2007**, *7* (8), 573–584.

(98) Hanakova, A.; Bogdanova, K.; Tomankova, K.; Binder, S.; Bajgar, R.; Langova, K.; Kolar, M.; Mosinger, J.; Kolarova, H. Study of Photodynamic Effects on NIH 3T3 Cell Line and Bacteria. *Biomed. Pap.* **2014**, *158* (2), 201–207.

(99) Saeko Tada-Oikawa, Shinji Oikawa, Junya Hirayama, Kazutaka Hirakawa, S. K. DNA Damage and Apoptosis Induced by Photosensitization of 5, 10, 15, 20-Tetrakis (*N*-Methyl-4-Pyridyl)-21H, 23H-Porphyrin via Singlet Oxygen Generation. *Photochem. Photobiol.* **2009**, *85*, 1391–1399.

(100) Thomas, A. P.; Saneesh Babu, P. S.; Asha Nair, S.; Ramakrishnan, S.; Ramaiah, D.; Chandrashekar, T. K.; Srinivasan, A.; Radhakrishna Pillai, M. *Meso*-Tetrakis(*p*-sulfonatophenyl)*N*-Confused Porphyrin Tetrasodium Salt: A Potential Sensitizer for Photodynamic Therapy. *J. Med. Chem.* **2012**, *55*, 5110–5120.

(101) Xiao, Z.; Dolphin, D. Facile Synthesis of N , N 0 -Dimethylated N -Confused Porphyrins. *Tetrahedron* **2002**, *58*, 9111–9116.

(102) Ikawa, Y.; Moriyama, S.; Harada, H.; Furuta, H. Acid–base Properties and DNA-Binding of Water Soluble *N*-Confused Porphyrins with Cationic Side-Arms. *Org. Biomol. Chem.* **2008**, *6* (22), 4157–4166.

(103) Du, Y.; Zhang, D.; Chen, W.; Zhang, M.; Zhou, Y.; Zhou, X. Cationic *N*-Confused Porphyrin Derivative as a Better Molecule Scaffold for G-Quadruplex Recognition. *Bioorgan. Med. Chem.* **2010**, *18* (3), 1111–1116.

(104) Silva, S.; Pereira, P. M. R.; Silva, P.; Almeida Paz, F. a.; Faustino, M. a. F.; Cavaleiro, J. a. S.; Tomé, J. P. C. Porphyrin and Phthalocyanine Glycodendritic Conjugates: Synthesis, Photophysical and Photochemical Properties. *Chem. Commun.* **2012**, *48*, 3608–3610.

(105) Simões, C.; Gomes, M. C.; Neves, M. G. P. M. S.; Cunha, Â.; Tomé, J. P. C.; Tomé, A. C.; Cavaleiro, J. A. S.; Almeida, A.; Faustino, M. A. F. Photodynamic Inactivation of Escherichia Coli with Cationic *Meso*-Tetraarylporphyrins - The Charge Number and Charge Distribution Effects. *Catal. Today* **2016**, *266*, 197–204.

(106) Belair, J. P.; Ziegler, C. J.; Rajesh, C. S.; Modarelli, D. A. Photophysical Characterization of Free-Base *N*-Confused Tetraphenylporphyrins. *J. Phys. Chem*

A **2002**, *106* (27), 6445–6451.

(107) Lee, J. S.; Lim, J. M.; Toganoh, M.; Furuta, H.; Kim, D. Comparative Spectroscopic Studies on Porphyrin Derivatives: Electronic Perturbation of *N*-Confused and *N*-Fused Porphyrins. *Chem. Commun.* **2010**, *46*, 285–287.

(108) Bacellar, I. O. L.; Tsubone, T. M.; Pavani, C.; Baptista, M. S. Photodynamic Efficiency: From Molecular Photochemistry to Cell Death. *Int. J. Sci.* **2015**, *16* (9), 20523–20559.

(109) Roche. Cell Proliferation Reagent WST-1 https://pim-eservices.roche.com/LifeScience/Document/c4c412ae-96ed-e311-98a1-00215a9b0ba8.

(110) Berridge, M.; Tan, A.; McCoy, K.; Wang, R. The Biochemical and Cellular Basis of Cell Proliferation Assays That Use Tetrazolium Salts. *Biochemica* **1996**, No. 4, 4–9.

(111) Crouch, S. P. M.; Kozlowski, R.; Slater, K. J.; Fletcher, J. The Use of ATP Bioluminescence as a Measure of Cell Proliferation and Cytotoxicity. *J. Immunol. Methods.* 1993, pp 81–88.

(112) Petty, R. D.; Sutherland, L. a; Hunter, E. M.; Cree, I. a. Comparison of MTT and ATP-Based Assays for the Measurement of Viable Cell Number. *J. Biolumin. Chemilumin.* **1995**, *10*, 29–34.

(113) Strober, W. Trypan Blue Exclusion Test of Cell Viability. *Curr. Protoc. Immunol.* **1997**, *Appendix 3* (November), 2–3.

(114) MOAN, J.; BERG, K. The Photodegradation of Porphyrins in Cells Can Be Used To Estimate the Lifetime of Singlet Oxygen. *Photochem. Photobiol.* **1991**, *53* (4), 549–553.

(115) Rangasamy, S.; Ju, H.; Um, S.; Oh, D. C.; Song, J. M. Mitochondria and DNA Targeting of 5,10,15,20-Tetrakis(7-Sulfonatobenzo[b]thiophene) Porphyrin-Induced Photodynamic Therapy via Intrinsic and Extrinsic Apoptotic Cell Death. *J. Med. Chem.* **2015**, *58*, 6864–6874.

(116) McCormick, B. P. P.; Pansa, M. F.; Sanabria, L. N. M.; Carvalho, C. M. B.; Faustino, M. A. F.; Neves, M. G. P. M. S.; Cavaleiro, J. A. S.; Vittar, N. B. R.; Rivarola, V. A. Cationic Porphyrin Derivatives for Application in Photodynamic Therapy of Cancer. *Laser. Phys.* **2014**, *24*, 45603.

(117) Chaitanya, G. V; Steven, A. J.; Babu, P. P. PARP-1 Cleavage Fragments: Signatures of Cell-Death Proteases in Neurodegeneration. *Cell .Commun. Signal.*

2010, *8* (1), 31.

(118) Gobeil, S.; Boucher, C. C.; Nadeau, D.; Poirier, G. G. Characterization of the Necrotic Cleavage of poly(ADP-Ribose) Polymerase (PARP-1): Implication of Lysosomal Proteases. *Cell. Death. Differ.* **2001**, *8*, 588–594.

(119) Kessel, D.; Oleinick, N. L. Initiation of Autophagy by Photodynamic Therapy. *Method. Enzym.* **2009**, *453*, 1–16.

(120) Tanida, I.; Ueno, T.; Kominami, E. LC3 Conjugation System in Mammalian Autophagy. *Int. J. Bio. Cell. Biol.* **2004**, *36*, 2503–2518.

(121) Christofferson, D. E.; Yuan, J. Cyclophilin A Release as a Biomarker of Necrotic Cell Death. *Cell Death Differ.* **2010**, *17* (12), 1942–1943.

(122) Nemazanyy, I.; Panasyuk, G.; Breus, O.; Zhyvoloup, A.; Filonenko, V.; Gout, I. T. Identification of a Novel CoA Synthase Isoform, Which Is Primarily Expressed in the Brain. *Biochem. Bioph. Res. Co.* **2006**, *341*, 995–1000.

(123) NCBI. GenBank https://www.ncbi.nlm.nih.gov/genbank/ (accessed Oct 20, 2016).

(124) Díaz-Perales, A.; Quesada, V.; Peinado, J. R.; Ugalde, A. P.; Álvarez, J.; Suárez, M. F.; Gomis-Rüth, F. X.; López-Otín, C. Identification and Characterization of Human Archaemetzincin-1 and -2, Two Novel Members of a Family of Metalloproteases Widely Distributed in Archaea. *J. Biol. Chem.* **2005**, *280* (34), 30367–30375.

(125) Marcel, V.; Tran, P. L. T.; Sagne, C.; Martel-Planche, G.; Vaslin, L.; Teulade-Fichou, M. P.; Hall, J.; Mergny, J. L.; Hainaut, P.; van Dyck, E. G-Quadruplex Structures in TP53 Intron 3: Role in Alternative Splicing and in Production of p53 mRNA Isoforms. *Carcinogenesis* **2011**, *32* (3), 271–278.

(126) Cooper, G. M.; Hausman, R. E. *The Cell: A Molecular Approach*, Fourth.; University, B., Ed.; ASM Press: Washington D.C, 2007.

(127) Mahmood, T.; Yang, P. C. Western Blot: Technique, Theory, and Trouble Shooting. *N. Am. J. Med. Sci.* **2012**, *4* (9), 429–434.

(128) Buckingham, L.; Flaws, M. *Molecular Diagnostics: Fundamentals, Methods, and Clinical Applications*; F.A. Davis company: Philadelphia, 2007.

(129) Rodwell, V.; Bender, D.; Botham, K.; Kennelly, P.; Weil, A. *Harper's Illllustrated Biochemistry*, Thirtieth.; McGraw-Hill, 2015.

(130) Uzman, A. Fundamental Molecular Biology. *Biochem. Mol. Biol. Educ.* **2007**, *35*, 481–482.

(131) ThermoFisher Scientific. Loading Controls Antibodies https://www.thermofisher.com/pt/en/home/life-science/antibodies/primary-antibodies/control-antibodies/loading-control-antibodies.html (accessed Oct 30, 2016).